

**NASA TECHNICAL  
MEMORANDUM**

**N 7 2 - 2 7 5 1 6**

**NASA TM X-64666**

**May 30, 1972**

**CASE FILE  
COPY**

**NASA TM X-64666**

**QUALITY AND RELIABILITY ASSURANCE RESEARCH  
AT MSFC**

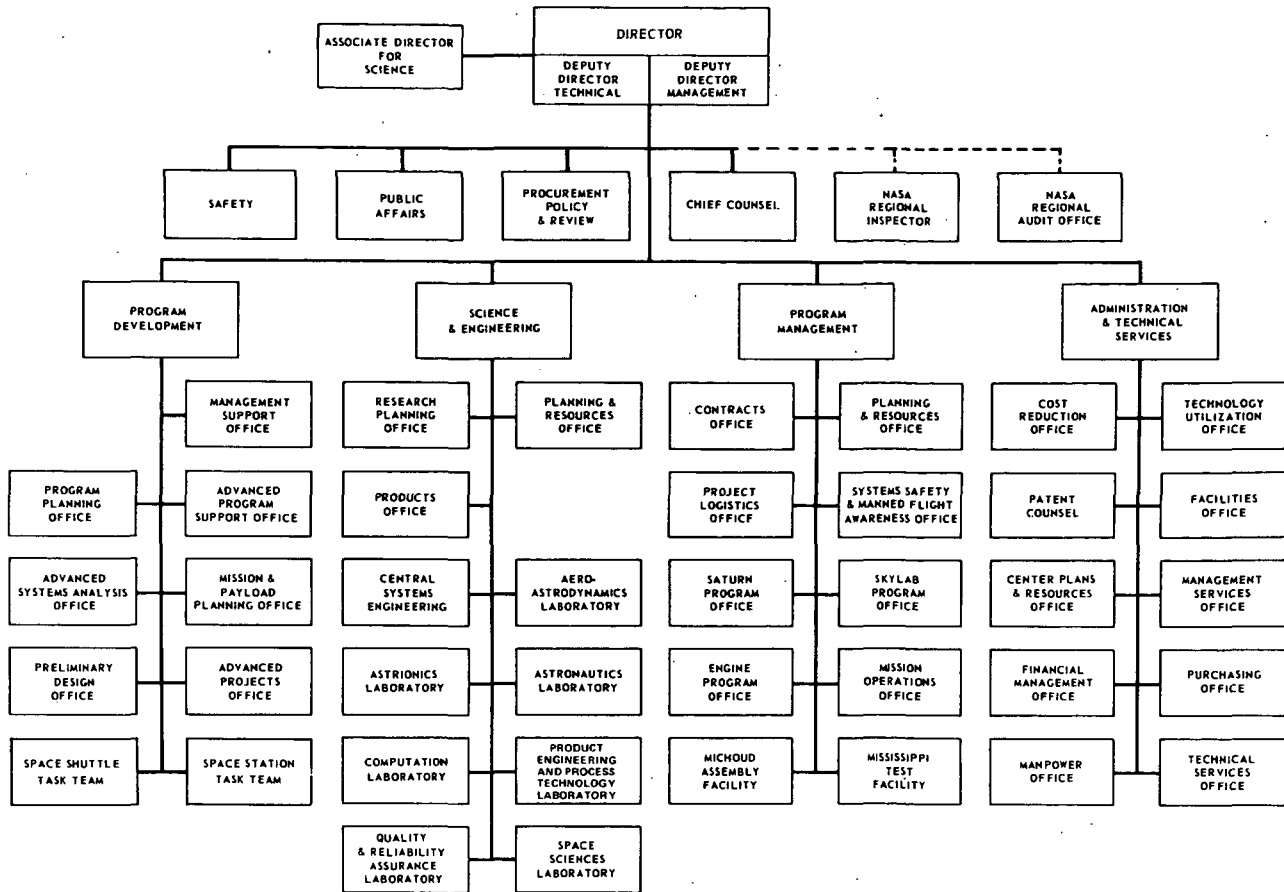
**RESEARCH ACHIEVEMENTS REVIEW**

**VOLUME IV**

**REPORT NO. 5**

**SCIENCE AND ENGINEERING DIRECTORATE  
GEORGE C. MARSHALL SPACE FLIGHT CENTER  
MARSHALL SPACE FLIGHT CENTER, ALABAMA**

GEORGE C. MARSHALL SPACE FLIGHT CENTER



RESEARCH ACHIEVEMENTS REVIEWS COVER THE FOLLOWING FIELDS OF RESEARCH

- Radiation Physics
- Thermophysics
- Chemical Propulsion
- Cryogenic Technology
- Electronics
- Control Systems
- Materials
- Manufacturing
- Ground Testing
- Quality Assurance and Checkout
- Terrestrial and Space Environment
- Aerodynamics
- Instrumentation
- Power Systems
- Guidance Concepts
- Astrodynamics
- Advanced Tracking Systems
- Communication Systems
- Structures
- Mathematics and Computation
- Advanced Propulsion
- Lunar and Meteoroid Physics

## PREFACE

The Research Achievement Reviews document research accomplished by the laboratories of Marshall Space Flight Center. Each review covers one or two fields of research and attempts to present the results in a form readily useable by specialists, system engineers, and program managers.

Reviews of this fourth series are designated Volume IV and will span the period from May 1970 through May 1972.

In accordance with NASA policy the International System of Units (SI Units), as defined in NASA SP-7012, are used in this publication.

The papers in this report were presented May 27, 1971

William G. Johnson  
Director  
Research Planning Office

CONTENTS. . .

ADVANCED RADIOGRAPHIC IMAGING TECHNIQUES

By J. B. Beal

	Page
SUMMARY . . . . .	1
LIST OF SYMBOLS . . . . .	1
GLOSSARY OF TERMS . . . . .	1
INTRODUCTION . . . . .	2
SOLID-STATE RADIOGRAPHIC X-RAY IMAGE AMPLIFIERS . . . . .	3
NEUTRON RADIATION IMAGING SYSTEM . . . . .	13
REFERENCES . . . . .	20
BIBLIOGRAPHY . . . . .	20

LIST OF TABLES

Table	Title	Page
1.	Comparison of X-Ray Imaging Systems . . . . .	9
2.	Comparison of N-Ray Imaging Systems . . . . .	18

LIST OF ILLUSTRATIONS

Figure	Title	Page
1.	Solid-state radiographic X-ray imaging systems . . . . .	4
2.	Basic circuit . . . . .	4
3.	Image amplifier panel construction . . . . .	5
4.	Transfer characteristics comparison -- fluoroscope versus nonstorage panel display . . . .	6
5.	Exposure time versus aluminum thickness for image storage panel display . . . . .	7
6.	Modified X-ray cabinet for use with nonstorage panel system . . . . .	10
7.	Nonstorage panel image of luggage interior . . . . .	10
8.	Nonstorage panel image of internal fixture in graphite/epoxy strut . . . . .	11

CONTENTS (Continued) . . .

LIST OF ILLUSTRATIONS

Figure	Title	Page
9.	Laboratory X-ray cabinet with wide-range radiographic application capabilities . . . . .	12
10.	Image storage panel display of stratoscope electrical connections . . . . .	12
11.	Schematic of radiographic system . . . . .	13
12.	Absorption of neutrons and X-radiation by the elements . . . . .	14
13.	Comparison of N-ray versus X-ray radiographs . . . . .	14
14.	Van de Graaff accelerator and neutron viewing system . . . . .	16
15.	TV direct-viewing N-ray system block diagram . . . . .	16
16.	Typical application of neutron radiography: explosive squib evaluation . . . . .	19

ADVANCED MATERIALS INSPECTION TECHNIQUES

By M. C. McIlwain

	Page
SUMMARY . . . . .	21
INTRODUCTION . . . . .	21
COATED REFRACTORY METALS . . . . .	21
FILAMENTARY COMPOSITES . . . . .	24
REFERENCES . . . . .	28

LIST OF TABLES

Table	Title	Page
1.	NDT Assessment Matrix . . . . .	26
2.	NDT Results Matrix . . . . .	28

LIST OF ILLUSTRATIONS

Figure	Title	Page
1.	Silicide coating with characteristic cracks . . . . .	21
2.	NDE technique schematic for coated refractory metals . . . . .	22

CONTENTS (Continued) . . .

LIST OF ILLUSTRATIONS

Figure	Title	Page
3.	Dermatron calibration curve . . . . .	23
4.	Stimulated emission radiograph . . . . .	24
5.	Current program schedule . . . . .	24
6.	Schematic of composite fabrication . . . . .	25
7.	Typical standard panel design . . . . .	26
8.	NDT schematic for composites . . . . .	27
9.	Ultrasonic C-scan of typical standard panel . . . . .	27

GASEOUS FLOW DETECTION TECHNIQUES FOR IN-SPACE APPLICATION

By T. F. Morris

	Page
SUMMARY . . . . .	29
INTRODUCTION . . . . .	29
FLOWMETER . . . . .	29
LEAK DETECTOR . . . . .	32
CURRENT STATUS . . . . .	34

LIST OF TABLES

Table	Title	Page
1.	Summary of Flowmeter Characteristics . . . . .	32
2.	Summary of Leak Detector Characteristics . . . . .	34

CONTENTS (Continued) . . .

LIST OF ILLUSTRATIONS

Figure	Title	Page
1.	Flowmeter for space environment . . . . .	30
2.	Leak detector for space environment . . . . .	30
3.	Flowmeter pictorial schematic . . . . .	31
4.	Block diagram of leak detector . . . . .	33

QUALITY AND RELIABILITY REQUIREMENTS FOR HYBRID MICROCIRCUITS

By M. J. Berkebile

	Page
SUMMARY . . . . .	35
INTRODUCTION . . . . .	35
CUSTOM HYBRIDS . . . . .	36
TEST SPECIMENS . . . . .	37
TEST PROGRAM . . . . .	39
PROBLEM AREAS . . . . .	44
ALUMINUM BUMP CHIPS . . . . .	45
HIGHER FREQUENCY RANGES . . . . .	45
HIGHER POWER REQUIREMENTS . . . . .	46
RELIABILITY . . . . .	47

LIST OF TABLES

Table	Title	Page
1.	Comparison of Hybrid Microcircuits and PC Board Construction . . . . .	37
2.	Typical Deposition Materials for Producing Hybrid Conductors and Passive Devices . . . . .	38
3.	Test Specimen Description . . . . .	39

CONTENTS (Continued) . . .

LIST OF TABLES

Table	Title	Page
4.	Test Program . . . . .	40
5.	Voltage Regulator Test Circuit Failures . . . . .	40
6.	Chip-to-Substrate Interface . . . . .	43
7.	Reliability Projection . . . . .	47

LIST OF ILLUSTRATIONS

Figure	Title	Page
1.	Comparison of printed circuit board and hybrid packaging techniques . . . . .	36
2.	A typical thick film hybrid microcircuit . . . . .	38
3.	Fractured substrate caused by poor substrate-to-header bond . . . . .	41
4.	Side-view X-ray photos (Manufacturer D) . . . . .	42
5.	A typical beam-led device . . . . .	43
6.	Test substrate for beam-led devices . . . . .	44
7.	Flip-chip test substrate . . . . .	45
8.	Power supply circuit using flip chips and beam-led devices . . . . .	46

BOND PROBLEMS CAUSED BY THERMAL EXCURSION

By F. Vilella

	Page
ABSTRACT . . . . .	49
SUMMARY . . . . .	49
POWER CYCLING TESTS . . . . .	49
SCANNING ELECTRON MICROSCOPE . . . . .	52

CONTENTS (Concluded) . . .

	Page
BOND PULLING TESTS . . . . .	54
CONCLUSIONS . . . . .	57
BIBLIOGRAPHY . . . . .	58

LIST OF TABLES

Table	Title	Page
1.	Summary of Power Cycling Tests Performed by Manufacturer A on their own Aluminum Thermocompression Wedge Bonds . . . . .	51
2.	Summary of Power Cycling Tests Performed by MSFC on Aluminum Ultrasonic Bonds (Maximum Device-Rated Power) . . . . .	52
3.	Summary of Power Cycling Tests Performed by MSFC on Aluminum Ultrasonic Bonds (Derated Conditions) . . . . .	52
4.	Summary of Power Cycling Tests Performed by MSFC on Gold Thermocompression Bonds (Maximum Device-Rated Power) . . . . .	53
5.	Results of Bond Pulling Tests Performed by MSFC . . . . .	57

LIST OF ILLUSTRATIONS

Figure	Title	Page
1.	Manufacturer A transistor 2N2222A from ECA Ignition Phase Timer, typical TC wedge bond (220X magnification) . . . . .	50
2.	Power cycling test circuit . . . . .	51
3.	Percentage of failures . . . . .	53
4.	Manufacturer A transistor 2N2222A from ECA Ignition Phase Timer, TC wedge bond, emitter bond failed after 2240 power cycles . . . . .	54
5.	Manufacturer A transistor 2N2222A, group 1, die side bond, ultrasonic, open at heel . . . . .	55
6.	Manufacturer B transistor 2N2222A, serial number 75, die side bond, ultrasonic; evidence of microcracks at the heel before power cycling . . . . .	55
7.	Manufacturer B transistor 2N2222A, serial number 75, die side bond, ultrasonic; microcrack depth increased after 3152 power cycles . . . . .	56
8.	Manufacturer B transistor 2N2222A, serial number 75, die side bond, ultrasonic; open at heel after 14 500 power cycles . . . . .	56

# ADVANCED RADIOGRAPHIC IMAGING TECHNIQUES

By

J. B. Beal

## SUMMARY

The need for reduction of space vehicle costs coupled with increased demands for high reliability, as dictated by long duration mission requirements, has required that the National Aeronautics and Space Administration (NASA) continuously scrutinize and improve quality assurance methods wherever possible. X-radiography has been extensively employed as a primary hardware inspection method. Neutron radiography has been applied to the analysis of ordnance devices.

This paper examines the nature and operational constraints of conventional X-radiographic and neutron imaging methods, thereby providing a foundation for the discussion of advanced radiographic imaging systems. Two types of solid-state image amplifiers designed to image X-rays are described. Operational theory, panel construction, and performance characteristics are discussed. A closed-circuit television system for imaging neutrons is described also; and the system design, operational theory, and performance characteristics are outlined. Emphasis is placed on a description of the advantages of these imaging systems over conventional methods.

## LIST OF SYMBOLS

<u>Symbol</u>	<u>Definition</u>
Au	Gold
$B_0$	Constant of EL cells
C	Capacitance
CdS	Cadmium sulfide
CdSe	Cadmium selenide
EL	Electroluminescent, electroluminescence
f	Frequency in hertz
fl	Foot-lamberts (lumens/ft <sup>2</sup> )

$\gamma$	Measure of contrast (gamma)
$\lambda$	Wavelength
P	Capacitance ratio
PbO	Lead oxide
PC	Photoconductive, photoconductor
R	Resistance or Röntgen
SnO	Tin oxide
ZnS	Zinc sulfide

## GLOSSARY OF TERMS

Brightness	Measure of visual sensation of luminous intensity; often used instead of luminescence or luminous emittance.
Electro-luminescence (EL)	Luminescence excited by an electrical field of current.
Gamma ( $\gamma$ )	Measure of the image contrast of an intensifier panel; equal to the slope of the transfer characteristics drawn on double logarithmic paper: $\gamma = d(\log B)/d(\log L)$ (where L is the input light intensity and B is the output brightness).
Illumination	Density of the luminous flux on an illuminated surface; its units are the lux (lumens/m <sup>2</sup> ) and phot (lumens/cm <sup>2</sup> ).
Image Amplifier or Image Intensifier	Device for increasing the brightness of an image; two varieties of such image

	intensifiers are under development: (1) vacuum-tube type using photoelectric emission, electron optics, and cathodoluminescence; and (2) solid-state type using PC and EL materials.
Lambert	See luminous emittance.
Lumen (lm)	Unit of luminous flux; equal to the flux through a unit solid angle (steradian) from a uniform point source of 1 candle.
Luminescence	Phenomenon of light emission caused by an effect other than high temperature (thermal radiation), as electroluminescence (EL), photoluminescence (PL), bioluminescence, cathodoluminescence, etc.
Luminous Emittance	Luminous flux emitted per unit area; its units are lumen/cm <sup>2</sup> (lambert) and lumen/ft <sup>2</sup> (foot-lambert).
Luminous Flux	The total visible energy emitted by a source per unit time; its unit is the lumen.
Luminous Gain	The ratio of the total output flux in luminous units to the corresponding input flux in the same units; the input spectrum, the output phosphor, and the input or output flux level must be specified.
Photoluminescence (PL)	Luminescence excited by electromagnetic radiation as ultraviolet light, visible light, or X-rays.
Resolution	Measure of the optical quality of an image regarding the separation of close elements; its units are (1) optical lines/mm (in.), (2) line-pairs/mm (in.), (3) TV lines/mm (in.), and (4) elements or cells/mm (in.); units (3) and (4) differ by a factor of two from units (1) and (2).

Röntgen (R)	Unit of X-ray dose; R/sec and R/min are units of X-ray intensity.
Standard Luminous Gain	Same as luminous gain if the input flux is 2870°K color temperature tungsten lamp radiation.
Transfer Characteristics	Curve representing the output brightness as a function of the input light intensity of the image intensifier; drawn generally on double logarithmic paper.

## INTRODUCTION

Nondestructive testing (NDT) is the ability to evaluate, without damage, a structure or part for defects and material characteristics. Nondestructive testing of aerospace structures draws on all areas of science and adopts whatever it finds useful. It also contributes useful evaluation methods for biomedical, industrial, and public-sector applications. It uses all types of energy from the single thump of dynamite through sonics to ultrasonics, radio frequency up to light, and ultraviolet to X-, gamma-, and neutron-rays.

Radiography (utilizing X-, gamma-, or neutron-rays) is one of the most useful tools in the NDT engineer's kit. The information obtained from radiographs is well worth the cost per shot, but when tens of thousands of radiographs are made on a single project, the cost factor has to be considered. This kind of evaluation has highlighted the desirability of eliminating direct film radiography wherever possible [1].

This paper will be concerned with two imaging techniques developed at MSFC, the solid-state radiographic image amplifier and a neutron-radiation direct-viewing system. The solid-state image amplifier development was initiated when a contractual study, "Nondestructive Testing for Space Application", conducted by Marshall Space Flight Center (MSFC) indicated problems of film storage, development, and evaluation in the space environment for the optimum NDT method of radiography [2]. To solve the film problems, contracts were issued with Westinghouse Electric Corp. to

develop the solid-state imaging system, both with and without image retention capabilities, as a direct film replacement. The delivered panels, as a result of a decision to concentrate the effort on developing the simplest possible construction, are inherently easy to manufacture and thus have many advantages over more complex electronic devices for both immediate terrestrial applications as well as any potential space uses. Other in-house uses for production and receiving inspection evaluations are now being explored. The feasibility of producing flexible panels (plastic base instead of glass base) and light-sensitive storage panels has been proven, but such panels have not been developed in MSFC program efforts [1].

Neutron radiography has recently entered the NDT tool kit as a result of the unique behavior of a collimated beam of neutrons. Such a beam penetrates most materials easily. The opacity of the elements to neutrons varies randomly, with hydrogen, boron, cadmium, and some of the rare earth elements being much more opaque than the rest. The hydrogen content of organics makes them optimum materials for neutron radiography through thicknesses that are astonishing in comparison to usual structural metals.

The MSFC study concluded that generators of low neutron-radiation output (such as the Van de Graaff type) were the best choice as sources of neutron radiography; closed circuit television, with recorder memory abilities, was selected as the best imaging system. A Van de Graaff generator and facility, formerly used in studies of high energy particle effects on materials, was modified for neutron radiographic purposes. A closed-circuit television system was then developed under contract and designed around an imaging system utilizing a recently developed vidicon camera tube. All neutron indications are stored in the SEC vidicon camera tube until enough events are recorded for suitable image display. The image is then scanned and stored in a data disc recorder system and displayed out of this system. A method of image enhancement by lighter or darker contrast adjustment of grey levels is built-in. The system's ability to be used in "in-motion" studies as well as its ability to detect very low levels of tracers such as cadmium, carbon, and boron compounds should be quite valuable [1].

## SOLID-STATE RADIOGRAPHIC X-RAY IMAGE AMPLIFIERS

### Discussion

#### DEVELOPMENT OF IMAGE AMPLIFIERS [3]

The history of this type of amplifier dates back to 1952 when it was invented. Since 1952, more than a hundred patents have been awarded that propose a large variety of construction techniques, materials, and applications. The device is similar in general appearance to a fluorescent screen, but it converts input radiation into electric current, amplifies, and excites an electroluminescent material to form an image on the panel output side. The panel's activating power may be either ac or dc at quite low voltages and low power. The contractual study with Westinghouse produced two noteworthy developments: (1) a means of producing a fine grain, high contrast, high sensitivity nonstorage image panel; and (2) methods and materials for fabricating an amplifier panel having image retention properties, meeting requirements for X-ray film resolution, and also having fine grain, high contrast, and high sensitivity.

Figure 1 shows the various imaging systems developed. The two panels on the left are the non-storage type and are sensitive to electromagnetic spectrum wavelengths from near-light infrared through X-radiation ( $10^4$  to  $10^{-3}$  Å). The panel with the picture frame is the image storage type. The smaller panel in the plastic envelope is the prototype flexible image storage panel developed. The battery-operated power supply shown may be used with all the panels illustrated here since operational requirements are similar for both types of image amplifiers, which is a definite advantage.

#### CONSTRUCTION

The X-ray sensitive image amplifiers, both the nonstorage and image storage type, developed in this program are of the photoconductor-electroluminescent (PC-EL) sandwich-type construction.

Figure 2 shows the basic circuit. The sensor element, a photoconductor (PC), is connected in series with the display element, an electroluminescent



Figure 1. Solid-state radiographic X-ray imaging systems.

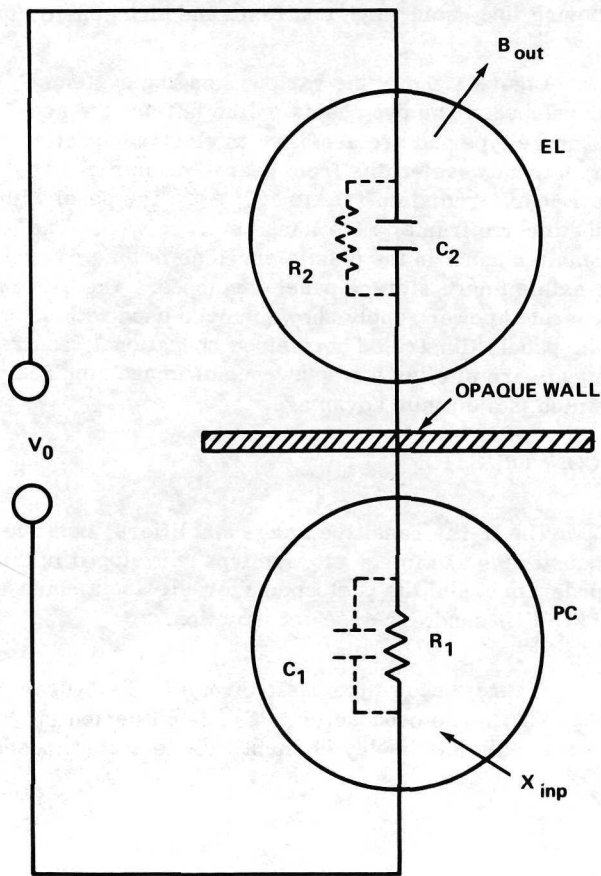


Figure 2. Basic circuit.

(EL) cell. An ac voltage is necessary to obtain high brightness and good efficiency on the EL layer. When the PC layer is exposed to an irradiation pattern, the same electric field pattern is created on the EL layer, giving a visible image.

The first condition for an acceptable image amplifier is that the brightness of the EL element be very low when the input light intensity is zero. To achieve this, the impedance of the PC element should be much higher than that of the EL element. This requires not only a high dark resistance of the photoconductor, but a high capacitance ratio of the EL to the PC element; i.e.,  $C_{EL}/C_{PC} > 1$ . Since the voltage is divided between the EL and PC elements as the impedance ratio, the EL element will have a low voltage and consequently a very low light output in this case.

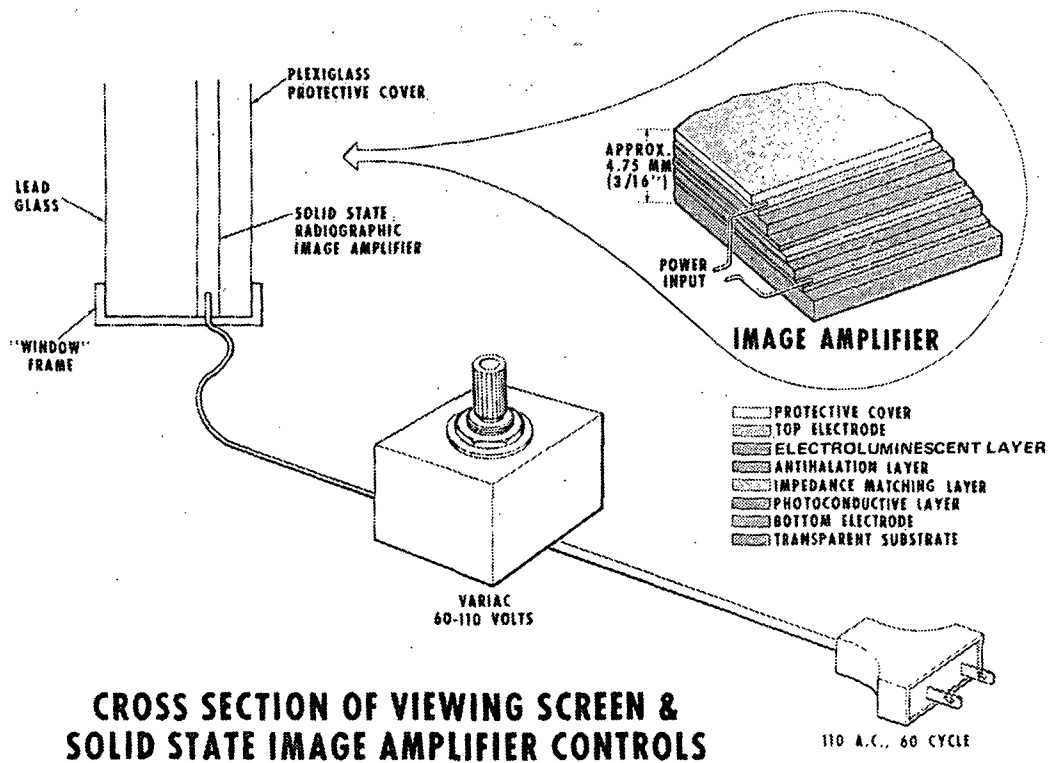
When the PC element is irradiated, its resistance decreases, the voltage across the EL element increases, and the output light is increased. If the PC cell is sensitive to the light emitted by the EL cell, a positive feedback is present that can give increased light output or that results in a bistable device, if the gain at the emitted wavelength is high enough. In this case the output light stays on after the input radiation is switched off; thus, this phenomenon enables one to make storage displays. Without special construction, however, the light feedback can cause lateral spreading and resolution loss. An

opaque film placed between the PC and EL elements eliminates this feedback effect.

When the optoelectronic characteristics of the PC and EL cells are properly chosen, the light output is higher than the radiation input within a given intensity region and light intensification is achieved. By building a two-dimensional mosaic array of such PC-EL pairs, an image amplifier can be constructed. Also, continuous thin layers of the PC and EL materials sandwiched between two electrodes should, in principle, give an image amplifier that works well. The first patents described just this construction. However, it was difficult to satisfy the requirement of the high capacitance ratio of the EL to the PC layer. Luminous gain in the order of unity was the highest obtained with this sandwich-type construction. The problem was caused by the fact that for a high enough capacitance ratio, a thick PC layer was required and such a layer in volume conduction (through the thickness) had low light sensitivity because the light was absorbed in a very thin layer on the surface. Recently high dielectric plastic materials became available for the embedment of the EL powder, thus luminous gains in excess of  $10^{-2}$  lamberts (10 foot-lamberts) were achieved in the sandwich construction at

Westinghouse. The continuous layer sandwich-type construction is the simple way to fabricate solid-state image amplifiers. Figure 3 shows construction details of such a practical working panel of the nonstorage image type; image retention panels are of the same general layered construction, but they require fewer layers and use a different PC material. Construction of the two types of panels is discussed in the following.

Nonstorage Image Panels (Fluoroscope-Type Radiographic Amplifier Screens). The nonstorage image panel PC layer is deposited on a glass plate coated with tin oxide (SnO), and is a cadmium selenide/cadmium sulfide (CdSe/CdS) mixture doped with copper and applied by a settling and sintering operation. Its thickness may be between 100 and 150  $\mu\text{m}$  (4 to 6 mils). The intermediate, vacuum-deposited, semiconductive film of CdSe has a higher donor concentration than that of the contacted PC layer, thereby offering an ohmic contact. Consequently, electron injection and high gain can be obtained in the PC layer. The sprayed opaque antihalation layer prevents light feedback; however, this layer is not needed if the PC layer has low response to the EL light (as is the case with the image storage panel). The conductivities of



**CROSS SECTION OF VIEWING SCREEN & SOLID STATE IMAGE AMPLIFIER CONTROLS**

Figure 3. Image amplifier panel construction.

both the semiconductive and the opaque films must not be excessive to prevent spreading of the current in a lateral direction. The sprayed EL layer is zinc sulfide (ZnS), embedded in a high dielectric constant plastic. An evaporated lead oxide-gold (PbO-Au) film serves as one of the electrodes of the panel, and then a protective cover of glass is applied. The SnO coating is the other electrode. Total panel thickness is approximately 4.7 mm (0.187 in.). The panel can be obtained commercially in sizes from 7.5 cm x 7.5 cm (3 in. x 3 in.) to 25 cm x 25 cm (10 in. x 10 in.) with a lead glass radiation plate bonded on, if desired, for immediate installation in the X-ray cabinet viewing system.

**Image Storage Panels (Radiographic Storage Screens).** The image storage panels are similar in construction to the nonstorage image panels, except that the EL layer of ZnS is first spray-deposited on the SnO-coated glass plate. No intermediate antihalation or impedance-matching layers are required. The PC layer of X-ray sensitive zinc oxide (ZnO) is then bladed on top of the EL layer. An evaporated PbO-Au film applied to the dried PC layer serves as one of the electrodes of the panel; the SnO electrode serves double duty as a resistive heater for the image erasing circuit. A gap between the protective cover glass and the last layer of the PbO-Au film is provided for air circulation during the erasing cycle of heating and cooling. Total panel thickness is approximately 6.4 mm (0.250 in.). The panel can be obtained commercially in sizes from 7.5 cm x 7.5 cm (3 in. x 3 in.) to 20 cm x 25 cm (8 in. x 10 in.).

Since the construction of the storage radiographic amplifier screen requires no high temperature processing, it is possible, in principle, to fabricate a flexible storage panel in the same construction as that of the nonflexible type by substituting sheet plastic for the glass substrate. A prototype flexible storage panel was fabricated and delivered but was not optimized for applications because of program limitations.

**OPERATIONAL CHARACTERISTICS AND SYSTEM DESCRIPTION**

**Nonstorage Panels [4].** This radiographic image amplifier panel is similar to a fluoroscopic screen. There is no image storage on these panels; when the exciting radiation source is turned off, the image disappears within 1 sec. As shown in Figure 4, the light output from the panel is brighter under a wide range of operating conditions than that of the

conventional fluoroscopic screen used under identical conditions. The high contrast achievable (up to  $\gamma = 6$ ) from these panels compared to the standard fluoroscopic screens ( $\gamma = 1$ ) makes these devices ideal for detection of small foreign objects or flaws and results in high-definition images. The reasonably fast response time of the imaging panel makes it useful in production-line testing where higher resolution and greater image sharpness than are achievable with standard fluoroscopic screens are required, and where cost and time delay make film radiography undesirable. Permanent records, if needed, can be made by using a camera or a TV camera with video tape.

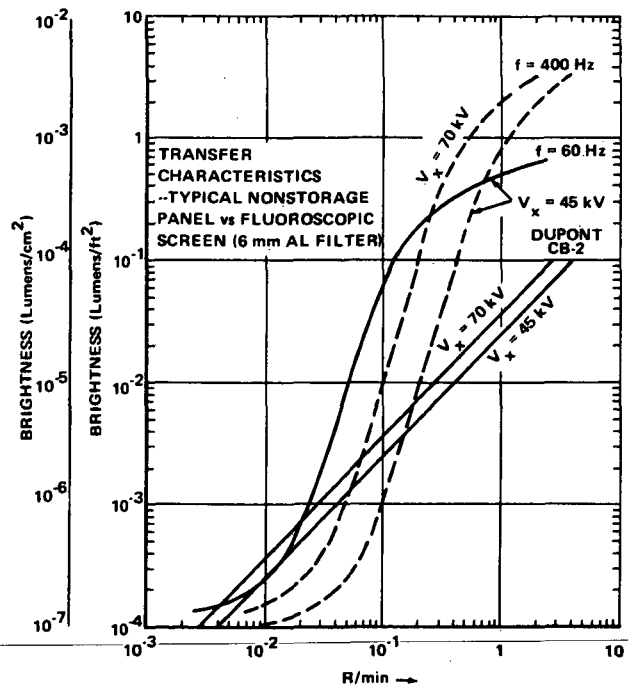


Figure 4. Transfer characteristics comparison — fluoroscope versus nonstorage panel display.

Such a panel, as all other PC-EL types, can be used as an image amplifier in the visible waveband if the PC material is sensitive in this region. CdS and CdSe are sensitive PC materials in the visible, near infrared, and X-ray regions; consequently, the image amplifiers using these materials are infrared converters and radiographic amplifiers also. Features of this system are as follows:

- X-ray to visible image converter.

- Replacement for fluoroscopic screen or X-ray (image) intensifier tube offering:

- Three times higher resolution (6 line pairs/mm or 300 TV lines/in. ).

- Two to six times higher contrast (2 to 6  $\gamma$ , depending on driving voltage).

- Ten to fifty times higher brightness than that of fluoroscopic screen (Dupont CB-2).

- Radiographic quality level of 8 percent of thickness resolution in a 6.3-mm (0.25-in.) aluminum plate.

- Flat, lightweight, solid-state construction, and easy to operate.

- Power supply may be of simple construction; i.e., 100- to 200-V adjustable output at 60 Hz with a current of approximately 0.155 mA/cm<sup>2</sup> (1 mA/in.<sup>2</sup>) required.

- Can be obtained commercially in sizes from 7.5 cm  $\times$  7.5 cm (3 in.  $\times$  3 in.) to 25 cm  $\times$  25 cm (10 in.  $\times$  10 in. ).

- Minimum detectable radiation is 20 mR/min at 70 keV.

- Image decay time is 1 sec or less.

- Lifetime of panel to half-brightness output is 100 to 1000 hr depending on driving frequency.

- Complete system would consist of imaging panel, power supply, continuous X- or gamma-radiation source, and radiation-proof viewing cabinet with lead glass.

(Note: The glass substrate of the panel is not flexible and must be handled with care to avoid breakage.)

Image Storage Panels [5]. This radiographic image amplifier with image storage capabilities was designed for use primarily in nondestructive testing applications as a reusable replacement for expensive X-ray film. Permanent records may be obtained conveniently by photographing the panel image with a camera or by using a TV camera with video tape.

Figure 5 shows exposure time versus aluminum thickness for this type of panel, holding panel and X-ray operating parameters constant.

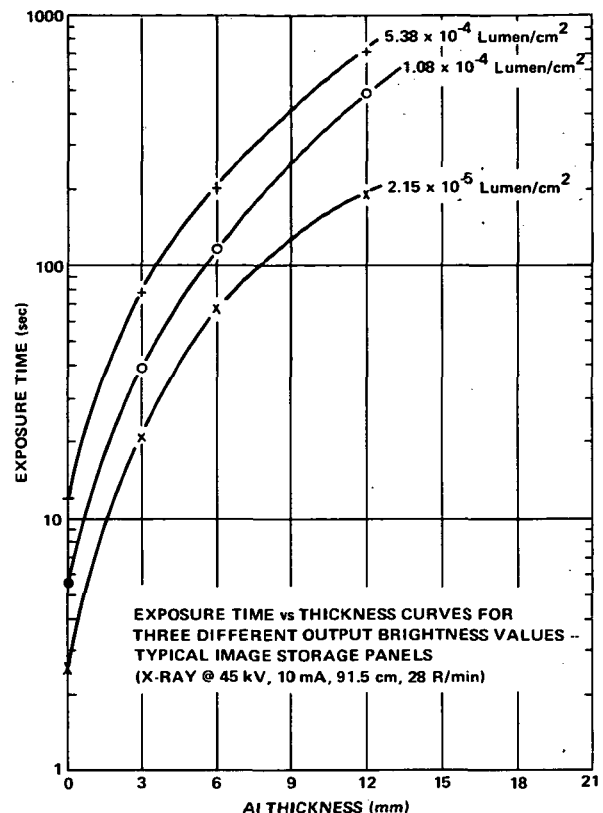


Figure 5. Exposure time versus aluminum thickness for image storage panel display.

Upon exposure, the radiographic image can immediately be seen without processing. A continuously displayed image can be stored with little deterioration for 10 to 60 min, depending on the characteristics of the various layers within the panel.

The X-ray sensitive ZnO has very low sensitivity for visible light, which is convenient when working with these panels. Also, there is no need to apply an electric field to the panel during exposure. The panel is energized only if one wants to see the image.

It should be noted here that "storage time" refers to the total time the panel is energized for viewing. When the panel has been exposed but not energized, it will hold the image for many hours without any appreciable reduction in brightness, resolution, and contrast when the viewing period begins.

The stored image can be erased by heating the panel with an oven or heat lamp to about 100° C (212° F) for 2 to 30 min, depending on the storage capability (panels with short storage need shorter baking). Erasure time is an inconvenience in ZnO storage panels. A fast way of erasing the image was found by heating electrically (approximately 5 min at 50 V) the SnO electrode of the panel. In practice, using 2 or 3 panels successively, no delay would result from the slow erasure.

Features of this system are as follows:

- X-ray to visible image converter.
- Reusable replacement for X-ray photographic film.
- Stores a visible image up to 60 min and a high contrast image for at least 10 min.
- Requires no processing after exposure to view the image.
- Simple to fabricate and is inexpensive.
- Radiographic quality level of 2-2T, per MIL-STD-453.
- Flat, lightweight, solid state construction, and easy to operate.
- Can be obtained commercially in sizes from 7.5 cm × 7.5 cm (3 in. × 3 in.) to 20 cm × 25 cm (8 in. × 10 in.).
- Power supply may be of simple construction; i. e., 200 to 300 V adjustable output at 60 cycles with a current of approximately  $32 \mu\text{A}/\text{cm}^2$  ( $200 \mu\text{A}/\text{in.}^2$ ) required. A panel image-erasing circuit is required that may be 50 to 100 V, dc or ac, 60 cycle. An audible timer with automatic circuit cutoff is preferred for the required erasure time of 4 to 5 min.
- Minimum detectable radiation is 0.1 R at 70 kV.
- Resolution is 6 to 8 line pairs/mm (300 to 400 TV lines/in.).
- Contrast is 2 to 6  $\gamma$ , depending on driving voltage.
- Panel lifetime is more than 100 hr to half-brightness output.

- Complete system would consist of the image panel, power supply, and pulsed or continuous radiation source. The system weighs less than 13.61 kg (30 lb) and will fit in a small suitcase.

(NOTE: The glass substrate of the panel is not flexible and must be handled with care to avoid breakage.)

Table 1 presents a comparison of imaging systems and characteristics for fluoroscope, X-ray film, and the storage and nonstorage image amplifiers.

#### APPLICATIONS OF SOLID-STATE IMAGING SYSTEMS

##### Current Applications.

**Nonstorage Imaging Panel.** Figure 6 shows a prototype of a radiation-shielded X-ray cabinet with a lead glass viewing window that was modified for use with the nonstorage panels and a continuous X-ray source. This X-ray cabinet has an internal conveyor belt for back-and-forth movement of the object being evaluated in front of the viewing panel.

Figure 7 shows a panel image of the interior of a piece of luggage. This application was developed and demonstrated as an adaptation of aerospace inspection equipment in surveillance of airline baggage for detection of concealed weapons and contraband. Articles such as pistols, toothpaste tubes, wire, electric switches, zippers, and snaps may be clearly seen on the 15 cm × 23 cm (6 in. × 9 in.) panel area.

Figure 8 shows an application to determine the position of an internally erectable ultrasonic beam reflector bar inside a graphite-epoxy prototype Space Shuttle engine actuator strut. This display is composed of four image panels arranged vertically to provide a viewing area of 15 cm × 66 cm (6 in. × 26 in.). The continuous source X-ray system operated at 90 kV, 5 mA during viewing sessions.

**Image Storage Panel.** Figure 9 shows another type of radiation-shielded X-ray cabinet. This is a recently procured laboratory evaluation system with wide range kilovolt and milliampere capabilities for thorough evaluation of all image amplifier capabilities. It has both continuous-duty fluoroscopic capabilities (for up to 5-min observation) and pulsed X-ray (variable time exposure) capabilities for nonstorage image and image storage panels, respectively. The lead glass viewing window is installed in the top;

TABLE 1. COMPARISON OF X-RAY IMAGING SYSTEMS

System Characteristic	Fluoroscope	X-Ray Film	Image Amplifier (Nonstorage)	Image Amplifier (Storage)
Resolution (Detail Definition)	1.6 Line Pairs/mm (80 Lines/in.)	8 Line Pairs/mm (400 Lines/in.)	6 Line Pairs/mm (300 Lines/in.)	6 to 8 Line Pairs/mm (300 to 400 Lines/in.)
Penetrameter Sensitivity (MIL-STD-453)	7 to 13 percent	1 percent or Less (1-1T)	8 percent	2 percent (2-2T)
Typical Input Radiation Required 6-mm Aluminum Specimen	6 R/min (Approximate)	6 to 8 R/min (Approximate)	1 R/min	28 R/min
Image Storage	No	Yes	No	Yes
Image Brightness	Very Dim, Approximately $10^{-4}$ lamberts (0.1 ft-L)	High, Variable with Illuminator	Medium, Self-Illuminated, $10^{-4}$ to $10^{-2}$ lamberts (0.1 to 10 ft-L), De- pending on Panel Frequency and Voltage	
Dark Adaptation Required	Yes, 20 min	No, But Dim Room Helpful	No, But Dim Room Helpful	
Contrast ( $\gamma$ , Input Energy Versus Out- put Brightness)	1 (Fixed)	2.5 (Typical Film Density, Fixed)	2 to 6 (Adjustable Output Brightness by Voltage Variation)	
Lifetime	Indefinite	Indefinite	Greater than 100 hr Activation to Half-Brightness Output	
Cost	High	Low But Continual	Low	

thus, the development of the image on the storage panel can be directly observed and correlated with amount and time of X-ray exposure.

Figure 10 illustrates a recent application in the evaluation of electrical connectors utilized on the in-house Stratoscope program. Note the clarity with which the internal pins and wires are shown on this panel. This panel exposure required 200 mA, 80 kV, and 12 sec.

#### Other Possible Applications (X-Ray and Light Sensitive).

##### Nonstorage Imaging Panel.

- Improved fluoroscopy for NDT or medical applications.
- Evaluations in the field using an isotope radiation source and a portable radiation shield.

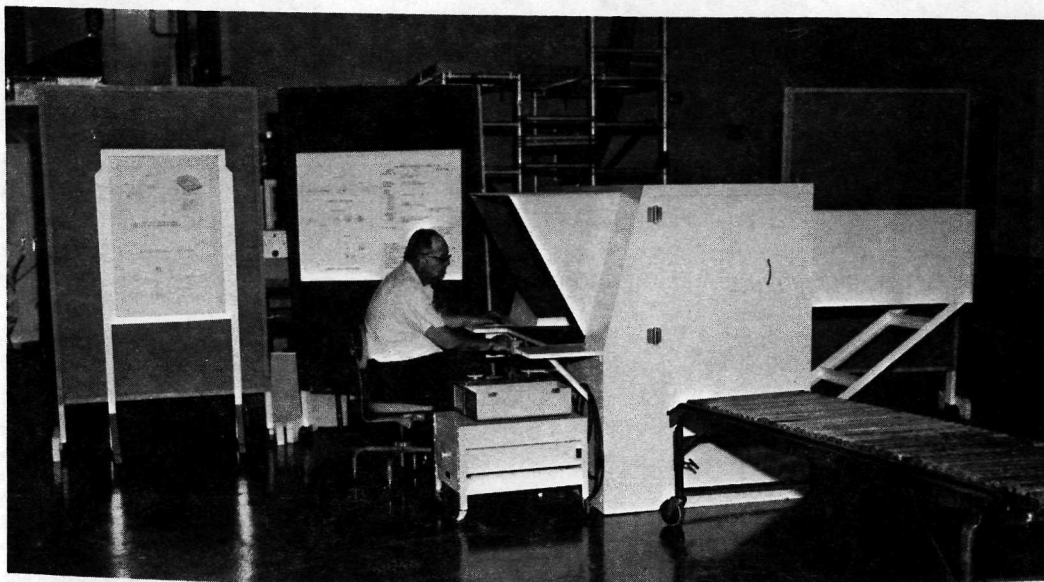


Figure 6. Modified X-ray cabinet for use with nonstorage panel system.

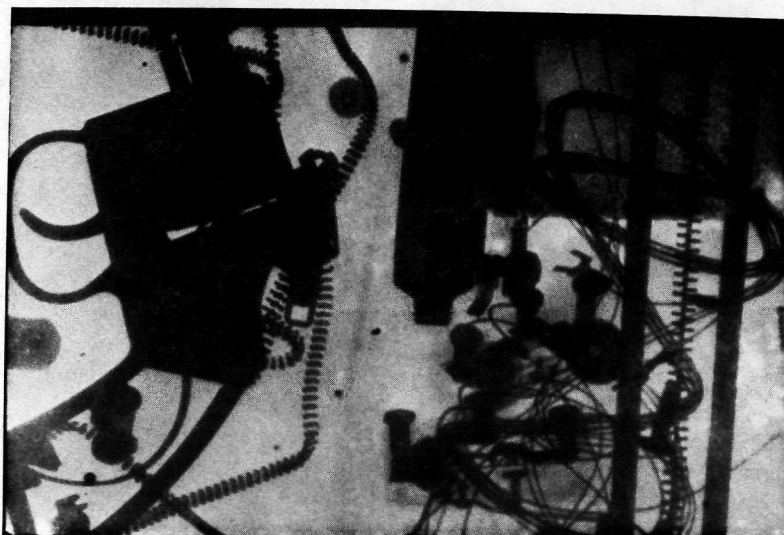


Figure 7. Nonstorage panel image of luggage interior.

- Use in hazardous terrestrial, oceanographic, and space environments.

- Back-lighted projection screens.

- Light amplifier for data displays — increased brightness.

Image Storage Panel (X-Ray and Light Sensitive).

- Evaluations in the field, NDT or medical, using a pulsed, cold-cathode, battery-operated X-ray source. The total system weighs less than 13.61 kg (30 lb) and is portable in a small suitcase.

- Use in hazardous terrestrial, oceanographic, and space environments.

The extent of these applications depends largely on the characteristics, availability, and price of the panels. Since their fabrication is quite simple, especially the storage panels, the price consideration appears to be very favorable, and fabrication of these panels in quantity will be started in the near future. Several nonstorage type radiographic amplifiers have already been sold.

## Conclusions

When required, a suitable solid-state X-ray imaging system may be developed for applications in a space environment. The original problems of expendable film storage, film development, and evaluation in the space environment no longer apply, based on characteristics of the solid-state X-ray image amplifier systems developed.

Solid-state imaging panels with storage capabilities have been delivered that meet contractual requirements of fine grain, high sensitivity, and the radiographic quality level (2-2T) per MIL-STD-453; i.e., resolving a 2-percent penetrometer minimum thickness of 0.12 mm (0.005 in.), and a hole diameter of 0.5 mm (0.020 in.) in a 6.3 mm (0.25 in.) thick aluminum plate.

Solid-state image nonretention panels of the fluoroscopic type still do not have the capability to meet MIL-STD-453 radiographic quality levels. The best attainable resolution delivered to date is about 8 percent, or 0.5 mm (0.020 in.) thickness, and a

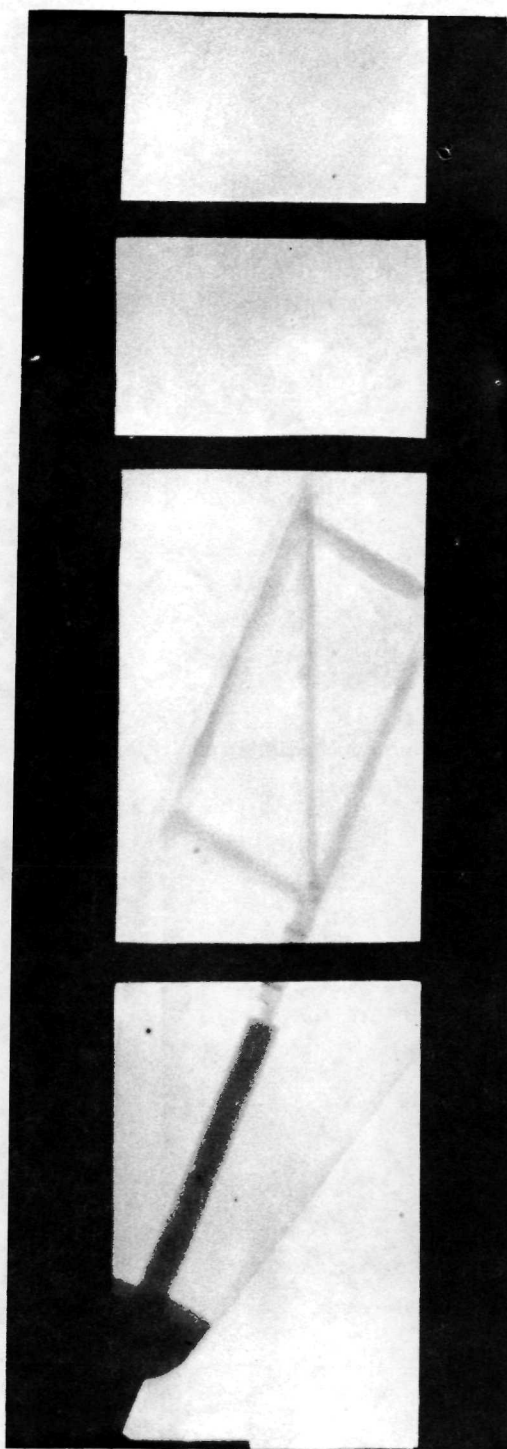


Figure 8. Nonstorage panel image of internal fixture in graphite/epoxy strut.



Figure 9. Laboratory X-ray cabinet with wide-range radiographic application capabilities.

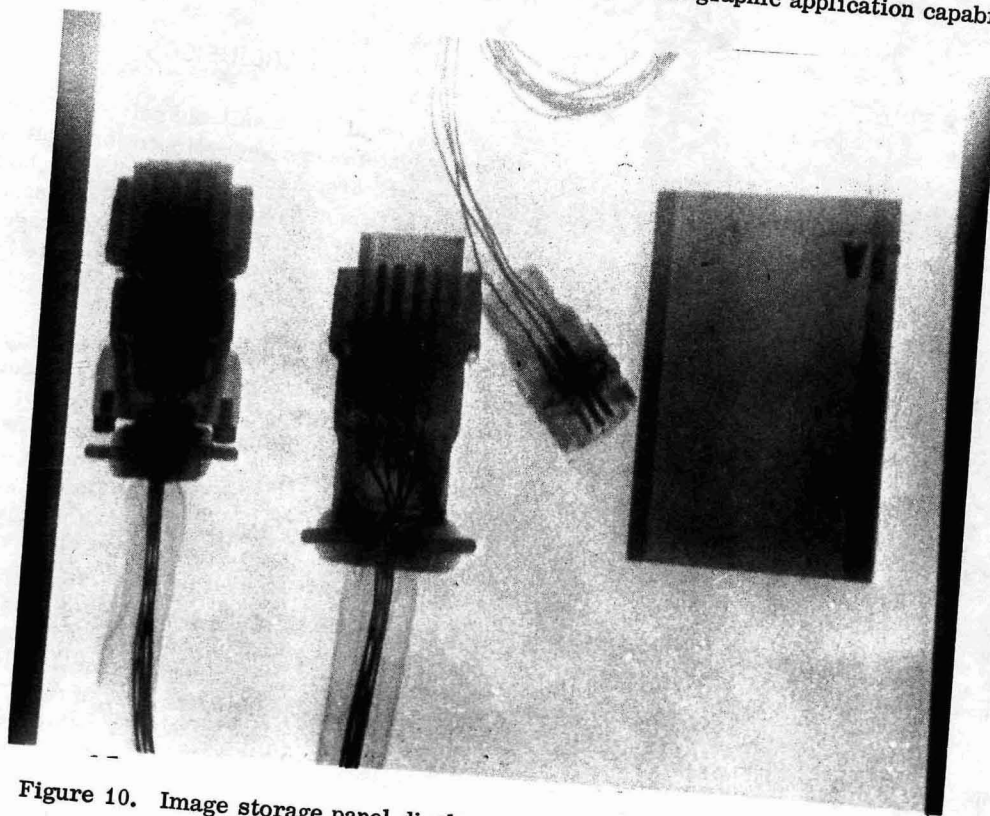


Figure 10. Image storage panel display of stratoscope electrical connections.

1-mm (0.040-in. hole) in a 6 mm (0.25 in.) thick aluminum plate. This still meets the best fluorescent screen definition. Contractual work is proceeding to improve panel resolution to meet MIL-STD-453 requirements.

All panels are fabricated on a glass substrate, are not flexible, and must be handled with care. This, at present, is the biggest limitation to applications.

Flexible image storage panels, both light and X-ray sensitive, can be built based on prototype results. Additional funding will be required to refine processes and to fabricate.

## Future Activities

Future activities include the following:

1. A thorough in-house evaluation of panel characteristics for optimum utilization with radiographic equipment and aerospace materials to be encountered will be conducted.
2. Image retention and image nonretention panels will be combined with in-house built power supplies and issued as complete imaging systems for production and receiving inspection evaluation and implementation (already begun).
3. Further development of flexible image amplifier panels may be pursued.
4. The use of nonstorage image panels in the modified X-ray cabinet available for production evaluations will be implemented.

## NEUTRON RADIATION IMAGING SYSTEM

### Discussion

#### DEVELOPMENT OF N-RAY FOR SPACE VEHICLE COMPONENTS

Radiography, whether X-ray or neutron, works by generally similar methods. This always involves a radiation source, a detector, and the object that is to be examined (Fig. 11). The object is placed between the source and the detector so that radiation from the source penetrates the object and forms an image on the detector, which is usually film. This image has variations because of changes in the

object's density or thickness; this information can be very useful in determining conditions inside the radiographed object.

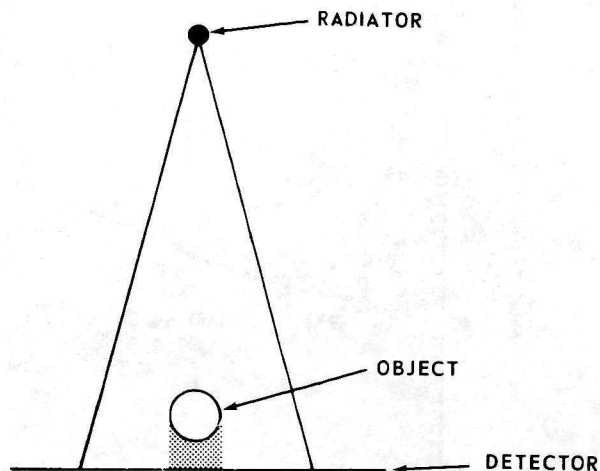


Figure 11. Schematic of radiographic system.

X-radiography dates to before 1900, but neutron radiography is much more recent. Theory had predicted the neutron, which is a single electron bound to a single proton; and the theoretical properties and behavior of the neutron were already well known when the first neutrons were isolated in 1932, thus confirming the existence of the particle.

These properties — high mass, zero electrical charge, and very small size compared even to atomic dimensions — were enough to assure interest in the "new" particle. It had been theorized that the neutron would penetrate ordinary matter with ease.

Neutron radiography offers results that cannot be duplicated by X-ray. Figure 12, which compares X-ray opacity with neutron opacity (mass attenuation), shows the basis of these advantages. The solid line shows the orderly way that X-ray opacity increases with atomic weight. Between hydrogen, the lightest element, and uranium, the heaviest element, there is about a 15:1 increase in the X-ray opacity (mass attenuation) coefficient [6].

The neutron opacity pattern, or rather the lack of a pattern, defies all theory. No one has ever been able to explain the disorder in the neutron opacity of the elements. Hydrogen is extremely opaque to neutrons, and uranium is transparent.

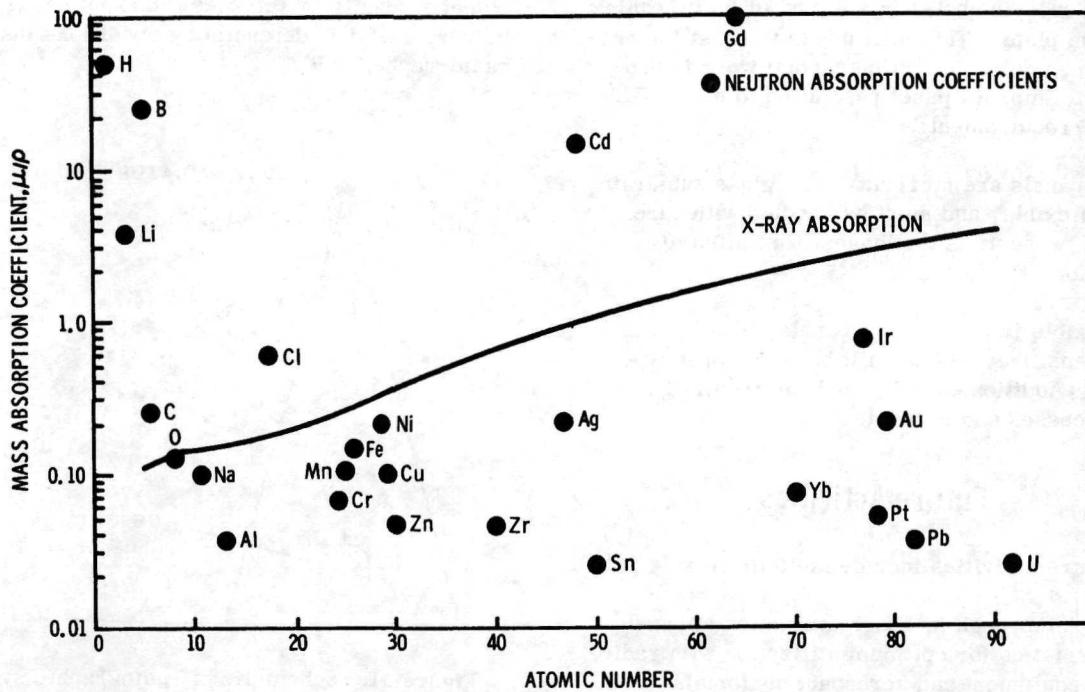
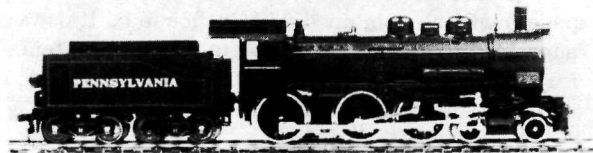


Figure 12. Absorption of neutrons and X-radiation by the elements.

Nondestructive testing exploits the favorable characteristics of neutron radiography that are lacking in X-radiography; e. g. , the high hydrogen content of organic materials such as explosives, rubber, plastics, and oils make these materials much more opaque to neutrons than most of the metals such as lead, steel, or aluminum, so that organic materials can be neutron-radiographed clearly through thick sections of these common metals.

Figure 13 shows a good example of the different results obtained with X-radiography and neutron radiography [7]. The top view is a photograph, the middle view is an X-radiograph, and the bottom is a neutron radiograph of an HO model locomotive.

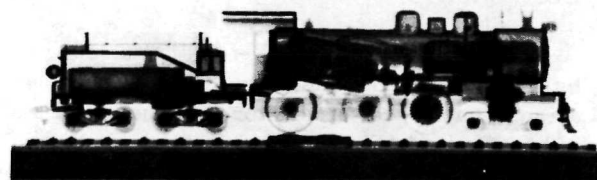
Significant differences are easily seen between the X-ray and neutron radiograph. The plastic casing of the model is almost invisible in the X-ray, and its metal parts blank silhouettes without detail. The neutron radiograph gives a very different pattern in which the housing and many parts, such as the organic fiber gears, are shown in considerable detail, a condition that could not be seen with X-radiography. Results such as this graphically illustrate the results obtainable in inspecting a wide range of devices by neutron radiography.



PHOTOGRAPH  
HO SCALE LOCOMOTIVE



X-RADIOGRAPH



NEUTROGRAPH

Figure 13. Comparison of N-ray versus X-ray radiographs.

In spite of the knowledge of the superior results obtainable by proper use of neutron radiography, the high cost of the process led to a general neglect of the possibilities until about 1960, when the space program's demand for ultrahigh reliability led to a rapid expansion made possible by the high neutron flux levels generated by atomic piles.

Possible sources for neutrons include accelerators, generators, atomic piles, and isotopes. All of the early work in neutron radiography was done with cyclotron generators, but machines big enough to produce adequate neutron flux for neutron radiography were scarce and were used for more important work. During the late thirties, linear accelerators were developed, but these are still of limited usefulness because of low output and the inefficiencies of conventional film radiographic methods and the radioactive foil sheet-to-film transfer processes. The Van de Graaff electrostatic generator, also invented in the thirties, can, in the modern version, reach ten times the flux of an accelerator, but its output is still considered of borderline usefulness since atomic piles can easily generate neutron flux at rates many times higher than are possible with a Van de Graaff generator. Most commercially available isotope neutron sources have flux levels that are too low to be seriously considered in production radiography, although it seems certain that isotope Californium 252 (available in experimental quantities now) will become increasingly important [8, 9]. It has good neutron flux levels, is moderate in cost, and, with the development of better imaging systems, will make neutron radiography portable.

#### PLANNED MSFC N-RAY SYSTEM

The in-house effort at MSFC is being carried out jointly by the Astronautics and Quality and Reliability Assurance Laboratories. The Astronautics Laboratory is furnishing an upgraded Van de Graaff accelerator that has been converted to generate neutrons, and a facility. The Quality and Reliability Assurance Laboratory will furnish a unique closed circuit television system that is designed to work in the low, available, neutron-flux characteristic of generators. This facility (Fig. 14) is to be jointly operated by both laboratories and is to be available to both.

The prior availability of a facility and generator at MSFC has, of course, influenced the direction in which work was initiated to establish a facility for neutron radiography. As mentioned earlier, the

Van de Graaff generator is the best available neutron generator but is too low in total flux to be a satisfactory production device with existing techniques. A considerable effort to improve imaging systems was justifiable on the basis of very evident cost benefits in being able to use the existing facility and Van de Graaff generator, taking advantage of recent developments in electronic imaging devices and incorporating them into a new class, closed-circuit, television viewing system for neutron radiography.

#### OPERATIONAL CHARACTERISTICS OF THE TV DIRECT VIEWING SYSTEM

Design of this system centered about the unique ability of a newly developed television camera tube, the "secondary electron conduction" (SEC) vidicon, to integrate in very dim light for long times to produce a daylight-quality single frame of television when scanned. This ability is analogous to using time exposures with a camera to gather light for a good image when the light is poor, with the exception that the SEC vidicon is about a thousand times as sensitive as photographic film.

An analysis of the proposed system was made which showed that performance should be high enough to make the Van de Graaff generator an adequate neutron source for high speed repetitive neutron radiography, the only limitations being in the television system's ability to reproduce an image.

Since design of the neutron viewing television system is unusual, Figure 15 aids in understanding its functions and the philosophy behind its design.

Neutrons from a Van de Graaff generator are exactly the same as neutrons from an atomic pile, except that the generator will not produce, by several orders of magnitude, as many neutrons as a pile.

After slowing or "moderating" the flux to useful levels and collimating to a reasonably parallel beam, the original flux has been decreased by several orders of magnitude. When shooting this beam through a specimen to radiograph, it loses more neutrons, so that very few indeed are left to form images.

Since the neutron is a particle, each just like all others, each neutron can be regarded as a "bit", their uneven distribution against an even background forming the neutron image. The problem is to accumulate enough "bits" to form an acceptable image. This, in most cases, will require about 10 000 000 neutrons. The system starts with a scintillator,

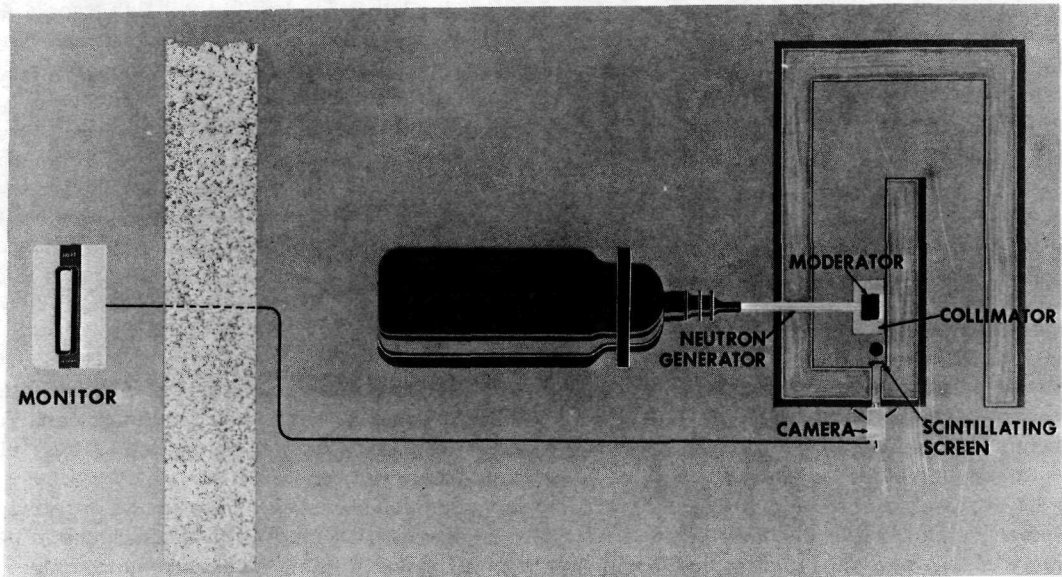


Figure 14. Van de Graaff accelerator and neutron viewing system.

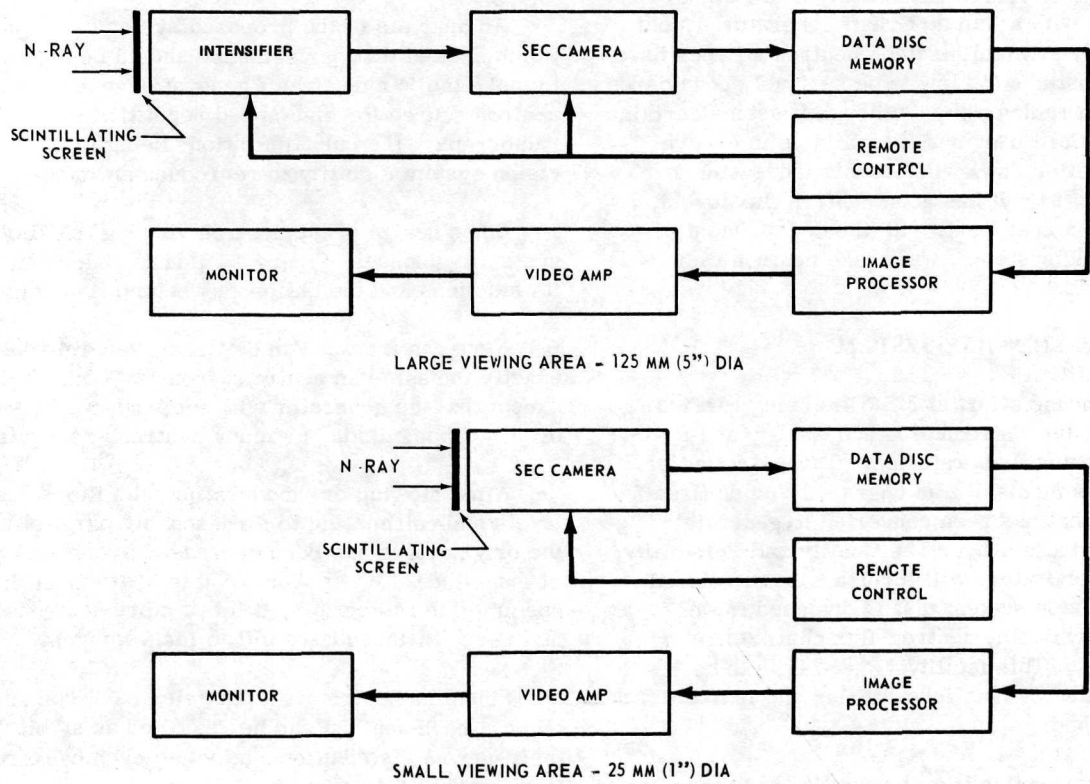


Figure 15. TV direct-viewing N-ray system block diagram.

which is made of material that emits a speck of light when it stops a neutron. It is thin, so that light scattered sideways in the scintillator will not degrade the image. The system's small-area, high-resolution camera can image a 25 mm (1 in.) diameter circle on such a scintillator with 0.05 mm (0.002 in.) resolution, which is near the limiting value resolution that can be displayed by a 12 line pairs/mm (600 lines/in.) television system.

Large area viewing, 125 mm (5 in.) diameter, 0.5 mm (0.020 in.) resolution, is through a neutron image-intensifier tube. This tube is optically coupled into a second SEC camera; if desired, cameras can be quickly interchanged to vary image magnification and resolution. The efficiency of these front ends is high, and the gain is enough to make each intercepted neutron visible.

After an image is accumulated, the tube is scanned, a single image is generated, and the stored image is destroyed. The single frame is stored in the "Data Disc" magnetic memory and can be replayed for observation, study, and processing in a continuous display when desired [10].

Many of the functions of image enhancement can be carried out in the image processor. Grey levels can be shifted toward black or white, and the contrast can be expanded or compressed for clarity of imaging, a feature already known to offer much help in interpretation.

The output image is on a standard 40-cm (16-in.) black and white monitor. It is, of course, possible to photograph the monitor for records.

Design values indicate that the MSFC Van de Graaff generator will produce sufficient neutron flux for viewing system operation at near its peak performance; less than 5 min exposure will be required to assure that the limiting factor in detail viewing will be the limitations of the 12 line pairs/mm (600 lines/in.) television system.

The viewing system has been thoroughly tested at the Juggernaut Pile at Argonne National Laboratory. These tests were considered positive proof that design goals can be met or surpassed.

Present scheduling calls for the facility to be complete with the generator and viewing system operational by November 1971. A training and familiarization period will be required to reach operational status. This will lead into scheduled

use in feasibility studies and research by March 1972 on a routine day-to-day basis. It is anticipated that this work will be primarily visual.

A camera will be used to make a permanent record by photographing the monitor when discontinuities or other features of interest are found. It is expected that the short exposures of less than 5 min required for a delivered visual readout will be a considerable advantage when compared with the long time periods (up to 24 hr) for conventional neutron radiography.

Table 2 provides a good comparison of the various neutron radiation imaging systems and their operational characteristics.

#### APPLICATIONS OF THE N-RAY IMAGING SYSTEM

Neutron radiograph applications to space hardware were investigated by the Manned Spacecraft Center (MSC) at least as early as 1964. This was primarily for inspection of ordnance devices, which are explosives encased in steel or lead. These cannot be nondestructively tested by X-ray because the explosive cannot be seen in X-radiographs. Figure 16 is a neutron radiograph of several such items and illustrates the visibility of the explosive [7]. It is apparent that one device is not properly filled with the explosive charge. Records indicate that, historically, about 10 percent of ordnance is found to be defective to some extent [6].

By 1967, MSC had developed sufficient confidence in the process to require neutron radiography of all Apollo ordnance, over two hundred items, and had issued specifications to make this a mandatory requirement [11].

At MSFC neutron radiography was carefully watched as it emerged as a visual inspection tool. Work was initiated in 1966 with the ultimate intent of providing at least a minimum neutron radiographic facility at MSFC.

At the present time, Quality and Reliability Assurance Laboratory and Astronautics Laboratory agree on the value of neutron radiography, and the Program Management Office proposes to utilize neutron radiographic inspection on the remaining items of Saturn V ordnance and on all ordnance to be used on future programs.

The earlier discussion on the nature of neutron opacity should lead, and is intended to lead, to the

TABLE 2. COMPARISON OF N-RAY IMAGING SYSTEMS

System Characteristics	Direct Film Method (Gadolinium Converter Foil Between Two Films)	Indirect or Transfer Method (Indium Foil to Film)	Direct Viewing Remote TV Monitor With SEC Vidicon Camera	Comments	
Resolution Obtained (Detail Definition)	0.025-mm (0.001-in.) Spot Visible	0.025-mm (0.001-in.) Spot Visible	0.05-mm (0.002-in.) Spot Visible - Smaller Linear Object Visible	Resolution With Minimum Listed Flux	
Time Required	24 hr	24 hr	15 min	Based on Minimum Flux Listed, Direct View Can Use Lower	
Neutron Radiation Flux Required for Suitable Image (N/cm <sup>2</sup> -sec)	10 <sup>6</sup> N/cm <sup>2</sup> -sec, Collimated and Moderated	10 <sup>6</sup> N/cm <sup>2</sup> -sec Collimated and Moderated	10 <sup>5</sup> N/cm <sup>2</sup> -sec Collimated and Moderated	1 to 5 percent Efficiency With Film Methods, 30 percent plus With Direct Viewing	
Compatible With Sources				Source Cost	
				Initial	Yearly
	1. Accelerator	No, Too Costly	No	Yes	1. 40K 16K
	2. Generator	No, Too Costly	Too Slow	Yes	2. 100K 16K
	3. Atomic Pile	Yes	Yes	Yes	3. 500K 100K
4. Isotope (Californium 252)	Yes	Yes	Yes	4. 50K 5K	
System Costs				Procurement and Installation	
1. Initial	Low	Low	High	Assuming Large Number of Production Items Evaluated	
2. Yearly	Continual Costs, High	Continual Costs, High	Parts and Maintenance, Low		
System Complexity	Low	Low	Complex Electronics, High		

idea of neutron radiography as a widely useful NDT method. MSFC's first application will be on explosive devices, but many other applications are possible and a few are in production use. The following applications have been shown feasible [9]:

1. Inspection of ordnance hardware.
2. Detection of, or the lack of, oil in bearings.
3. Detection of hydrogen contamination in titanium welds.
4. Inspection of adhesive in bonded structures for porosity and filleting conditions.
5. Radiography of heavy sections of structural metals.

6. Detection of borated steel.

7. General failure analyses - valves, electronics, etc., having organic parts such as O-rings and gaskets.

Studies have already been made of a gamma-ray sensing version of the imaging system and its possible adaptation to "tracer" medicine, where it has been shown to have both higher resolution and higher sensitivity than existing "tracer" medical imaging systems. The image is displayed in a conventional serial television format that is very suitable for computer manipulation and processing, all of which indicates high value in this and other areas of the medical field [10].

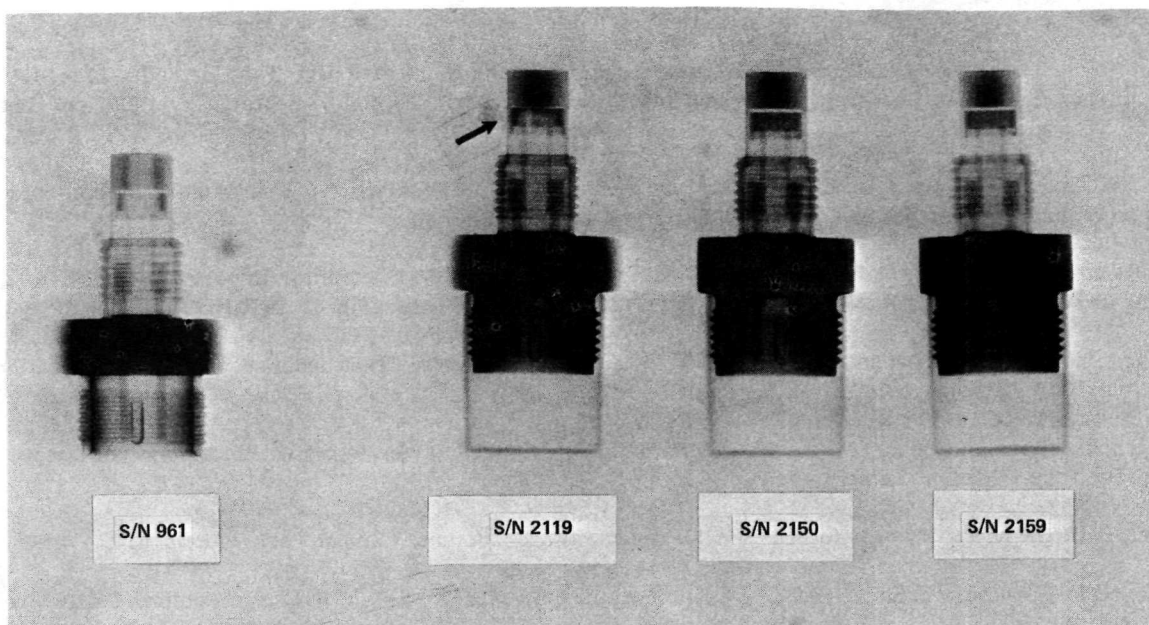


Figure 16. Typical application of neutron radiography: explosive squib evaluation.

The various applications discussed above are just a sampling; the entire area of neutron radiography is still in the development stage and is rapidly growing. We can be sure that it will continue to grow into more important roles as portable isotope radiation sources and improved solid-state imaging systems are developed.

### Conclusions

The MSFC Van de Graaff generator, when operational, will produce sufficient neutron flux for peak-performance use of the direct viewing system. Crude imaging was obtained in March 1971 at MSFC. (See the following topic, Future Activities.) The imaging system was thoroughly tested and accepted at Juggernaut Pile, Argonne National Laboratory, before shipment to MSFC [10].

Inspection of ordnance, failure analyses, and nondestructive testing of space hardware, as described herein, can be accomplished by this equipment when a suitable neutron flux is obtained. Real-time neutron imaging, short-time neutron radiography (from a video monitor screen), storage playback, and enhancement of recorded information will be accomplished also.

### Future Activities

Future activities in the area of neutron radiography include the following:

1. The neutron radiation imaging system and facility is scheduled to become operational by November 1971, and implementation is planned by March 1972. The primary work remaining consists of Van de Graaff equipment modification and the proper moderation and collimation adjustments of the resulting neutron flux.
2. Experimental quantities of Californium 252 isotope will be received at MSFC in the near future. It is anticipated that evaluation of the imaging system with this portable neutron source will be undertaken.
3. Neutron activation analysis for detection of trace elements will be considered for this system. The high sensitivity of the imaging system to neutron flux makes this analysis application highly feasible.

## REFERENCES

1. Brown, Robert L.: Potential Biomedical Applications of Saturn Nondestructive Test Methods. *Journal of the Assoc. for the Advancement of Medical Instrumentation*, vol. 3, no. 5, September, 1969, pp. 154-161.
2. Zoran, W. A.: Nondestructive Testing For Space Application -- Feasibility & Preliminary Design Study. Hamilton Standard, Contract No. NAS8-20630, Final Report, November, 1967.
3. Szepesi, Dr. Z.: Solid State Radiographic Image Amplifiers. NASA Contractor Report CR-61328, Westinghouse Electric Corp., Contract No. NAS8-21206 (Part B), November, 1969.
4. Radiographic Amplifier Screen. Westinghouse Data Sheet WX-31661, Westinghouse Electric Corporation, Electronic Tube Division, Elmira, N. Y., April, 1971.
5. Radiographic Storage Screen. Westinghouse Data Sheet WX-31980, Westinghouse Electric Corporation, Electronic Tube Division, Elmira, N. Y.
6. Neutron Radiography. Atomics International Presentation Document, Canoga Park, California, 1969.
7. Neutrography Service. General Electric Co. Brochure GEA-8311A, 5M (2-69), Pleasanton, California.
8. Californium -- 252, Its Use & Market Potential. AEC Brochure, U. S. Atomic Energy Commission, Aiken, S. Carolina, May, 1969.
9. Ray, J. W.: Neutron Radiography -- A Solution in Search of Problems. *Research/Development*, July, 1969, pp. 18-24.
10. Brown, Robert L.: Television System for Neutron Radiography Using Small Sources. *American Nuclear Society Proceedings*, December, 1969.
11. Neutron Radiographic Inspection of Apollo Ordnance. North American Rockwell Corp. Specification MA0222-0003, September, 1967.

## BIBLIOGRAPHY

Beal, James B.: Space -- for All. Presentation at Southern Illinois University, April 1971.

Gerrard, Martha: Uses of Neutron Radiography --- A Literature Review. Report ORNL-IIC-16, Isotopes Information Center, Oak Ridge National Laboratory, Oak Ridge, Tennessee, January, 1969.

Improved Radiographic Image Amplifier Panel. NASA Technical Brief 68-10363.

Szepesi, A.; Novice, M.; and Keeton, T.: Solid State Radiographic Image Amplifiers. Westinghouse Report on Part A of Contract No. NAS8-21206, May 1968.

Szepesi, Z; and Novice, M.: Solid-State Radiographic Amplifiers & Infra-red Converters. *Advances in Electronics & Electron Physics*, vol. 28, pp. 1087-1098.

# ADVANCED MATERIALS INSPECTION TECHNIQUES

By

M. C. McIlwain

## SUMMARY

The Space Shuttle program has introduced two new materials that have had little previous application in space vehicle structures. These materials, coated refractory metals and filamentary composites, present new and somewhat unique inspection problems that must be addressed. In-house and contractual efforts aimed at solving these problems are discussed herein.

## INTRODUCTION

Stringent mission performance requirements have been imposed upon the Space Shuttle. Two specific materials are being investigated to assist in meeting these requirements: (1) refractory metals, to meet the high temperatures that the Shuttle thermal protection system must withstand during reentry; and (2) filamentary composites, to meet the need for high-strength, lightweight material to minimize gross liftoff weights. This paper discusses the developmental efforts being exerted to ensure that the usefulness of these materials is not compromised by inadequate inspection techniques.

## COATED REFRACTORY METALS

Refractory metals, specifically columbium alloys, are being considered as prime candidates for the Shuttle thermal protection system over areas of the vehicle where temperatures will exceed  $1100^{\circ}\text{C}$ . At these temperatures, columbium alloys still possess sufficient strength and creep resistance to render adequate service lives. However, these alloys cannot be used unless a protective coating is provided to prevent oxidation. At temperatures above  $425^{\circ}\text{C}$ , these alloys react rapidly with oxygen which results in embrittlement as well as actual loss of the material in the form of an oxide. To prevent this oxidation, a silicide coating is used as a protective layer. This coating is produced by spraying,

or dipping, the precleaned columbium parts with a slurry of elemental silicon and metal powders blended together with a lacquer binder. After the coating has dried, the part is placed in a vacuum furnace where it is fired for 1 hr at approximately  $1375^{\circ}\text{C}$ . At this temperature, the slurry constituents fuse and combine with the base metal to form a complex silicide coating, as shown in Figure 1. The composition of the coating is tailored to each specific alloy to achieve maximum utility. The cracks in this coating (Fig. 1) are characteristic of silicide coatings. They are formed during cooldown of the part after coating and are a result of differences in the thermal expansion characteristics of the coating and the metal substrate. When the part is reheated, the differential expansion of the substrate and coating forces the cracks closed, thus preventing oxidation of the substrate.



Figure 1. Silicide coating with characteristic cracks.

If components fabricated from these coated refractory metals are to be used with confidence, inspection procedures must be evolved which will assure that an adequate coating exists. In fact, not only must inprocess and acceptance type inspections be performed, but techniques must be available to

periodically determine the condition of the part after the Shuttle is placed into service. A survey of the test data available indicated the following variables to be the most important as far as coating reliability is concerned: thickness, homogeneity, and defect content. The initial coating must be thick enough to provide oxidation protection, but not so thick that differential expansion stresses cause spalling of the coating. Segregation of elemental constituents in the slurry can result in areas of improper coating chemistry in the fired coating. These areas of segregation do not possess the required oxidation resistant properties and thus become potential failure sites. The coated refractory metals, as with any material, show a reduced service life when defects are present. The exact nature and significance of defects in the coated refractory metals are not completely defined at this time; however, it is known that mechanical damage or chipping of the coating is detrimental.

Three potential inspection techniques were investigated at MSFC for potential application as in-process/acceptance type techniques (Fig. 2). The Dermatron, an eddy current device, and the Betascope, a beta backscatter instrument, were examined

for measuring thickness of coating, and stimulated emission radiography was used to detect inhomogeneities in the coating chemistry. With the Dermatron, a sinusoidal varying potential is applied across a bridge network where a pencil-like test coil forms one leg of the bridge circuit. When the test coil is placed on a conductive sample, the impedance of the coil is changed, resulting in a bridge unbalance that causes a voltage difference across the bridge. This voltage difference can be measured and empirically related to coating thickness.

The Betascope is used to measure the beta back-scattering characteristics of the material, which can then be related to coating thickness and chemistry. A small isotope source is used to supply beta particles. The particles are directed toward the coated sample where they interact with and are scattered by the atoms of the sample. A certain number of the beta particles are backscattered in the general direction of the source. These particles are counted by a Geiger Mueller Counter. The number of counts recorded is proportional to the average atomic number of the sample. If the coating and base metal chemistry remain essentially constant, the count rate at the detector will be proportional to the coating thickness.

TECHNIQUES EVALUATED

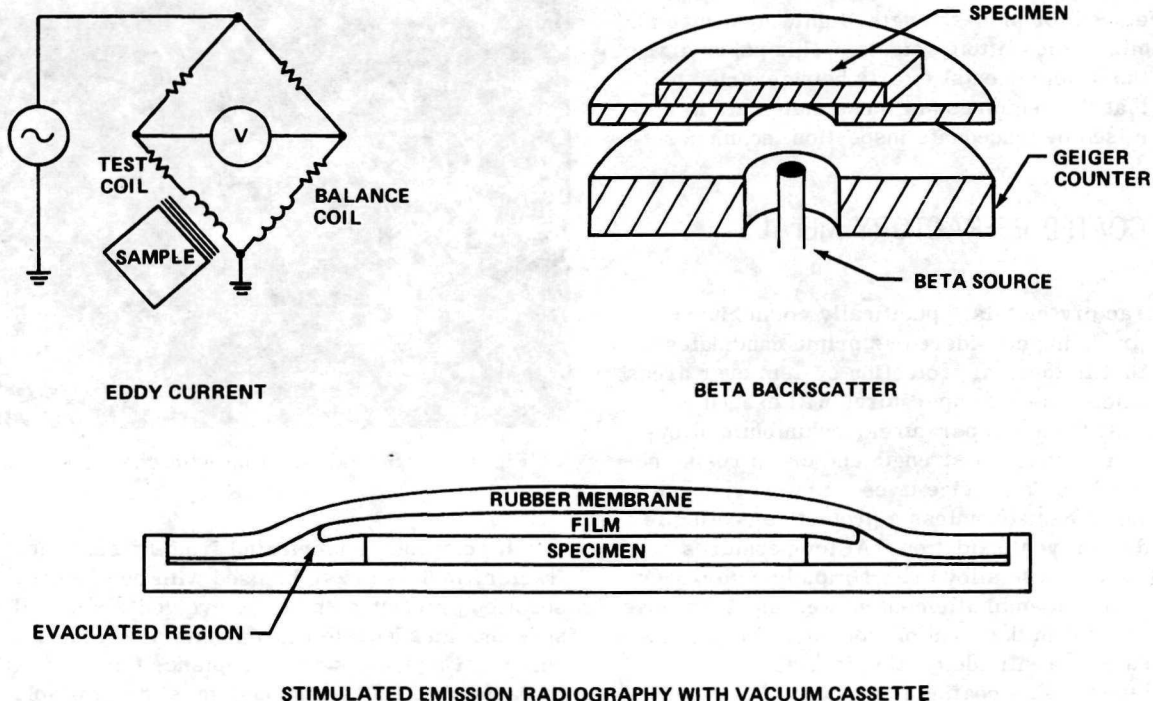


Figure 2. NDE technique schematic for coated refractory metals.

The detection of inhomogeneities in coating chemistry is also based on a radiation method. In stimulated emission radiography, the specimen and film are placed in a vacuum cassette to ensure intimate contact. The film is placed on the source side of the specimen and the setup is irradiated with hard X-rays, 240 to 300 keV. These X-rays interact with the specimen through Compton scattering or through photoelectric ejection, resulting in the ejection of photoelectrons and the emission of characteristic X-radiation of the specimen. Since these emissions are random in direction, a certain number are directed back toward the source where they expose the film. The probability of an X-ray interaction increases as the atomic number of the absorber increases; thus, areas where segregation occurs will appear lighter or darker than the surroundings, depending on whether the segregated area is lower or higher in atomic number than the surroundings.

A calibration curve for the Dermitron developed during MSFC studies [1] is shown in Figure 3. This curve was generated by preparing specimens of varying coating thickness and testing each specimen with the Dermitron. The samples were then metallographically sectioned and measured. A regression analysis of coating thickness versus instrument reading was then performed. The centerline point shown in Figure 3 is the regression line, while the upper and lower lines represent the statistically determined 95-percent confidence limits. Using this approach, thickness measurements to an accuracy of  $\pm 2.5 \times 10^{-3}$  mm can be made. Similar accuracies were attained in experiments with the Betascope, but it was decided to eliminate this instrument as an inspection tool because of its size-related lack of versatility and because of the required stability of the environment in which it must be used. A typical stimulated emission radiograph showing light element segregation in a Vac-Hyd coating is depicted in Figure 4. Since this is a positive print, the segregated area appears darker than the surroundings, rather than lighter as it was in the initial radiograph. An exposure of 60 sec, using operating parameters of 240 kV and 3 mA, was used to produce this radiograph. Note that the segregation shown in the stimulated emission radiograph is not shown in the standard radiograph.

As a result of these studies, it is believed that adequate determinations of whether coated refractory metal parts are prepared to the thickness specified by the designer can be made, and the homogeneity of the coating can be evaluated. Additional work is

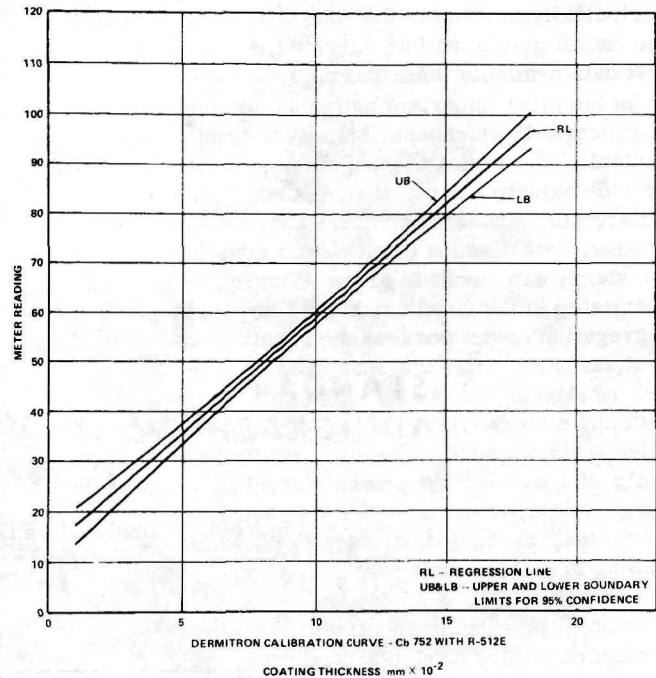


Figure 3. Dermitron calibration curve.

currently being pursued to determine the response of these and other nondestructive evaluation (NDE) techniques to defects in coatings and to subtle changes in the chemistry and structure of the coatings that might occur during service. The project schedule for these efforts is shown in Figure 5.

The evaluation of the phase master will be similar to the work performed with the Dermitron. This instrument, although it is an eddy current instrument, operates on a phase-sensing principle rather than by measuring impedance change. Its operating characteristics make it less sensitive to liftoff and probe angulation errors than the Dermitron. At the completion of this evaluation, studies to define the response characteristics of the eddy current instruments and the radiographic technique to various defects will be conducted. The studies will use samples that were intentionally processed improperly and samples containing mechanically damaged coatings. The response of the various instruments to the defected samples will be recorded. The defected samples will be subjected to destructive analyses to determine the nature and extent of defects present. The destructive and nondestructive data will be correlated to define the sensitivity limits of the inspections.

In the third phase of future efforts, both defected and optimally coated samples will be inspected by the

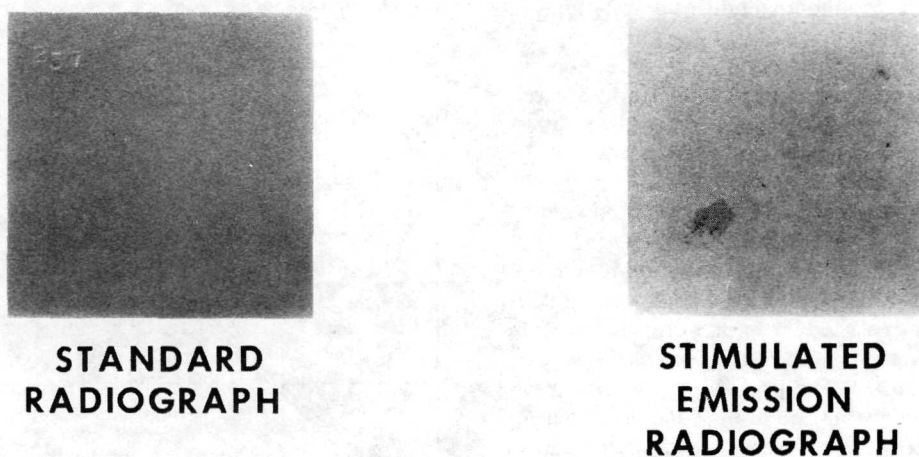


Figure 4. Stimulated emission radiograph.

	CY-71							CY-72						
	MAY	JUN	JUL	AUG	SEPT	OCT	NOV	DEC	JAN	FEB	MAR	APR	MAY	JUN
PHASE MASTER EVALUATION	█													
DEFECT RESPONSE CHARACTERIZATION				█										
PERIODIC INSPECTION DEVELOPMENT							█							

Figure 5. Current program schedule.

NDE techniques used to date. These samples will then be subjected to temperature and pressure profiles that simulate reentry conditions. The samples will be retested periodically using the NDE techniques, and samples will be removed from test for destructive analyses. A correlation of the NDE test with a metallography analysis, a mechanical properties test, and an X-ray diffraction analysis will be performed to evolve an NDE system for condition evaluation.

### FILAMENTARY COMPOSITES

Filamentary composites of boron epoxy and graphite epoxy are currently being designed, fabricated, and tested at MSFC. These composites consist of preferentially directed filaments of boron

or graphite embedded in a matrix of epoxy. Composites of this type combine high-strength, lightweight characteristics with the ease of fabrication of the epoxy matrix. By using materials such as these, tensile strengths in excess of  $1.033 \times 10^6 \text{ N/m}^2$  can be achieved at low densities; however these high strengths can only be achieved if the composite is free from defects.

To aid in understanding the composites, a schematic of the fabrication process used to produce unidirectional flat panels is depicted in Figure 6. As shown in the figure, a "prepreg" tape is wound on a mandrel. The prepreg tape consists of a tape and the fibers of interest, preimpregnated with epoxy. The fibers are aligned with the axis of the tape. Winding of the tape is continued until the desired number of layers or plies has been built up. The mandrel and uncured composite are then placed in a heated press

## METHOD FOR MAKING UNIDIRECTIONAL FLAT PANELS

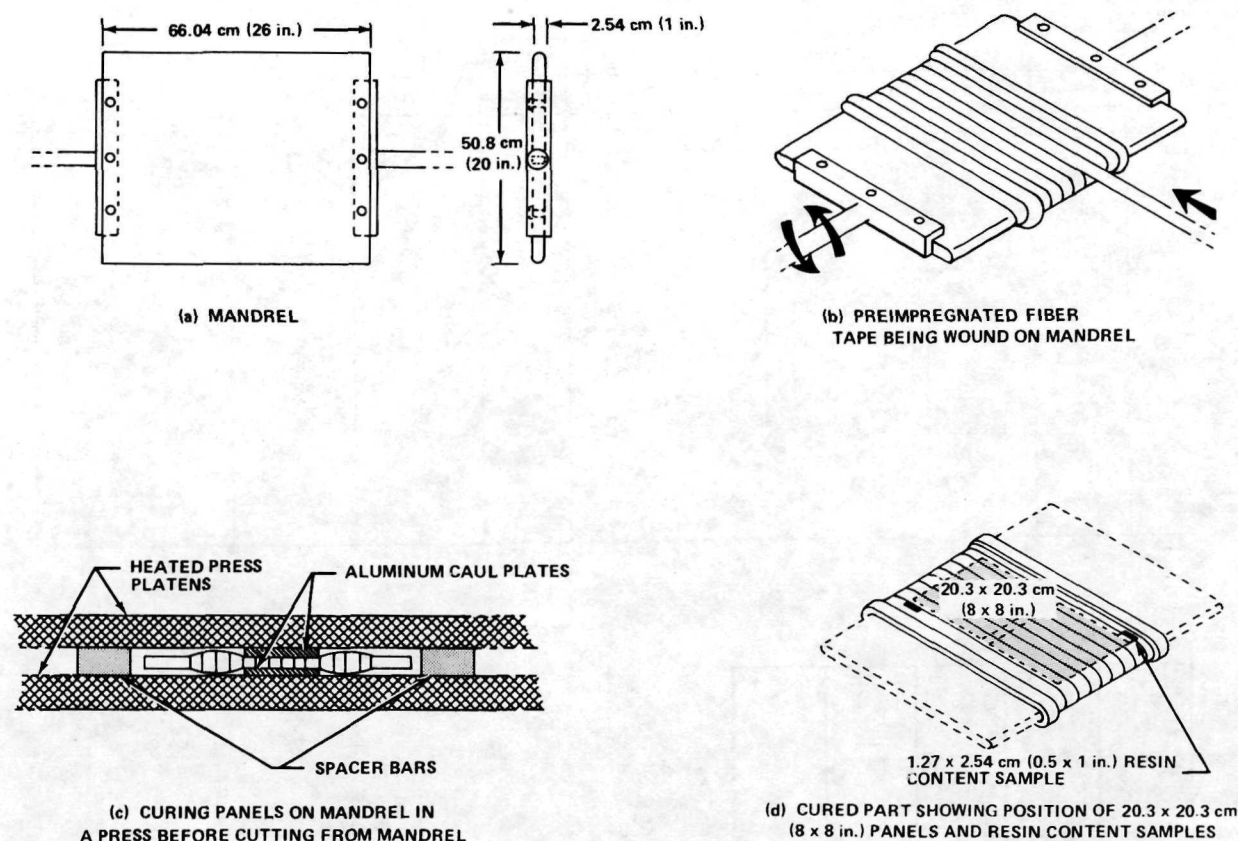


Figure 6. Schematic of composite fabrication.

for compaction and curing of the composite. An alternate technique for the curing cycle is to vacuum-bag the composite and cure it in an autoclave. After curing, the mandrel is removed and the desired shapes are cut from the composite. It can be seen that the process contains many potential sources of defects such as variations in the cure state of the epoxy, delaminations between plies, broken fibers, inclusions, etc.

A survey of current literature and industrial sources was conducted to assess the nondestructive test (NDT) capability in the area of composites. The results of the survey are shown in matrix form in Table 1. As can be seen, very little quantitative data were available. In most cases only the qualitative detectability of a defect was stated, with no lower size limit specified.

In an effort to fill the blanks in this matrix and to generate more quantitative data, a series of standards were prepared [2]. These standards incorporated various sizes and types of defects. A typical panel is illustrated in Figure 7. Each panel had five different section thicknesses and had various defect simulations incorporated at specified locations.

To ensure that the intended defects were incorporated, the vendor was required to perform a preliminary inspection using available techniques. The techniques selected are illustrated in Figure 8. Both ultrasonic techniques use attenuation of the ultrasonic beam as a measure of the integrity of the material. In the pulse-echo technique, a focused beam of ultrasonic energy is directed through the composite onto a reflection plate. The energy is reflected back through the composite to the probe where the signal

TABLE 1. NDT ASSESSMENT MATRIX

NDT ASSESSMENT CAPABILITIES - LAMINATES (BORON EPOXY AND GRAPHITE EPOXY)

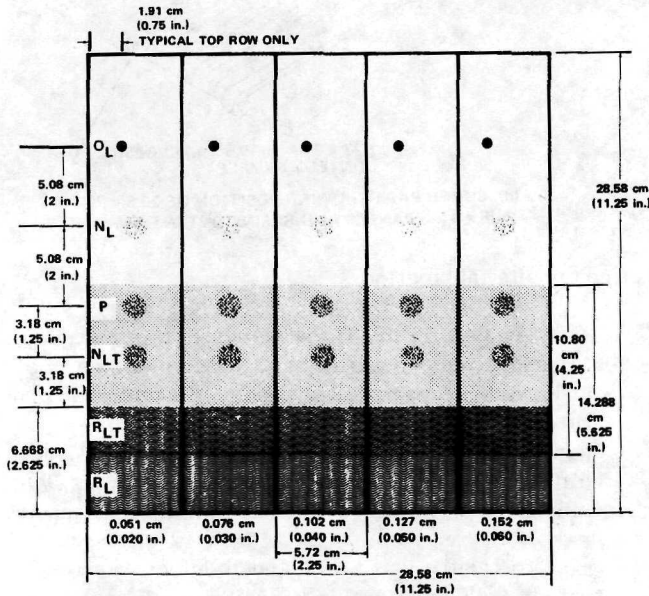
LEGEND

T = Thickness  
D = Diameter

N/A - Not Applicable  
✓ - Can Identify But Quantitative Limits Not Established

X - Can Be Detected, But Difficult To Identify  
? - Unknown

Measures-Detect	Ultrasonics				Thermal		Radiography	
	Impedance	Pulse Echo	Through Emission	Velocity	Infrared	Liquid Crystal	X-Ray	Gamma Radiometric
Density/Porosity Modulus Variations	X	✓	✓	±2.5 percent In T = 0.094 To 0.373 cm (0.037 To 0.147 in.)	✓	✓	X	±2.5 percent In T = 0.094 To 0.373 cm (0.037 To 0.147 in.)
Cure State	?	?	?	✓	?	?	NA	NA
Fiber Spacing And Misalignment	?	?	?	?	?	?	✓ (If Enhanced)	NA
Delamination	X	✓	✓	1.27 cm (0.5 in.) D In T = 0.094 To 0.373 cm (0.037 To 0.147 in.)	✓	✓	NA	NA
Overlap	?	?	?	X	?	?	NA	?
Broken Fibers	?	?	?	?	?	?	✓ (If Enhanced)	NA
Inclusion	X	✓	✓	✓	✓	✓	✓	✓
Filament/Resin Volume Ratios	?	?	?	±2 percent In T = 0.094 - 0.373 cm (0.037 - 0.147 in.)	?	?	NA	±2 percent In T = 0.094 To 0.373 cm (0.037 To 0.147 in.)



PANEL NO.

- LAY UP ONE GRAPHITE-EPOXY LAMINATE, AS SHOWN. CURE.  
525 1a. BOND TITANIUM PANEL TO BACK OF LAMINATE.
- LAY UP ONE BORON-EPOXY LAMINATE, AS SHOWN. CURE.  
526 2a. SAME AS 1a. ABOVE.

N<sub>L</sub> - INTERLAMINAR DISBOND, 1.27 cm (0.5 in.)      N<sub>LT</sub> - WITH TITANIUM.  
 P - DISBOND BETWEEN TITANIUM AND LAMINATE.  
 R<sub>L</sub> - INTERLAMINAR DISBOND, GENERAL.      R<sub>LT</sub> - WITH TITANIUM.  
 O<sub>L</sub> - INTERLAMINAR DISBOND, 0.635 cm (0.25 in.)

Figure 7. Typical standard panel design.

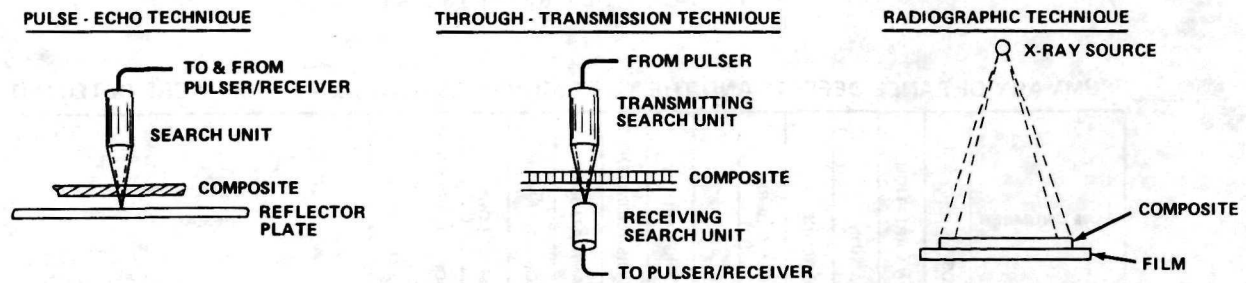


Figure 8. NDT schematic for composites.

originated. The magnitude of the reflected signal is then taken as a measure of the composite integrity. Should a defect such as delamination be present in the material, the ultrasonics beam will be attenuated, resulting in no reflected signal. Through-transmission ultrasonics works on the same basic principle of relating integrity to ultrasonic attenuation. The difference lies in the use of separate transmitter and receiver transducers, and the fact that the ultrasonic beam penetrates the composite only once. The radiographic techniques employed were standard and used low energy X-rays, 35 to 50 keV.

A typical ultrasonic pulse-echo record is shown in Figure 9. The blank areas represent strong attenuation of the ultrasonic beam. These blank areas correlate with locations where inserts were implanted to simulate interlaminar disbonds. The half-moon shaped area represents an insert that was accidentally installed.

A summary of the vendor inspections is shown in Table 2. As can be seen, most of the incorporated defects were detectable. Only the undercured resin condition was completely missed.

Currently, these standards are being used to optimize inspection techniques and to define the limits of detectability for the various techniques. The techniques being studied include those previously discussed as well as infrared scanning and electric field measurements.

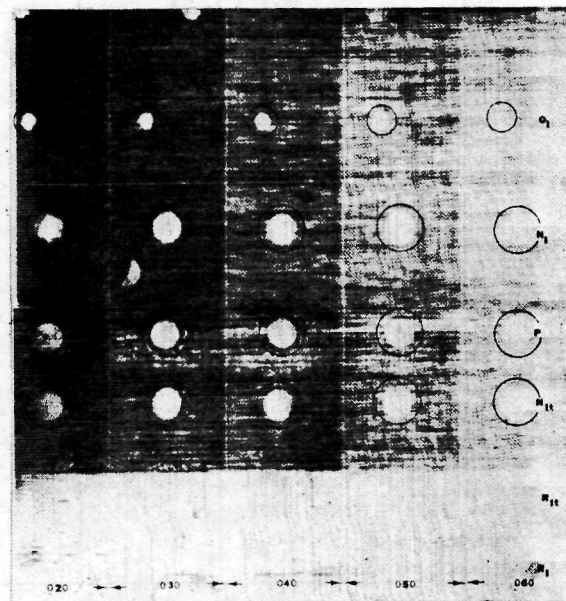


Figure 9. Ultrasonic C-scan of typical standard panel.

At the completion of this program, suitable techniques will be available to handle in-house inspection problems, and a sound experience base will be available from which to evaluate contractor-incurred problems.

TABLE 2. NDT RESULTS MATRIX

## SUMMARY OF PANEL DEFECTS AND THE NDT TECHNIQUES WITH WHICH THEY WERE DETECTED

PANEL NUMBER	POROSITY	RESIN VARIATION	INCLUSION	UNDERCURE	BROKEN FIBERS	OVERLAP	SPACING VOID	BIAS MISALIGNMENT	DELAMINATION	DISBOND-TITANIUM	CRUSHED CORE	DISBOND-HONEYCOMB	PRE-AGED AREA	REMARKS
101 102 103 104 105 106	1 1 1 1 1 1	1 0 0 1 0												EXCEPT IN SUBSTRATED AREAS.
207 208 209 210 211 212			111 1 1 1 1 1	0 0 0 0 0 0										
313 314 315 316 317 318								1 0 0 111 111 11						10° MISALIGNMENT VISIBLE IN 0.051 cm (0.020 in.) STEP  MISALIGNMENT NOT VISIBLE IN THE 0.127 cm (0.050 in.) & 0.152 cm (0.060 in.)
419 420 421 422 423 424					111 0 11 11 0 0	111 11 11 111 11 11	111 11 11 111 11 11							0.635 cm (0.25 in.) SLOT VISIBLE ONLY IN 0.051 cm (0.020 in.)
525 526 527 528  529 530								111 1 111 111  1 1	111 1      		111 111 111 111  111 1 1	111 111 111 111  111 1 0 0		PRE-AGED AREA ONLY SLIGHTLY VISIBLE WITH X-RAY  DELAMINATIONS PARTIALLY REVEALED BY U/S  DELAMINATIONS PARTIALLY REVEALED BY U/S

1 - DETECTED WITH ULTRASONIC C-SCAN TECH.

111 - DETECTED WITH BOTH ULTRASONIC AND X-RAY TECH.

11 - DETECTED WITH X-RAY TECHNIQUE

0 - NOT DETECTED BY EITHER METHOD

## REFERENCES

1. Wages, C. ; and Parks, M. : Evaluation of an Eddy Current and a Beta Backscatter Instrument for Measuring the Thickness of Refractory Coatings. Contract No. NAS8-20081, SPACO, Inc. , Huntsville, Ala.
2. Pless, W. M. ; et al. : Development, Fabrication, Testing, and Delivery of Advanced Filamentary Composite Nondestructive Test Standards. NASA CR-61340, Lockheed-Georgia Co. , Marietta, Ga.

# GASEOUS FLOW DETECTION TECHNIQUES FOR IN-SPACE APPLICATION

By

T. F. Morris

## SUMMARY

To meet the requirement for gaseous flow detection in the environment of space, a flowmeter and a leak detector have been developed. The operation of the flowmeter is based on the orifice-meter measuring system and the flowmeter makes corrections for gas temperature variation internally. The flowmeter is self-contained, portable, and hand-held and is capable of handling hydrogen, helium, nitrogen, oxygen, organic vapors, and other common gases found in flight systems over a flow range of 5 to 9500 standard cubic centimeters per minute (sccm).

The leak detector is basically a hand-held, self-powered ion pressure gauge designed to operate in an ambient pressure of  $133.32 \times 10^{-4} \text{ N/m}^2$  ( $10^{-4}$  torr). Tests in high-vacuum chambers have shown that at a pressure of  $133.32 \times 10^{-5} \text{ N/m}^2$  ( $10^{-5}$  torr), leaks as small as  $1 \times 10^{-7}$  standard cubic centimeters per second (sccs) can be detected. In the space environment, it is expected that leaks in the range of  $1 \times 10^{-9}$  sccs will be detected.

Prototypes of both units have been built and tested. Presently, flight qualification testing is in progress.

## INTRODUCTION

During the past few years, it has become apparent that there is a definite need for the development of gaseous flow detection techniques that are applicable for use in space. Suitable instruments are needed to support orbital inspection and checkout operations of space stations and interplanetary vehicles prior to launch from parking orbits. For damage assessment of any pneumatic system in space, leak detection and flow measurement are essential. The checkout of stages fabricated and assembled in space will surely require flow detection.

Likewise, orbital checkout of engines will include purge measurements and leak checks. To meet these needs, a flowmeter and a leak detector designed specifically for operation in the environment of space have been developed (Figs. 1 and 2).

## FLOWMETER

The flowmeter (Fig. 1) is a rather simple device and its operation is based on the orifice-meter measuring system. It is designed with three main sections: (1) the gas handling and conditioning system, (2) the orificing system, and (3) the pressure measuring system (Fig. 3).

The gas handling and conditioning system receives the flow from a leak or purge port, conducts it through the temperature conditioning chamber to the orifice manifold, and exhausts it to space.

Normally in flow measurements, a correction for variations in temperature is applied to the indicated flow, but in this unit the gas temperature is regulated within certain limits and the flow is read directly. The temperature stabilization chamber is a large heat sink that either warms or cools the gas. Electrical resistance elements supply heat as needed, while a cannister of dodecahydrate of sodium biphosphate absorbs any excessive amount of heat energy in the gas.

This hydrated salt loses its water of crystallization between the temperature of  $360^\circ \text{K}$  ( $92^\circ \text{F}$ ) and  $322^\circ \text{K}$  ( $120^\circ \text{F}$ ), and in the process of becoming a liquid, it absorbs heat from the heat sink, thereby cooling the gas. Since this process is fully reversible, the salt cannister, in conjunction with the thermostatically controlled electrical heaters, effectively regulates the temperature of the gas within the limits of  $297^\circ \text{K}$  ( $75^\circ \text{F}$ ) and  $325^\circ \text{K}$  ( $125^\circ \text{F}$ ).

The orificing system is the heart of the operation of the flowmeter and the principle of operation



Figure 1. Flowmeter for space environment.



Figure 2. Leak detector for space environment.

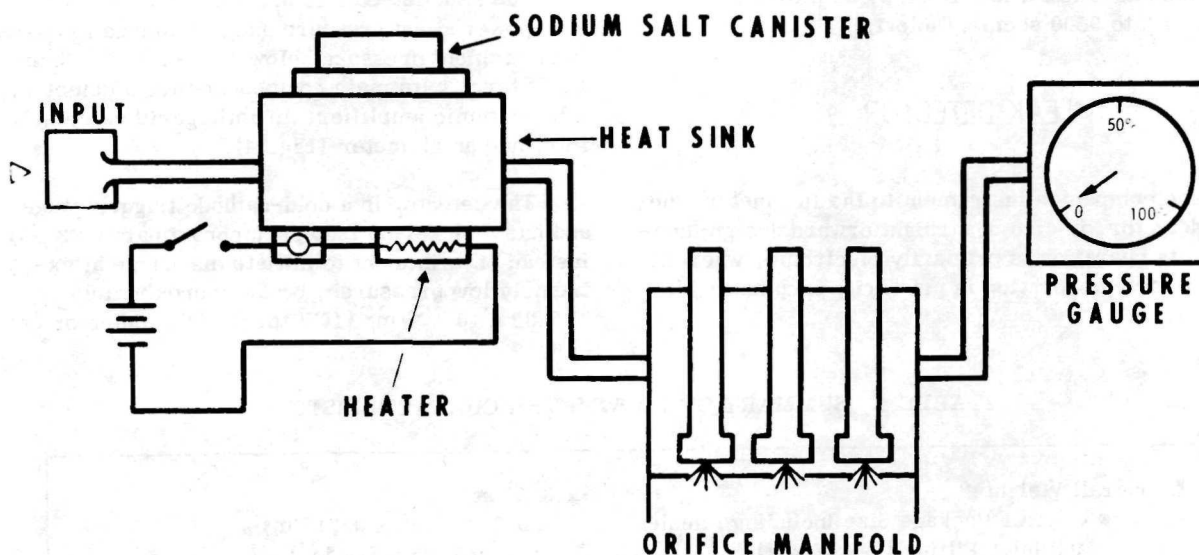


Figure 3. Flowmeter pictorial schematic.

is one of basic simplicity; i. e. , the temperature-conditioned gas is exhausted to space through an orifice.

In this application, the exhaust pressure, which is the vacuum of space, is very low, which virtually assures that the flow orifice is always operating in the supercritical regime where flow through the orifice is directly proportional to the upstream pressure and is dependent on downstream pressure. Thus, a pressure gauge and an orifice can be empirically calibrated to measure the mass flow of a gas directly. This is done by putting known rates of flow through the instrument and noting the indicated pressure.

Experimentation and calculations established that three orifices would be adequate to handle the wide range of flow rates of the various gases commonly found on space systems. The proper orifice for a particular measurement is selected by means of a toggle valve.

The pressure measuring system is the last major part of the flowmeter. It actually senses the flow and gives a numerical display. The main part of this system is the pressure gauge connected to the orifice manifold.

Since the orifices operate in the supercritical regime, it is a straightforward procedure to calibrate the meter for the various gases. The meter

scale can be either marked in percent of full scale with calibration curves used to give actual flowrate or a multiple scale can be used to read flow directly. Both approaches have merit, but the final selection will not be made until the flight specifications are more definable.

Two safety features have been incorporated to protect the instrument. A gauge guard is located in the line connecting the pressure gauge to the orifice manifold, and a pressure relief valve is located on the orifice manifold. The gauge guard is a fast acting valve that isolates the pressure gauge in the event of an overpressure surge or pressure spikes. This prevents the meter from being damaged because of excessive rates-of-change of pressure, even through total pressure may be well within the range of the instrument. The pressure relief valve on the orifice manifold prevents the orifice plates from being damaged by over-pressure. The orifice plates are very thin, approximately 0.05 mm, and are very susceptible to excess pressure. This valve has a relatively large bore and is very effective in preventing damage to the other components of the flowmeter as well as to the orifice plates.

The flowmeter is packaged as a self-contained, portable, hand-held unit. It is to be used by the astronaut during extra-vehicular activity (EVA) to measure the mass flow of gases from purges and leak ports. It is capable of handling hydrogen, helium, nitrogen, oxygen, organic vapors, and other

common gases found in a flight system over a flow range of 5 to 9500 sccm (Table 1).

## LEAK DETECTOR

The companion instrument to the flowmeter, the leak detector, is also of straightforward design; however, its operation is primarily electronic, whereas the flowmeter operation is primarily pneumatic (Fig. 2).

The leak detector is basically a hand-held, self-powered ion pressure gauge designed to operate in an ambient pressure below  $133.32 \times 10^{-4} \text{ N/m}^2$  ( $10^{-4}$  torr). Its main components are a detector, a logarithmic amplifier, an antilogarithmic amplifier, and an ammeter (Fig. 4).

The detector is a cold-cathode trigger gauge and has a nickel-63 isotope (approximately  $63 \mu\text{C}$ ) instead of a filament to initiate discharge at extremely low pressures, below approximately  $133.32 \times 10^{-7} \text{ N/m}^2$  ( $10^{-7}$  torr). The detector

TABLE 1. SUMMARY OF FLOWMETER CHARACTERISTICS

● Overall Weight	3.51 kg (7.75 lb)		
● Overall Package Size Including Handles and Inlet Fitting (L x W x H)	0.317 x 0.235 x 0.216 m (12.5 x 9.25 x 8.5 in.)		
● Battery Specifications	Storage, Sealed Silver Zinc		
● Type	6		
● Number of Cells	9 V		
● Voltage at Full Charge	$7.9 \times 10^4 \text{ J}$ (22 W-hr)		
● Approximate Full Charge Energy Recoverable			
● Heat Sink Specifications	Utilizes Latent Heat of Crystallization of $\text{NaH PO}_4 \cdot 0.12 \text{ H}_2\text{O}$ , Rechargeable		
● Type			
● Temperature Range of Crystallization Phase Change	306° K to 322° K (92° F to 120° F)		
● Ambient Temperature Range	20° K to 500° K (-424° F to 440° F)		
● Maximum Operating Back Pressure to Ensure Flow Metering Accuracy	1.333 pascals ( $10^{-2}$ torr)		
● Orifice Pressure at Full Scale Flow	$49.8 \times 10^2$ pascals (20 in. $\text{H}_2\text{O}$ )		
● Approximate Full Scale Flow at 297° K (75° F) [sccm at 293° K (68° F), $10.13 \times 10^4 \text{ N/m}^2$ (760 torr)]			
	<u>Orifice</u>	<u>1</u>	<u>2</u>
		<u>3</u>	
Hydrogen	9500	850	270
Helium	7000	650	200
Nitrogen	2500	250	75
Oxygen	2400	225	70

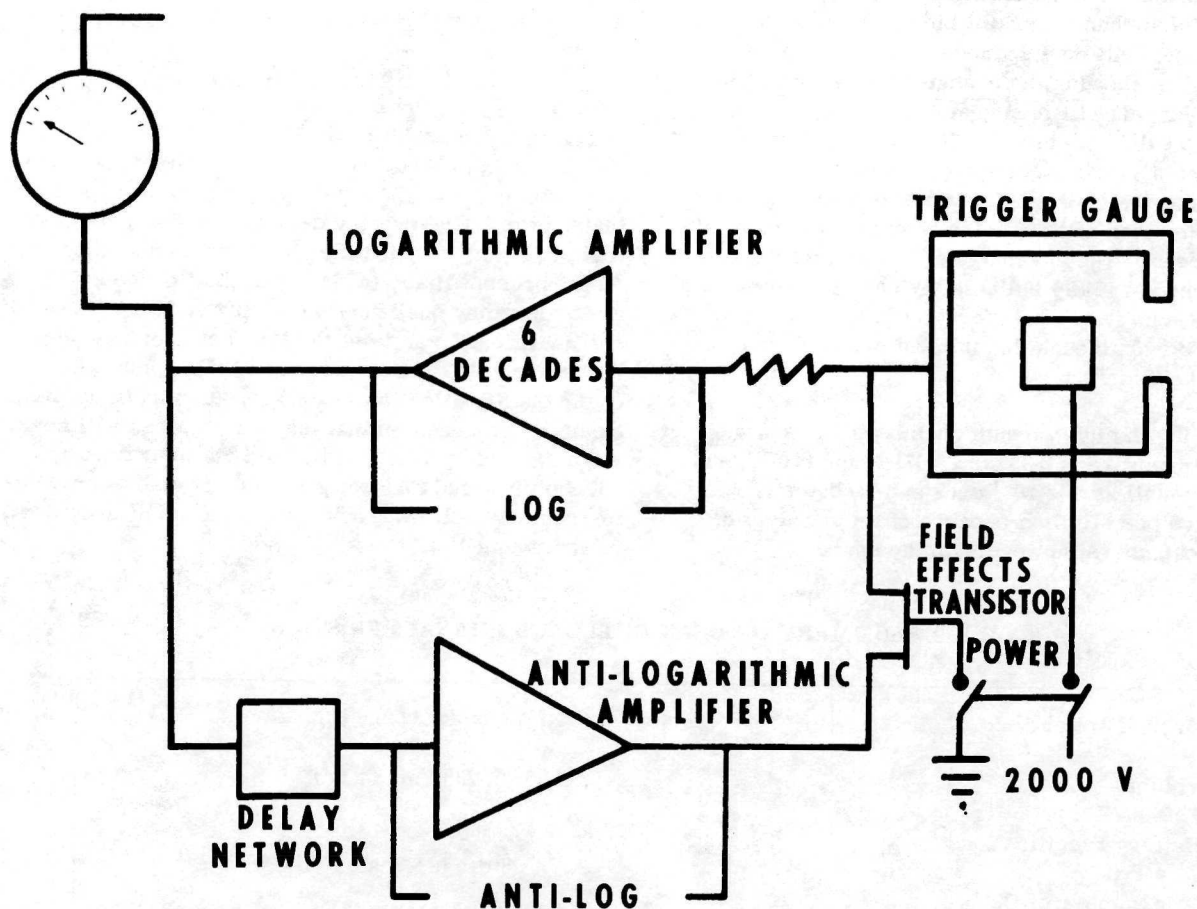


Figure 4. Block diagram of leak detector.

operates in the same manner as other ionization gauges commonly used to measure pressure in high-vacuum systems. Gas molecules enter the gauge, are ionized, and produce a current proportional to the gas pressure at the gauge. In the vacuum of space, as the instrument is brought into proximity to a leak, the number of gas molecules entering the detector increases producing a current proportional to the increase in pressure.

This current is processed by the logarithmic amplifier, where it is amplified and changed from an exponential function to a linear function. The amplifier is designed to cover six orders of magnitude of detector current representing pressures from  $133.32 \times 10^{-4} \text{ N/m}^2$  ( $10^{-4}$  torr) down to  $133.32 \times 10^{-10} \text{ N/m}^2$  ( $10^{-10}$  torr). The linearized current from the log amplifier then drives an ammeter that is calibrated to read pressure.

At this stage, the leak detector continuously measures and displays the ambient pressure. When it is placed near a leak, the change in pressure is sensed and read-out on the meter; however, small leaks in a relatively high ambient pressure [ $133.32 \times 10^{-4} \text{ N/m}^2$  ( $10^{-4}$  torr)] will give very small changes in the meter reading and could be missed very easily. To overcome this, a negative feedback circuit consisting of a delay network and an antilogarithmic amplifier was added.

A portion of the current driving the ammeter is fed back through the delay network to the anti-logarithmic amplifier. Here the linear current function is changed back to an exponential function and supplied to the input of the logarithmic amplifier, where it opposes the current from the trigger gauge. This results in a zero input to the log amplifier, and the meter indicates zero pressure.

This condition remains until the pressure at the trigger gauge changes again; then, the input to the log amplifier will be unbalanced and the meter will deflect, thus showing the change in pressure. The feedback circuit will then again feed back sufficient current to null the meter. Initially, the delay network gives a 10-sec delay before the feedback circuit actuates, but the delay network rapidly becomes saturated and the delay is reduced to approximately 2 sec. The advantage of this is that the instrument is rapidly nulled after each change in pressure, and it will be operating in a more sensitive range even though the ambient pressure may be relatively high.

Testing in high-vacuum chambers has shown that at a pressure of  $133.32 \times 10^{-5} \text{ N/m}^2$  ( $10^{-5}$  torr), leaks as small as  $1 \times 10^{-7}$  sccs can be detected. Tests have been limited because of the capacity of vacuum chambers; however, in the space

environment, it is expected that leaks in the range of  $1 \times 10^{-9}$  sccs will be detected (Table 2).

## CURRENT STATUS

The development of the flowmeter and the leak detector has progressed very satisfactorily through the design, prototype, and test phases. It appears that this is a flightworthy design, and the prototype test programs verified the operational capability. At the present time, two units of the flowmeter are undergoing qualification testing at MSFC, and two qualification units of the leak detector are due for delivery in the next 2 months. On completion of the qualification test program, any modifications, changes, or redesign that may be required will be incorporated. Flight models of both instruments will be procured and two gaseous flow detection instruments will be ready for off-the-shelf use on future manned missions.

TABLE 2. SUMMARY OF LEAK DETECTOR CHARACTERISTICS

● Overall Weight	2.85 kg (6.28 lb)
● Volume	28 200 cm <sup>3</sup> (1 ft <sup>3</sup> )
● Battery Specifications	
● Type	Storage, Sealed Silver Zinc
● Number of Cells	18
● Voltage at Full Charge	28 V
● Approximate Full Charge Energy Recoverable	$24 \times 10^4$ J (66 W-hr)
● Ambient Temperature Range	20°K to 500°K (-424° F to 440° F)
● Maximum Ambient Operating Pressure	$1.333 \times 10^{-2}$ pascals ( $1 \times 10^{-4}$ torr)
● Minimum Leak Detected During Tests	$1 \times 10^{-7}$ sccs @ $1 \times 10^{-5}$ torr
● Minimum Leak Detectable in Space (Projected)	$1 \times 10^{-9}$ sccs

# QUALITY AND RELIABILITY REQUIREMENTS FOR HYBRID MICROCIRCUITS

By

M. J. Berkebile

## SUMMARY

This paper discusses the methods and techniques used for deriving quality and reliability requirements applicable to the fabrication of hybrid microcircuits suitable for space flight application. The hybrid technology has evolved from printed circuit board packaging concepts. Printed circuit boards are being replaced by hybrids because of their size, weight, and cost advantages.

Two basic construction methods are used in the production of hybrids. They differ in the method of deposition and the type of material used in forming the metallized interconnect pattern on the ceramic substrate. Hybrid microcircuits using metallization produced by vacuum deposition are called thin film hybrids, and those produced by the silk screening method are referred to as thick film hybrids. After the formation of the interconnect pattern, thick film and thin film hybrids are completed in a similar fashion. The semiconductor die or chips and the appropriate resistor and capacitor chips are bonded and interconnected to the metallization on the substrate.

To establish high reliability requirements for the hybrid microcircuit technology, off-the-shelf voltage regulator circuits were purchased from four different manufacturers. These regulators were tested in a three-phase test program. Upon receipt of the regulators, their electrical parameters were checked and the devices were X-rayed. Afterwards, electrical testing was continued to determine the failure rates under normal use. Finally, the regulators were overstressed in an attempt to produce failures. A large number of wire-bond and chip-to-substrate interface failures occurred during this test program.

Additional studies were then initiated to investigate beam leads and flip chips in an effort to alleviate the bonding problems that occurred on the voltage regulator circuits. Problems were encountered

during the handling of the beam-leaded devices as a result of the fragile beams being bent and disoriented. The aluminum beam-leaded devices were very difficult to ultrasonically bond to the substrate because appropriate ultrasonic equipment was unavailable. The gold beam-leaded devices appear very promising; however, the test program is still incomplete.

Requirements are being generated for applying hybrid technology to higher frequency areas, such as microwave receivers and transmitters. As the design frequency increases, the substrate material, thickness, and smoothness become critical factors for substrate selection. Thin film circuits will dominate in this application.

Studies are also being conducted to determine the power limitations on hybrids. Again, the substrate material (heat dissipating qualities) is a very important consideration. Beryllium oxide appears to satisfy the heat dissipation requirement. Additionally, a monometallic interconnection system is a very desirable characteristic for power hybrids.

## INTRODUCTION

Hybrids are being used more and more in the home entertainment field, replacing printed circuit (PC) board and discrete electronic packaging concepts. This usage is spilling over into the aerospace and defense areas. The hybrid technology is related to PC board packaging in that a fiberglass epoxy board is populated with discrete parts, such as transistors, diodes, resistors, capacitors, etc. The big difference, of course, is that the parts added to the PC boards are individually complete entities, and those parts added to the hybrid assembly are in chip form. The obvious difference between PC boards and hybrid circuits is size. The uncased devices (chips) used in hybrid circuits are much smaller than the discrete parts used on PC boards. Ceramic substrates for hybrids are also

much smaller than PC boards. This increased density of the hybrid makes it attractive for aerospace usage.

The reliability of the hybrid packaging technology has not been determined to the extent of that of the PC board packaging technology, primarily because of the extensive usage of the PC board. The greatest deterrent to reliability for hybrids today is the inability to electrically test each chip prior to the time it is mounted on the ceramic carrier. With discrete parts and the PC board technology, it is almost routine to check all capacitors, resistors, or semiconductors prior to soldering to a PC board. One of the major advantages of hybrid packaging is the reduced number of electrical interconnections that are necessary to complete any given circuit, interconnections being the major cause of failure with both PC boards and hybrid packaging.

The present hybrid technology is being considered for usage in the higher frequency range, extending into the microwave region. Work is also being done to define requirements for power hybrids. Both extensions of the basic hybrid technology will require new and different processes, materials, screening requirements, and controls in the fabrication of these microcircuits.

### CUSTOM HYBRIDS

Figure 1 indicates the close relationship between the hybrid and the PC board technologies. One can see that they both have a base or carrier. In the hybrid microcircuit a ceramic substrate serves as the carrier, whereas the fiberglass epoxy board provides the carrier for the PC board. The conductor for PC boards is copper, and the hybrid uses

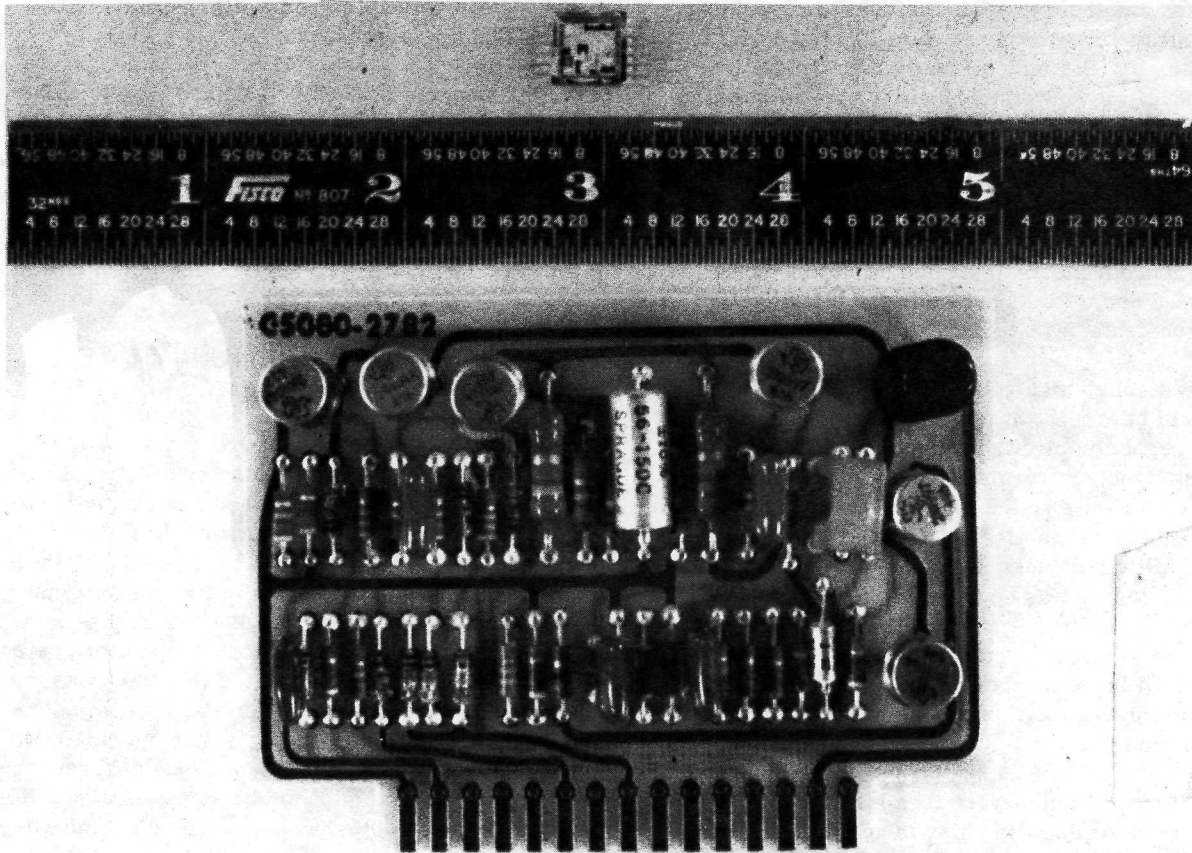


Figure 1. Comparison of printed circuit board and hybrid packaging techniques.

metal film deposition. The interconnect metallization pattern for thin film usually will be a nichrome base with an aluminum overcoat. In the case of the thick film, hybrid metallization probably will be palladium-gold.

Table 1 shows the equivalent circuit elements of a typical hybrid and a PC board. The resistor for the PC board is a standard part, whereas in the hybrid microcircuit a diffused chip, thin or thick film resistor is used. Capacitors are similar to resistors in both cases. Diodes and transistors are standard parts in the PC board packaging, whereas only the chip is used in the hybrids. In the transistor case, about 90 percent of the space is actually wasted since the only active part within that case is the small chip. External electrical connections in the PC board are plug-in types or connected by solder terminals, whereas in the hybrid microcircuit external electrical connections are interconnected like any other discrete part. Figure 2 shows a typical thick film hybrid using a palladium-gold interconnect pattern and resistors made of palladium-silver. Table 2 shows the typical materials used in the production of hybrids.

One of the biggest problems in stipulating the quality and reliability requirements for hybrids is to provide a means for obtaining electrically sound chips. The chip is so small that it is difficult to obtain its electrical characteristics without bonding it to a substrate and providing a means for electrical connection. It is also so small that it is difficult to place bonds and then remove them when it is to be placed in the actual assembly. Work is presently in progress to design a carrier mechanism that would accept chips. In turn, the chips would be electrically connected and heat-sunked for batch testing.

## TEST SPECIMENS

Table 3 presents a detailed description of the test specimens. A total of 100 commercially built voltage regulator circuits were purchased from 4 different manufacturers (25 each). This test was initiated to obtain a cross section of the technology that is used in commercially built hardware to determine what additional quality requirements and

TABLE 1. COMPARISON OF HYBRID MICROCIRCUITS AND PC BOARD CONSTRUCTION

Element	PC Board	Hybrid Microcircuit
Base or Carrier	Copper Clad Fiberglass Epoxy Board	Ceramic Substrate
Conductor Formation	Etch Away Unwanted Copper	Film Deposition
Resistors	Standard Part	Chip, Thin Film or Thick Film
Capacitors	Standard Part	Chip, Thin Film or Thick Film
Coils	Standard Part	Spiral Conductor Pattern
Transistors and Diodes	Standard Part	Transistor and Diode Chips
External Connections	PC Board Plug or Solder Terminals	Package Leads Similar to Standard Parts

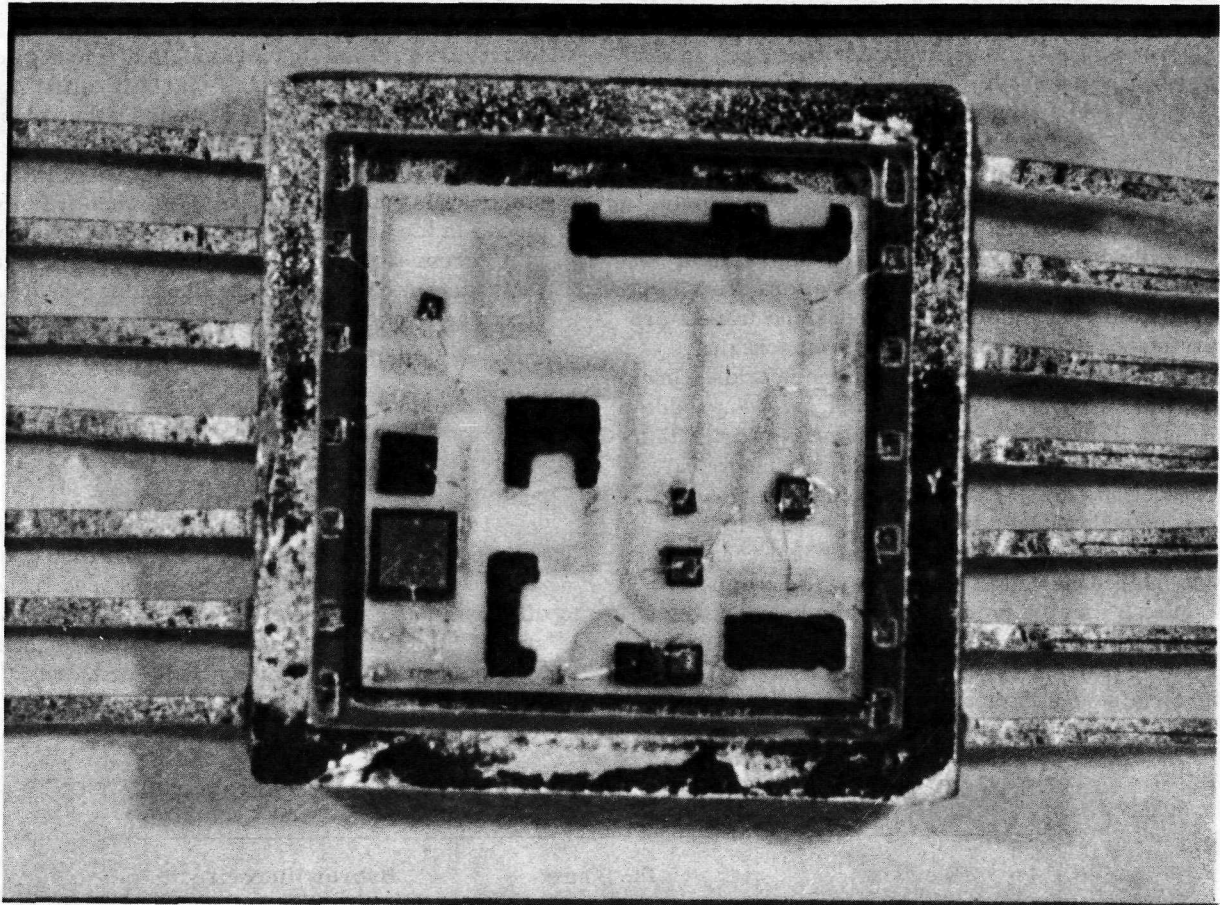


Figure 2. A typical thick film hybrid microcircuit.

TABLE 2. TYPICAL DEPOSITION MATERIALS FOR PRODUCING HYBRID CONDUCTORS AND PASSIVE DEVICES

Element	Thick Film	Thin Film
Conductor	Palladium-Gold	Aluminum Over Nichrome
Resistor	Palladium-Silver	Nichrome
Capacitor	Chip Capacitor or Two Conductors Separated by a Dielectric	Chip Capacitor or Two Conductors Separated by a Dielectric
Dielectric	Silicon Dioxide	Silicon Dioxide

TABLE 3. TEST SPECIMEN DESCRIPTION

Manufacturer	Assembly	Wire	Resistors	Capacitors	Semiconductors
A	Chip and Wire	Gold	Diffused Silicon Dice		Eutectically Bonded Dice
B	Thick Film	Gold	Diffused Silicon Dice		Moly-Tabbed Dice Eutectically Bonded
C	Thick Film	Gold	Thick Film		Eutectically Bonded Dice
D	Thin Film	Aluminum	Thick Film, Thin Film	Ceramic Chip	Eutectically Bonded Dice

controls were needed to produce highly reliable circuits for flight purposes. A description of the circuits from the four manufacturers is given in the following.

1. Manufacturer A — These regulator units are constructed on a single round alumina substrate that is eutectically bonded to the header. The electrical parts (transistors and resistors) are individual chip elements eutectically bonded to the substrate. Thermal-compression (gold wire) ball bonds and wedge bonds are made to the dice elements. The resistor elements are diffused silicon chips.

2. Manufacturer B — These regulator units are constructed using a single square substrate that is eutectically bonded to a 12-pin G-package. Thick film gold interconnection patterns are formed on the substrate. Resistors are diffused silicon dice. All resistors and transistor dice are moly-tabbed; i. e., mounted eutectically on small gold-plated Kovar rectangular sheet or tabs. The tabs are in turn eutectically bonded to the substrate (gold) intra-connection pattern. Thermal-compression (gold wire) ball bonds are made to the metallization patterns of the dice elements.

3. Manufacturer C — These regulator units are constructed using 2 substrates stacked on a 10-pin TO-5 header. The substrates are attached to the header by mounting posts passing through holes in the substrate, with small washers fitted over the posts and soldered to the posts and metallization on the substrates. The dice are eutectically bonded to the substrate. Thermal-compression (gold wire) ball bonds and wedge bonds are made to the

semiconductor dice. Thick film resistors are incorporated and are protected with an overcoat application.

4. Manufacturer D — These regulator units are constructed using two alumina substrates mounted on the same plane, each with thin film resistors and thin film (gold) intraconnections. The substrates are attached to the enclosure package by a high-temperature cure epoxy material. For jumpers and die interconnections,  $2.54 \times 10^{-5}$  m (1.0 mil) aluminum wire (ultrasonically bonded) is used. Ceramic chip capacitors are attached to the gold interconnection paths by means of solder reflow. A thick film resistor chip is also attached in this manner after its terminations are metallized. Crossover connections are made with aluminum jumper wires and an epoxy is used as insulating support.

## TEST PROGRAM

A test program was outlined to electrically, thermally, and mechanically exercise the regulator units and determine what prominent failure modes existed within the hybrid microcircuits. The test program was split into three phases as outlined in Table 4. Phase 1 consisted of electrical acceptance testing to make certain the device met all the manufacturer's specifications. In phase 2, a failure rate was established by testing each device within the constraints of the manufacturer's published literature. Phase 3 of this test program consisted of increasing severity until the device under test failed.

TABLE 4. TEST PROGRAM

Test	Purpose of Test
Phase 1 Electrical Test External Visual Test X-Ray Test	Verify Electrical Parameters Look for External Physical Damage Internal Anomalies
Phase 2 Life Test	To Determine a Representative Failure Rate
Phase 3 Step Stress Testing	This is a Method of Increasing the Severity of Test Stress until the Device Fails.

The failures experienced in the first two test phases are summarized in Table 5. The hybrids received from Manufacturer A experienced two failures, a wire bond failure and a chip failure. The chip failure occurred because a higher than normal temperature was used in mounting the chip to the substrate. The circuit failures from Manufacturer B consisted primarily of chip failures, with one substrate bond failure. This particular manufacturer uses a moly-tabbed mounting system to pre-test the chip prior to mounting it on the substrate. With this process, one would normally expect fewer chip failures. The only failures that were discovered from Manufacturer C were chip device failures, a total of six. Because of Manufacturer C's difficulty in testing the chips before attachment, marginal chips were often used, which is indicated by their high incidence of failure. Normally, a quality chip will be scribed and broken

on regular planes; however, the particular chips tested were not high reliability devices. The hybrids from Manufacturer D had the most failures of the four manufacturers tested, a total of 23. There were nine chip bond failures, seven wire bond failures, two excess temperature failures, and five loose particle failures; however, no chip failures were discovered. In summary, in-process monitoring on inspection points would have helped considerably in eliminating many chip bond, wire bond, and substrate bond failures. Testing of the chip before it was placed on the substrate could have eliminated many chip device failures.

One of the important quality and reliability jobs is to determine how to minimize conductor cross-over and to specify the minimum clearances between adjacent conductors. Knowing the size of the loose particles helps to determine what clearance can be

TABLE 5. VOLTAGE REGULATOR TEST CIRCUIT FAILURES

Manufacturer	Type of Failures					
	Chip Device	Chip Bond	Wire Bond	Substrate Bond	Excess Temperature	Loose Conductor Particles
A			1		1	
B	4			1		
C	6					
D		9	7		2	5

allowed within a particular circuit. A failure mode that appeared on the hybrids of Manufacturer B (Fig. 3) probably was caused by a lack of adhesion between the substrate and the Kovar header. The crack in the substrate severed the conductor pattern in many places, thus causing an open circuit. These particular chips are held in place on the ceramic substrate by an eutectic gold combination; the back of the chip is gold plated and palladium-gold is on the substrate. The two are diffused together by elevated temperature and a scrubbing action on the chip.

X-rays were taken at receiving inspection when the devices were first received. Examinations were conducted for parallelism between the ceramic substrate and the header, for broken leads if visible, for metallic particles, and to examine the eutectic bond of the chip. If something that looked like a particle was found, a routine X-ray was taken in another plane, which would help to indicate where the particle was located.

A large number of Manufacturer D's problems were caused by the use of pure gold. In producing a thin film hybrid microcircuit, the manufacturer used gold on the substrate and then soldered the chip in place. Whenever gold is used in a solid solution with solder, the tin within the solder alloy has an affinity for gold and the two come together and form a very brittle intermetallic system. This same problem occurred on PC boards where cracked solder connections were caused by this brittle gold-tin system. If all the gold from the printed circuitry is not erased before soldering, cracked connections will result. Some of the circuits from Manufacturer D had large capacitors that were loose when they were received, before any tests were conducted. The capacitors became loose during shipping operations. Manufacturer D also made redundant connections on his circuits. Several unsuccessful attempts to ultrasonically bond  $2.54 \times 10^{-5}$  m (1.0 mil) aluminum wire to the bond areas indicated that Manufacturer D had bonding problems. Figure 4 is an X-ray view of a typical circuit from

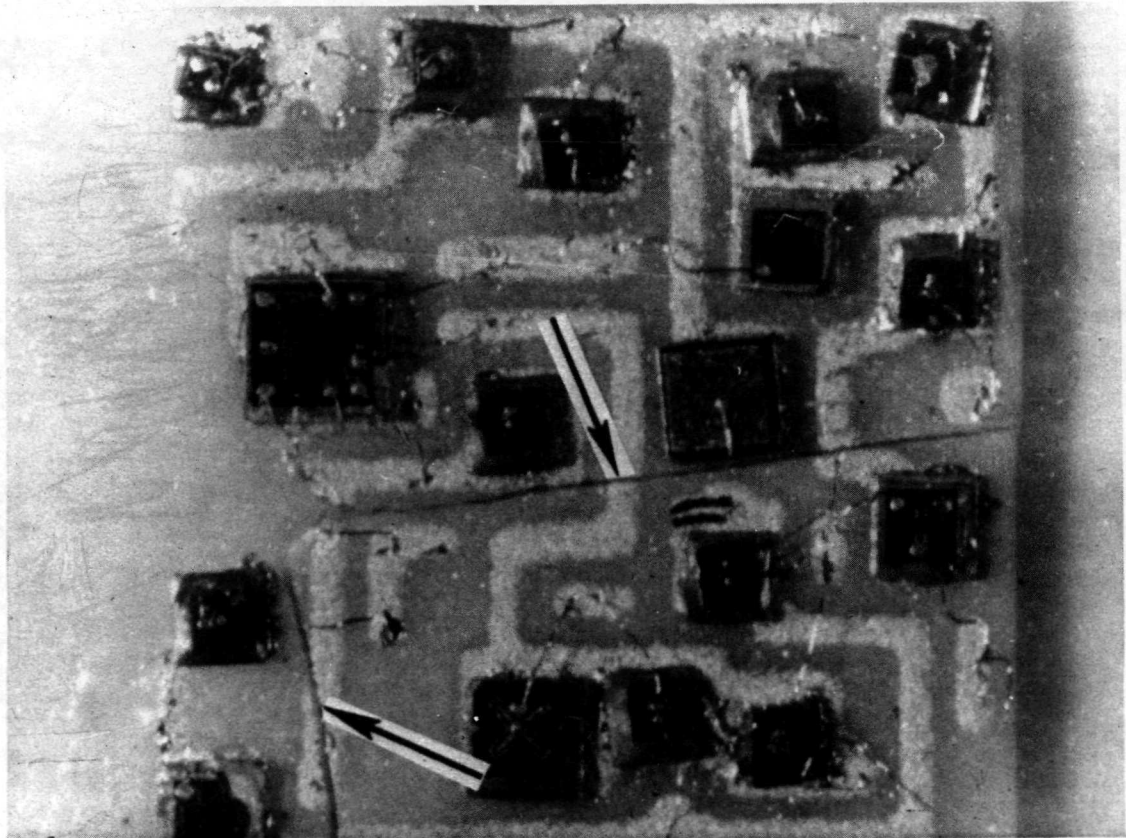


Figure 3. Fractured substrate caused by poor substrate-to-header bond.

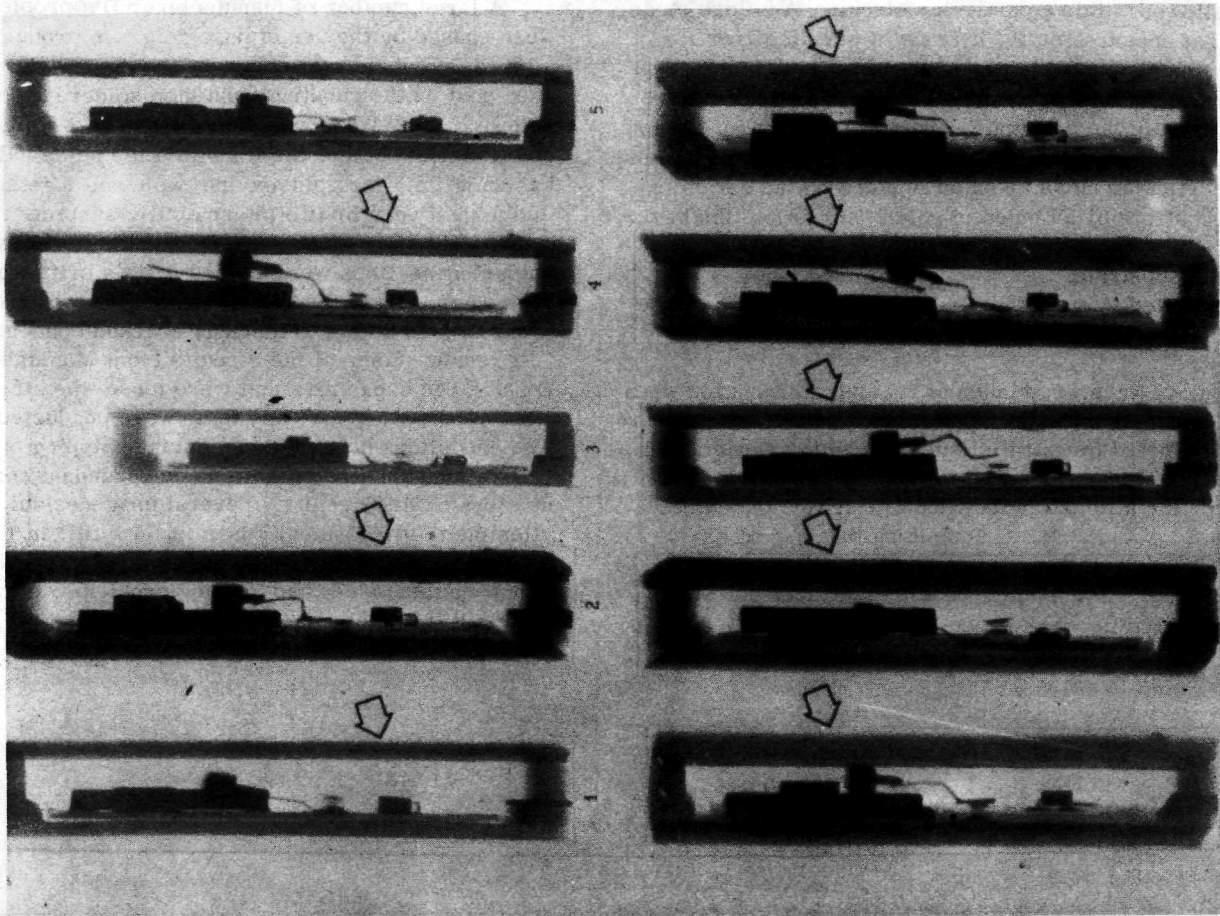


Figure 4. Side-view X-ray photos (Manufacturer D).

Manufacturer D, the one with the most problems. The figure indicates that during receiving inspection there were many problems, two loose capacitors and loose leads that caused a malfunction of the microcircuit.

Because of the problems that occur with wire bonds and the chip-to-substrate interface, beam leads were investigated and a test program was outlined. The objective of the program was to answer the following: What is involved in attaching a beam-leaded chip to a substrate? What are some of the quality control problems involved? The program was initiated to examine gold beam leads attached to gold over nichrome and aluminum beam leads attached to aluminum over nichrome. Flip chips, both solder and aluminum bump chips, were included in the test program (Table 6).

One of the things worth noting here is that the gold beam-leaded chips are rather prominent in the

United States, but in Europe aluminum beam leads are most prominent. A problem later developed in locating appropriate ultrasonic equipment to bond the aluminum beam leads to the thin film substrate.

Figure 5 is a photo of a beam-lead circuit, which derives its terminology from the very appearance of the beams. These are becoming more popular because of the problems associated with bonding aluminum and gold wires. There are many other metals used in the construction of the beams, and only the outer coating is gold. When one uses a beam-leaded device, he designs a circuit pattern on the substrate that will accommodate the particular beam spacing of that device.

In the test program, it was learned that the small gold-coated fingers (beams) are very susceptible to damage during handling, so they have to be packaged one at a time and handled very carefully.

TABLE 6. CHIP-TO-SUBSTRATE INTERFACE

Type of Chip	Substrate Metallization
Gold Beam Leads	Gold Over Nichrome (Thin Film)
Aluminum Beam Leads	Aluminum Over Nichrome (Thin Film)
Flip Chip (Solder Bumps)	Palladium-Gold Tinned with Silver Solder (Thick Film)
Flip Chip (Aluminum Bumps)	Aluminum Over Nichrome (Thin Film)

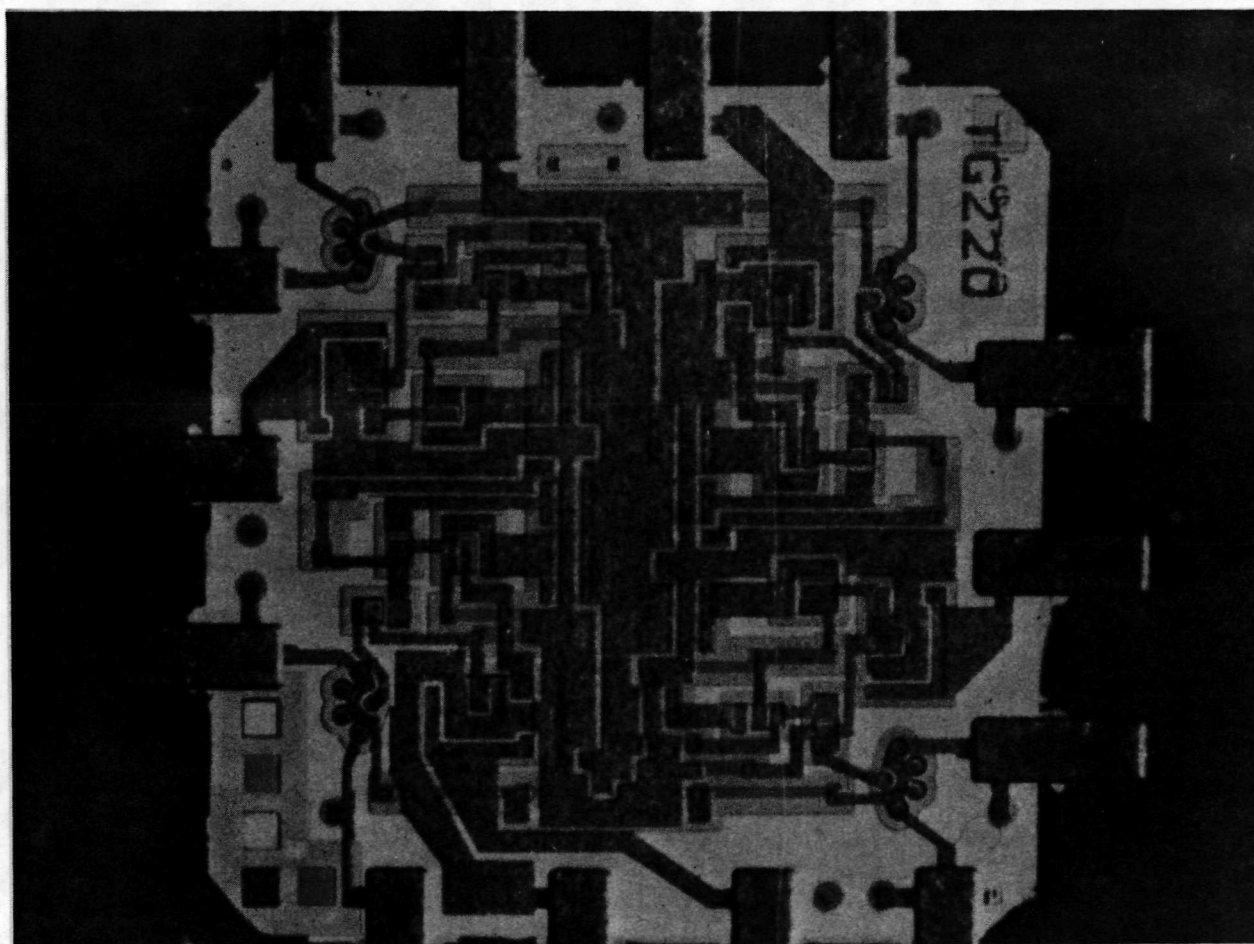


Figure 5. A typical beam-leaded device.

## PROBLEM AREAS

Many problems were observed in the tests. One of the major problems was in attaching the aluminum beam-lead device to the substrate, because no equipment was available for this operation. Later it was discovered that the ultrasonic equipment normally used in the United States to attach aluminum wire to aluminum land areas provides too much energy for the beam-lead device. The aluminum beam lead required lower energy and pressure parameters than the ultrasonic equipment is capable of producing at a close tolerance.

Variations of surface contacts of the aluminum bumps in different lots of devices delayed the construction of a weld schedule. A few electrical rejects having the same geometry as a good device were obtained. These devices were not from the lot that was procured later for test purposes. Although the specification sheet states that the geometry of the aluminum bumps is the same, it varied from lot to lot. Another problem that arose is that when too much pressure is put on the

aluminum flip chip to obtain a better bond, the bump might be depressed too far shorting out the bumps beneath the chip. One reason flip-chip devices must be thermally derated is to compensate for the lack of direct contact with the substrate. Derating factors have not been established for beam-leaded and flip-chip devices. Although some of the beam-lead manufacturers will say that thermal derating is not required, it seems that this position would be difficult to defend because of the lack of an intimate contact between the substrate and chip, as in a chip and wire assembly. All the heat must be dissipated through innerconnections, the beam leads, or flip-chip bumps.

A typical beam-leaded device (a 709 amplifier) is shown in Figure 5. In the test program for evaluating device bonds, a number were tested on test substrates. The two marks on the substrate area that accepts this beam-leaded device are visible in Figure 6. There is a hole in the center, which is used to dislodge the beam-leaded device from the substrate, and a mark to orient the manufacturer as to where to place the number one lead. The method used to attach the beam-leaded devices is thermal compression bonding, attaching one lead at a time. The wobble-head bonder technique bonds all of the

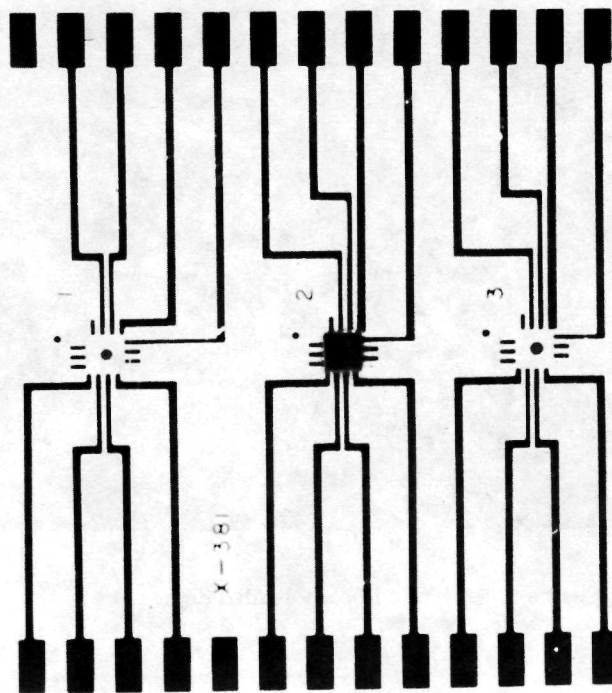


Figure 6. Test substrate for beam-leaded devices.

leads simultaneously and, thus, is a more efficient bonding method. Bonding each lead separately results in stronger bonds, but the difference in strength is not great enough to justify using the slower technique.

## ALUMINUM BUMP CHIPS

To determine how much pressure is required to remove a chip from the substrate, a lateral force was provided, putting the surfaces in shear. The force required to dislodge the chips was used to construct an optimum weld schedule. The chip was flipped over, and its surface and the substrate surface on which the chip was attached were examined. In studying these surfaces, an attempt was made to correlate weak and strong bonds. Surface studies proved negative, however.

A series of weld schedules for flip chips and beam leads were developed. These devices were bonded into a functional test circuit, shown in Figure 7. The flip chips and beam leads were bonded on the substrate of the power supply shown in Figure 8.

## HIGHER FREQUENCY RANGES

As mentioned earlier, the microwave regions are being examined for application of hybrid technology. A study is under way to find low dielectric loss substrates, which is important to prevent microwave power loss in coils, tune lines, and transmission lines.

Primarily, thin film probably will be used in hybrids for microwaves. The fuzzy uneven edges

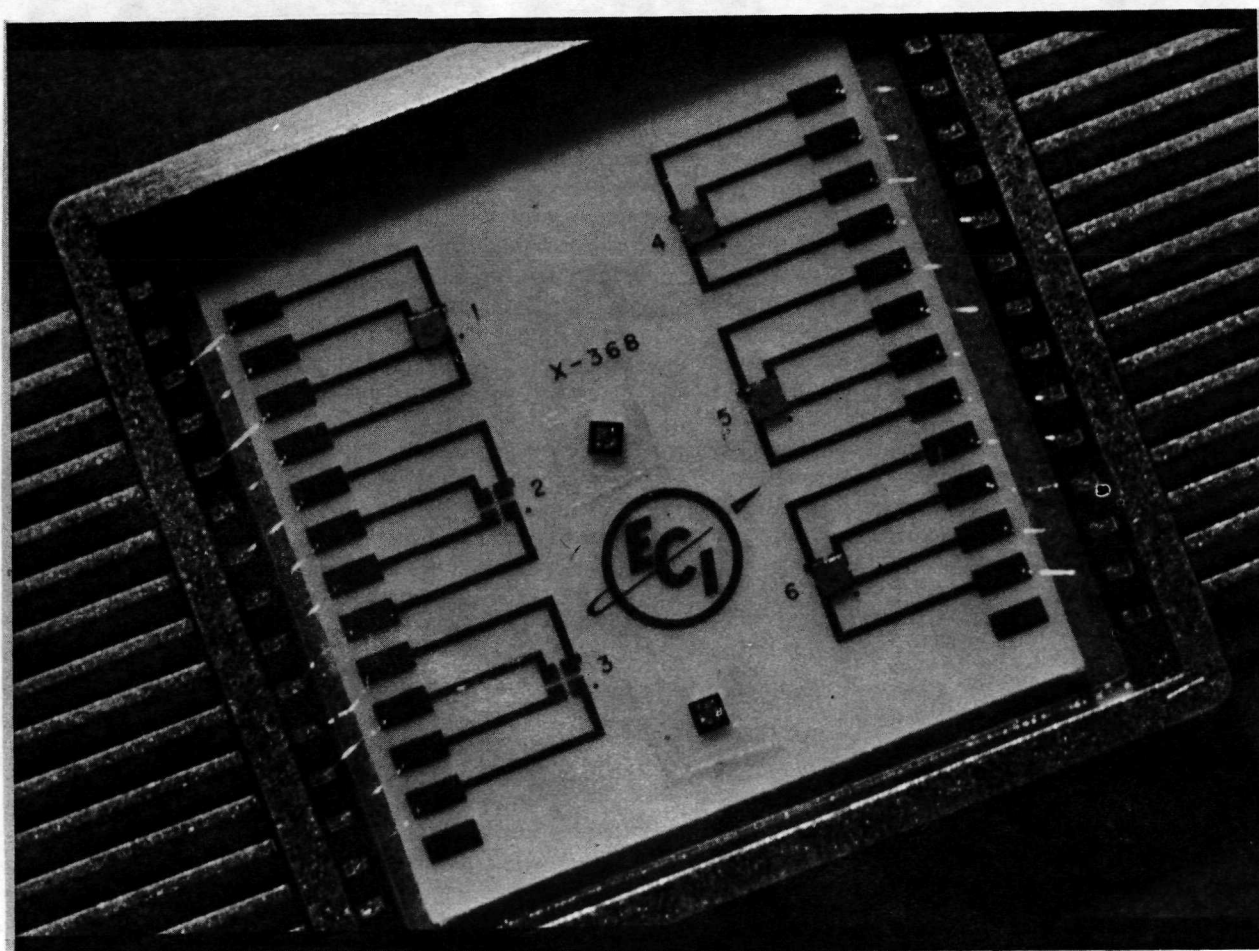


Figure 7. Flip-chip test substrate.

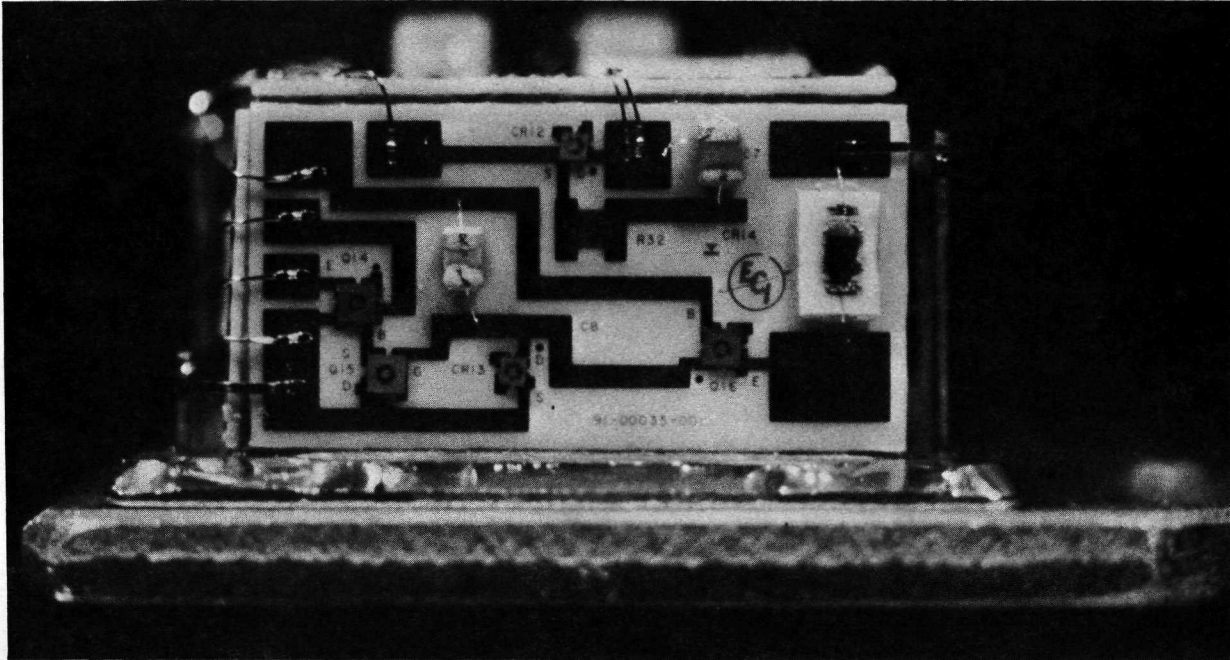


Figure 8. Power supply circuit using flip chips and beam-leaded devices.

and roughness of thick film will not accommodate requirements for the high frequency areas; therefore, the smooth (less than  $3 \times 10^{-6}$  cm) substrate is a requirement for hybrids in the microwave area. To partially overcome the chip failure problem, some manufacturers use more than one substrate in a package; if a problem develops with any one portion of a substrate, that substrate can be discarded and a new one inserted, rather than the whole component being discarded. This is one way of overcoming some of the problems of verifying the chip reliability prior to attachment to the substrate.

## HIGHER POWER REQUIREMENTS

As mentioned earlier, the hybrid requirements for power are being studied. When the power requirements were first evolved, thin film seemed out of place in the manufacture of power hybrids because of metallization thinness; however, the power hybrid technology now appears just as applicable for the thin film as for the thick film technology.

In the substrate requirements, though, alumina is seldom used. Something that is a better heat conductor than alumina must be used to get the heat

away from the chip, through the substrate, and down to the header where it can be dissipated. To do this, beryllium oxide is better; however, copper tabs that are somewhat bigger peripherally than the chip itself can be used with alumina substrates. Additionally, a larger substrate and larger conductor area are required to dissipate heat.

A reduction of the void area between the chip and substrate is very important for reliability, and X-rays will be the best means for determining the void area between the power chips and the substrate. On custom high reliability hybrids, a void between the chip and the substrate any larger than 50 percent of the chip area is not permitted. This will not be true with power hybrids. Power hybrids require that the void area between the chip and substrate be no larger than 15 to 20 percent of the chip area. This percentage will be verified as tests continue on this particular program. In power hybrids, of course, operation at a higher ambient temperature than is customary in other types of hybrids is to be expected. When temperature is increased, the metallization becomes very important. The "purple plague" problem with gold and aluminum is incurred at elevated temperature, so a monometallic (perhaps the aluminum to aluminum system) might be the best to use.

## RELIABILITY

Table 7 is a projection of how reliable the various interconnection methods appear today.

### Bond Strength

In tests thus far, the solder flip chip has shown superior bond strength to any of the rest. Flip chips also have their disadvantages, as will be shown later. The test program indicated that shear forces in the neighborhood of 1900 grams were necessary to dislodge one of the small chips from the substrate. It can be seen from Table 7 that wire is projected as one of the weaker materials in bond strength. Much is still unknown about the aluminum beam lead in this area, but tests indicate that the gold beam lead has average bond strength.

## Process Dependence

Process dependence is all important to reliability and quality assurance. The question is: How much variance in a process can you stand and still obtain a reliable product? The solder flip chip rates excellent in this category, the gold beam lead rates very high, and the wire rates about average. The aluminum-bump chip interconnections are weak. Generally, a highly controlled weld schedule for ultrasonic bonding is necessary.

### Handling Damage

As indicated before, the gold beam leads are very susceptible to deformation and, therefore, are weak in the handling damage category, as are the aluminum beam leads and the wire. The flip chips have shown excellence in this category.

TABLE 7. RELIABILITY PROJECTION

Characteristic	Beam Lead		Flip Chip		Wire
	Gold	Aluminum	Solder	Aluminum	
1. Bond Strength	A	U	E	A	W
2. Process Dependence	S	U	E	W	A
3. Handling Damage	W	W	E	E	W
4. Flexible Connection	A	A	W	W	E
5. Simple Metallurgy	W	E	A	E	S
6. Minimum Connections	S	S	S	S	W
7. Bonding Efficiency	E	U	S	S	W
8. Inspectability	S	S	W	W	E
9. Power Dissipation	A	W	S	S	E
10. Bond Reliability	E	U	S	A	A

Legend:

E - Excellent, S - Strong, A - Average, W - Weak, U - Unknown

## Flexible Connection

Flexible connections are desirable to permit expansions because of thermal excursions during cycling. Of course, the greater the flexibility, the better the interconnection method is. The beam leads have shown only average flexibility, whereas wire is unsurpassed in this respect. However,  $2.54 \times 10^{-5}$  m (1.0 mil) aluminum wire does have other problems.

## Simple Metallurgy

The gold beam leads are weak in this respect because, as mentioned before, they look like pure gold but are actually gold on the exterior surface only. Aluminum beam leads should have excellent reliability in this respect, as does the aluminum flip chip.

## Minimum Connections

With the beam-lead and flip-chip technology, a number of interconnections that would be used in a chip and wire assembly can be eliminated. On a typical transistor soldered to a PC board, there are eight interconnections to be made between the chip and PC board; with the hybrid, using the flip chip or the beam lead, there are only three connections between chip and substrate. By reducing the number of connections, the reliability will correspondingly increase.

## Bonding Efficiency

The gold beam lead rates much higher than all others in bonding efficiency since all 14 leads are bonded at one time, whereas with the wire each one is bonded separately. Incidentally, using beam-lead devices one is not restricted to 14 beam leads. There are beam-leaded devices available now that have 50 to 100 beam leads.

## Inspectability

Inspectability is another important aspect to reliability and quality assurance. The inspectability of the wire is better perhaps than that of either the flip chip or the beam leads because the wire connection can be seen readily from all angles. The beam is rated as good because only the top surface can be seen clearly, and the view from the side is limited because of the beam adjacent to it. The flip chip is rated as weak because the connections are beneath the chip and cannot be seen.

## Power Dissipation

The chip and wire are better for power dissipation, because the eutectic bond of the chip to the substrate provides a good thermal path. In the beam lead and flip chip, the power can be dissipated only through the interconnections.

## Bond Reliability

For bond reliability, the gold beam lead is better perhaps than all others, including conventional wire.

# BOND PROBLEMS CAUSED BY THERMAL EXCURSION

By

F. Vilella

## ABSTRACT

The failure mode caused by thermal deformation and thermal deformation effects on bond integrity are discussed herein. Thermocompression (TC) wedge bonding, ultrasonic bonding, and thermocompression ball (nailhead) bonding in small-signal transistors are considered. Repeated switching of these devices between high and low power at a rate that allows thermal expansion and contraction in the interconnecting wire causes the wire to flex at the point of reduced cross-sectional area until breakage finally occurs because of metal fatigue. This thermal deformation is related to many factors such as device power dissipation, current density in the wire, wire dress and length, the thermal time constant, and frequency of operation.

## SUMMARY

The failure modes and mechanisms discussed in this paper are presented to familiarize reliability and design engineers with fatigue failures that occur in  $2.54 \times 10^{-5}$  m (1 mil) aluminum lead wire of small-signal transistors when subjected to thermal excursions. In April 1969, during testing prior to hot firing of a J-2 engine at the Rocketdyne engine test stand, a screened 2N2222A transistor failed open between the base and emitter in the Electrical Control Assembly (ECA) Ignition Phase Timer. The failed transistor was decapped by the manufacturer, and visual inspection revealed that the base lead wire had fractured at the heel of the thermal compression wedge bond to the semiconductor chip. Many 2N2222A and other small-signal transistors with  $2.54 \times 10^{-5}$  m (1 mil) aluminum wire are used by MSFC; therefore, the Quality and Reliability Assurance Laboratory decided to investigate this problem further. A study of the problem, its causes, extent, and the possible screening tests and inspections was conducted. It was known from previous studies that abrupt changes in the cross section of the wire because of the bonding

operation can cause a significant reduction in the wire fatigue strength. Such a change in cross-sectional area can be found at the heel of a  $2.54 \times 10^{-5}$  m (1 mil) aluminum ultrasonic or TC wedge bond or at the neck of a gold ball bond (nailhead), and metal fatigue caused by thermal deformation usually breaks the wire at this, the weakest, point.

To verify the existence of several factors that might affect thermal deformation, thermal analyses at various power cycling conditions were conducted on actual devices (Fig. 1). Analyses with the Scanning Electron Microscope (SEM) were also performed. The effects of wire dress were investigated and bond pulling tests were performed on some of the devices that survived power cycling tests.

## POWER CYCLING TESTS

Since the failures to be investigated were mechanical in nature, namely cracking and separation of the bond wire at the heel of the bond, it was believed that accelerated stress testing such as by power cycling was the best approach for evaluating bond integrity and for duplicating the failure mode and mechanism of the failed transistor. To establish the extent to which thermal deformation caused by the temperature differential ( $\Delta T$ ) in the systems produces motion of the aluminum interconnecting wire, power cycling tests were conducted at various combinations of power level, current, and cycling time.

Parallel tests were conducted by MSFC and Manufacturer A. At the request of MSFC, Manufacturer A began power cycling tests at various operating conditions on devices using 0.0025 cm (0.001 in.) diameter aluminum interconnecting lead wire and TC wedge bonds, while MSFC began power cycling tests on devices using 0.0025 cm (0.001 in.) diameter ultrasonically bonded aluminum wire and devices using 0.0018 to 0.0025 cm (0.0007 to 0.001 in.) diameter gold TC bonds (wedge and nailhead).

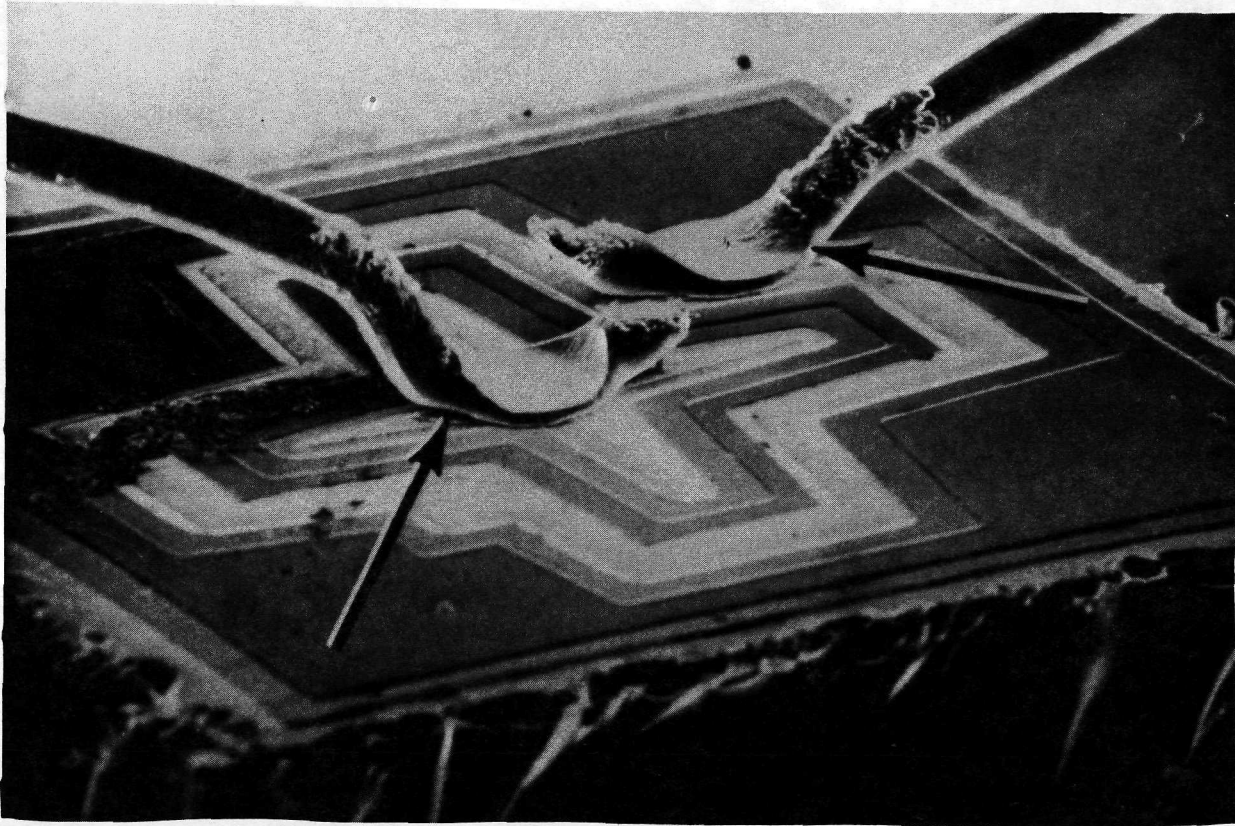


Figure 1. Manufacturer A transistor 2N2222A from ECA Ignition Phase Timer, typical TC wedge bond (220X magnification).

The common base configuration circuit shown in Figure 2 was used by MSFC. Each lead was inserted through five ferrite beads and attached directly at each transistor socket pin to minimize the occurrence of high frequency oscillations. The dc power was applied to each transistor by a common triple-pole contactor. At the end of the "on" cycle the contactor opened, simultaneously removing the dc power from the emitter, base, and collector.

The results of the tests performed by Manufacturer A on devices built with  $2.54 \times 10^{-5}$  (1 mil) TC wedge bonded aluminum lead wire are summarized in Table 1. The results of the tests performed by MSFC are summarized in Tables 2, 3, and 4. Table 2 summarizes the results of tests on devices manufactured by Manufacturers A and B, built with  $2.54 \times 10^{-5}$  m (1 mil) ultrasonically bonded aluminum lead wire and power cycled at maximum device-rated power. Table 3 summarizes the results of tests on devices from Manufacturer B, built with  $2.54 \times 10^{-5}$  m (1 mil) ultrasonically bonded

aluminum lead wire and power cycled under derated conditions. A cycling time of 1 min on and 1 min off was used, since thermal equilibrium on the TO-18 package under derated conditions can be reached in less than 1 min. Table 4 summarizes the results on devices manufactured by Manufacturers C, D, and E, built with  $1.78 \times 10^{-5}$  to  $2.54 \times 10^{-5}$  m (0.7 to 1 mil) TC bonded gold lead wire and power cycled at maximum device-rated power.

A plot of cumulative percent of failures versus cycles for devices operated under the same power current and repetition rates is shown in Figure 3. The data for the Manufacturer A 2N2222A (aluminum) TC bonds were not well correlated; therefore, the least squares method was used to determine the slope of the curve. Although the Manufacturer B ultrasonic bonds did not fail as early as the Manufacturer A TC bonds, the rate of failure of the Manufacturer B ultrasonic bonds after the initial failure is about the same as that experienced by the Manufacturer A TC bonds. This is illustrated by the fact that the two plots are nearly parallel.

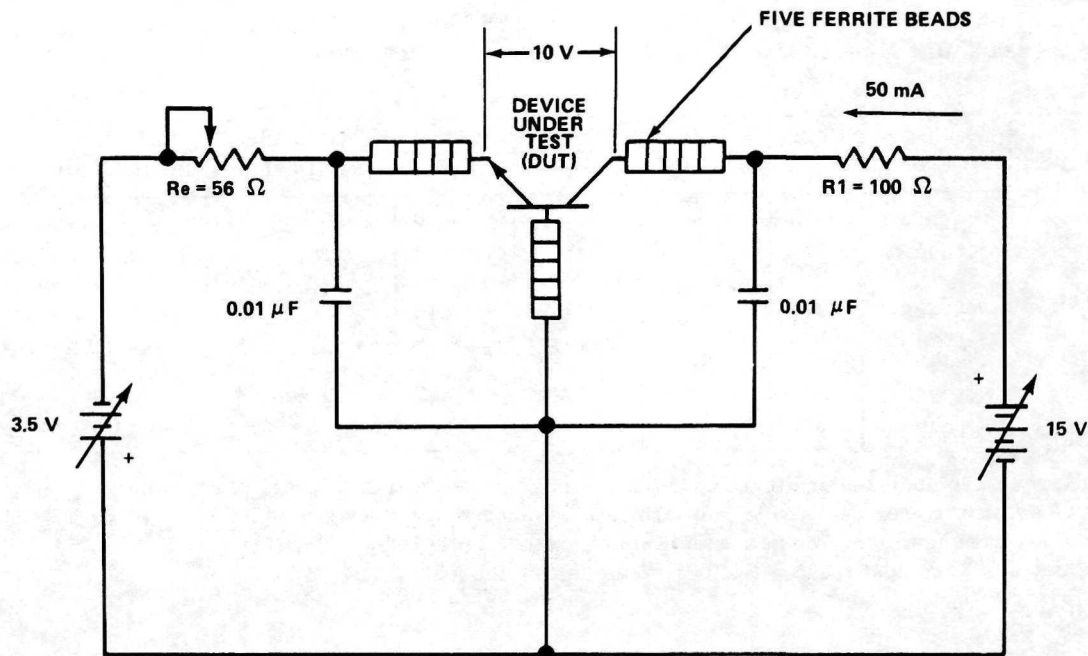


Figure 2. Power cycling test circuit.

TABLE 1. SUMMARY OF POWER CYCLING TESTS PERFORMED BY MANUFACTURER A ON THEIR OWN ALUMINUM THERMOCOMPRESSION WEDGE BONDS

Device Type	Date Code	Quantity	Test Conditions		Total Cycles Per Device <sup>a</sup>	Total Failures <sup>b</sup>
			$P_D$	$I_C$		
JAN2N2222A	6927A	85	500 mW	16.5 mA	8 058	13, First Occurred 2 at 2082 Cycles
JAN2N2222A	6927A	247	500 mW	50.0 mA	11 440	52, First Occurred 5 at 1600 Cycles
JAN2N2222A	6927A	750	165 mW	50.0 mA	23 640	38, First Occurred 10 at 1600 Cycles
JAN2N2222A	6927A	500	335 mW	50.0 mA	22 960	39, First Occurred 10 at 1600 Cycles
JAN2N2222A	6927A	500	165 mW	16.5 mA	21 902	3, First Occurred 1 at 588 Cycles
JAN2N2222A	6927A	500	335 mW	16.5 mA	22 630	43, First Occurred 4 at 588 Cycles

- a. Prior to 588 cycles the devices were power cycled at a rate of 5 min on and 5 min off, and thereafter at a rate of 3 min on and 3 min off.
- b. All failures were analyzed and found to be an open or broken lead at the heel of a semiconductor bond.

TABLE 2. SUMMARY OF POWER CYCLING TESTS PERFORMED BY MSFC ON ALUMINUM ULTRASONIC BONDS (MAXIMUM DEVICE-RATED POWER)

Manufacturer	Device Type	Date Code	Quantity	Test Conditions		Total Cycles Per Device	Total Failures <sup>a</sup>
				P <sub>D</sub>	I <sub>C</sub>		
A	2N2222A (Group 1)	7040	100	500 mW	50 mA <sup>b</sup>	45 720	23, First Occurred 1 at 11 520 Cycles
B	2N2222A (Group 2)	6949	29	500 mW	50 mA <sup>c</sup>	61 320	21, First Occurred 1 at 8190 Cycles
B	2N2222A (Group 3)	7007	25 <sup>d</sup>	500 mW	50 mA <sup>c</sup>	44 570	18, First Occurred 1 at 18 410 Cycles

- All failures were analyzed and found to be an open or broken lead at the heel of a bond.
- All devices were power cycled at a rate of 2 min on and 2 min off.
- All devices were power cycled at a rate of 3 min on and 3 min off.
- These devices were heat treated (baked) by the manufacturer.

TABLE 3. SUMMARY OF POWER CYCLING TESTS PERFORMED BY MSFC ON ALUMINUM ULTRASONIC BONDS (DERATED CONDITIONS)

Manufacturer	Device Type	Date Code	Quantity	Test Conditions		Total Cycles Per Device	Total Failures <sup>a</sup>
				P <sub>D</sub>	I <sub>C</sub>		
B	2N2222A (Group 4)	7007	25 <sup>b</sup>	100 mW	50 mA <sup>c</sup>	135 660	1 at 83 070 Cycles
B	2N2222A (Group 5)	7007	25 <sup>b</sup>	25 mW	10 mA <sup>c</sup>	138 660	0
B	2N2222A (Group 6)	7007	25 <sup>b</sup>	20 mW	10 mA <sup>c,d</sup>	135 660	0

- All failures were analyzed and found to be an open or broken lead at the heel of a bond.
- These devices were heat treated (baked) by the manufacturer.
- All devices were power cycled at a rate of 1 min on and 1 min off.
- Devices were in a steady-state environmental condition of  $85 \pm 3^\circ\text{C}$  during both the on and off power cycling.

The effects of lead dressing were studied also. It was noted that post-to-die leads that are dressed straight are more prone to fail than leads that are provided with a loop of the proper height [ $17.78 \times 10^{-5}$  to  $25.4 \times 10^{-5}$  m (7 to 10 mil)] when subjected to a given number of stress cycles. The explanation seems to be that when a service loop is present, the expansion and contraction of the wire caused by temperature changes causes only a very small flexion of the wire in the region of the bond heel. Calculations made by the National Bureau of Standards have shown that the increase in loop height, and

therefore the amount the heel flexed, is inversely proportional to the height of the loop measured at room temperature (initial height).

## SCANNING ELECTRON MICROSCOPE

The devices that failed during power cycling test were decapped and analyzed using the SEM. Examination of the failed bonds showed that the separation occurred at the heel of the bonds

TABLE 4. SUMMARY OF POWER CYCLING TESTS PERFORMED BY MSFC ON GOLD THERMOCOMPRESSION BONDS (MAXIMUM DEVICE-RATED POWER)

Manufacturer	Device Type	Date Code	Quantity	Test Conditions		Total Cycles Per Device <sup>a</sup>	Total Failures
				P <sub>D</sub>	I <sub>C</sub>		
C	2N2222A (Group 7)		19	500 mW	50 mA	50 320	0
D	JAN2N2222A (Group 8)		13	500 mW	50 mA	87 150	0
C	S2N910 (Group 9)	6750 6812 6815	49	500 mW	50 mA	72 120	0
E	S2N718 (Group 10)	6450 6520	49	500 mW	50 mA	72 930	1 at 42 060 Cycles
D	S2N718 (Group 10)	6948	49	500 mW	50 mA	72 930	1 at 19 880 Cycles

a. All devices were power cycled at a rate of 3 min on and 3 min off.

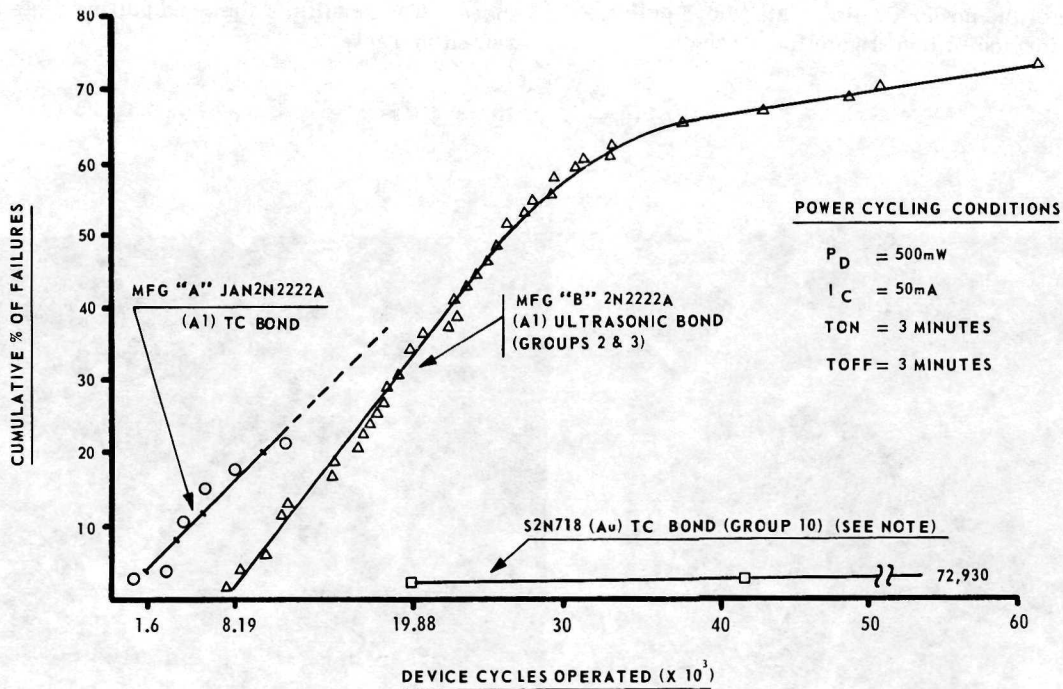


Figure 3. Percentage of failures.

(Figs. 4 and 5). The rough appearance of the wire in the areas of separation indicates a fatigue fracture mechanism. Also, to study the bond degradation during power cycling, a random sample of devices was taken from group 2, decapped, and analyzed using the SEM before and during power cycling and after failure. Figures 6, 7, and 8 depict clearly the increasing depth of the microcracks as a function of duration and severity of power cycling.

When examined with the SEM, electrically good devices from groups 4 and 5 that were power cycled under conditions (power, current, and repetition rates) less strenuous than the devices in groups 2 and 3 did not exhibit bond degradation at the heel even after 113 430 cycles. A sample of electrically good devices was taken from groups 2 and 3 after 41 650 cycles and analyzed using the SEM. It was found that these devices had deep microcracks at the heel of the bonds, such that the electrical continuity was about to be broken.

### BOND PULLING TESTS

At the end of the power cycling tests, bond pull tests were performed to investigate the strength of

the  $2.54 \times 10^{-5}$  m (1 mil) diameter aluminum and  $2.54 \times 10^{-5}$  m (1 mil) diameter gold interconnecting lead wires. The pull tests were performed on all bonds of the devices that had undergone SEM analysis. The pull tests were performed using a Micro Bond Tester. A thin molybdenum wire hook was carefully positioned under the loop of the interconnecting lead wire about midway between the die bond and the post bond of the transistor mounted on a fixed stage. The hook was attached to a retained reading dynamometer that was motor-driven at a constant angular velocity to apply a uniform loading rate. The loading rate used to pull the  $2.54 \times 10^{-5}$  m (1 mil) wire was 0.2 g/sec.

The failure loads for  $2.54 \times 10^{-5}$  m (1 mil) aluminum lead wire in the TO-18 packages were found to be in the range of 3.0 to 4.0 g for leads that are ultrasonically bonded to a system consisting of aluminum metallization on the die and gold-plated Kovar package posts. The failure loads for  $2.54 \times 10^{-5}$  m (1 mil) gold lead wire in the TO-18 packages were found to be in the range of 4.5 to 5.5 g for leads that are TC bonded in the same metallization system as above. The results of the bond pulling tests are presented in Table 5.

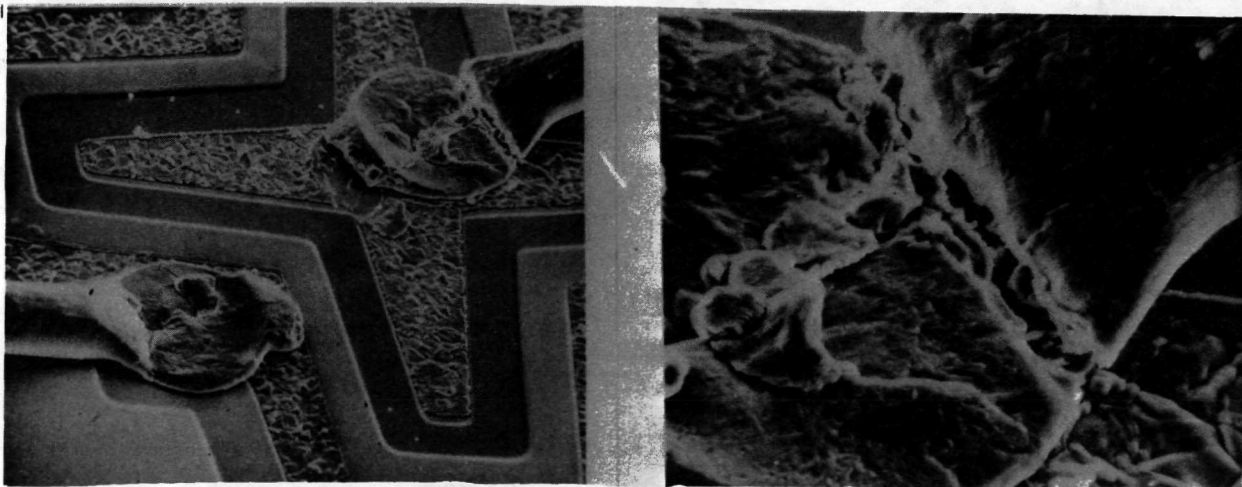


Figure 4. Manufacturer A transistor 2N2222A from ECA Ignition Phase Timer, TC wedge bond, emitter bond failed after 2240 power cycles.

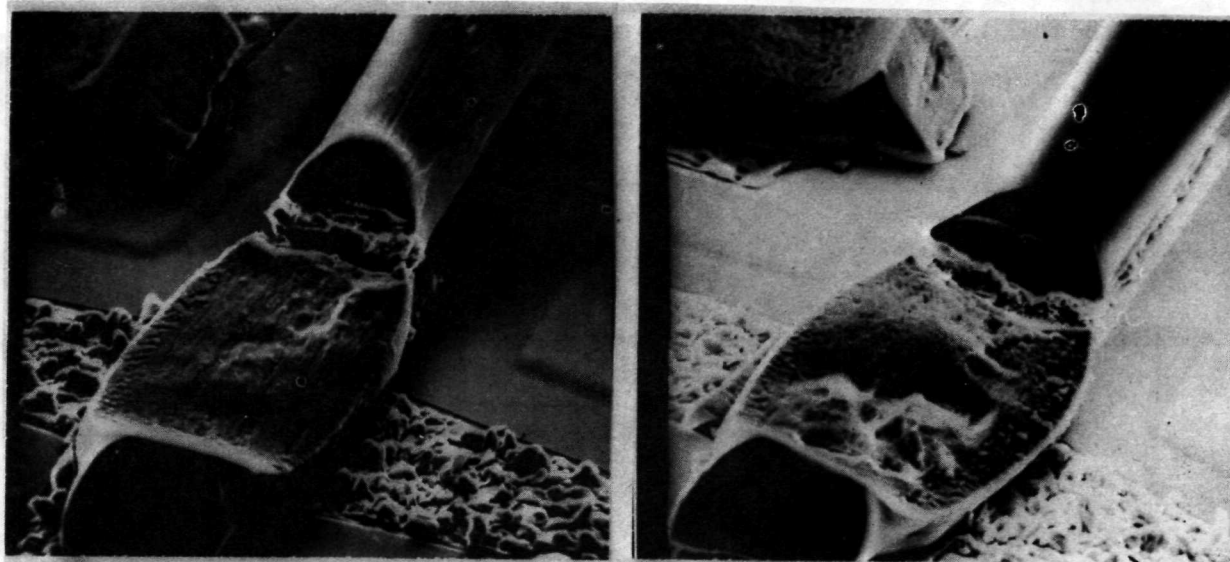


Figure 5. Manufacturer A transistor 2N2222A, group 1, die side bond, ultrasonic, open at heel.

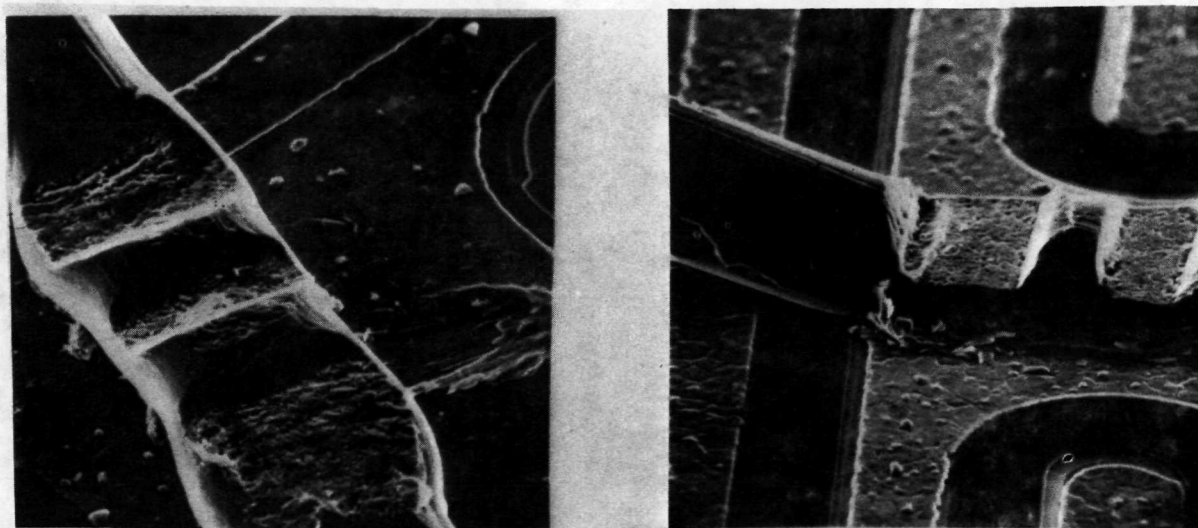


Figure 6. Manufacturer B transistor 2N2222A, serial number 75, die side bond, ultrasonic; evidence of microcracks at the heel before power cycling.

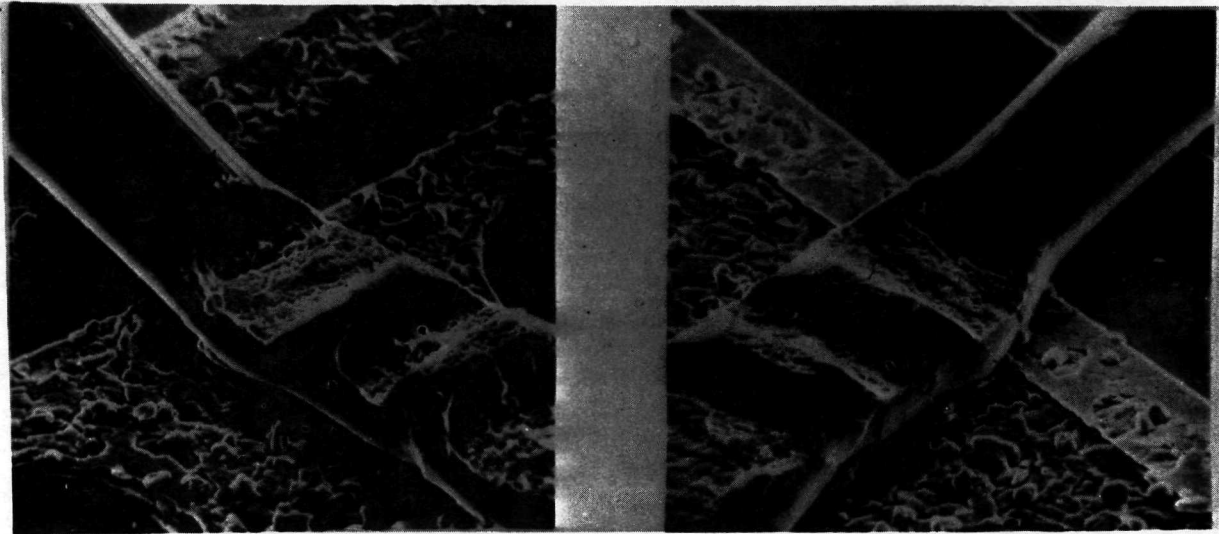


Figure 7. Manufacturer B transistor 2N2222A, serial number 75, die side bond, ultrasonic; microcrack depth increased after 3152 power cycles.

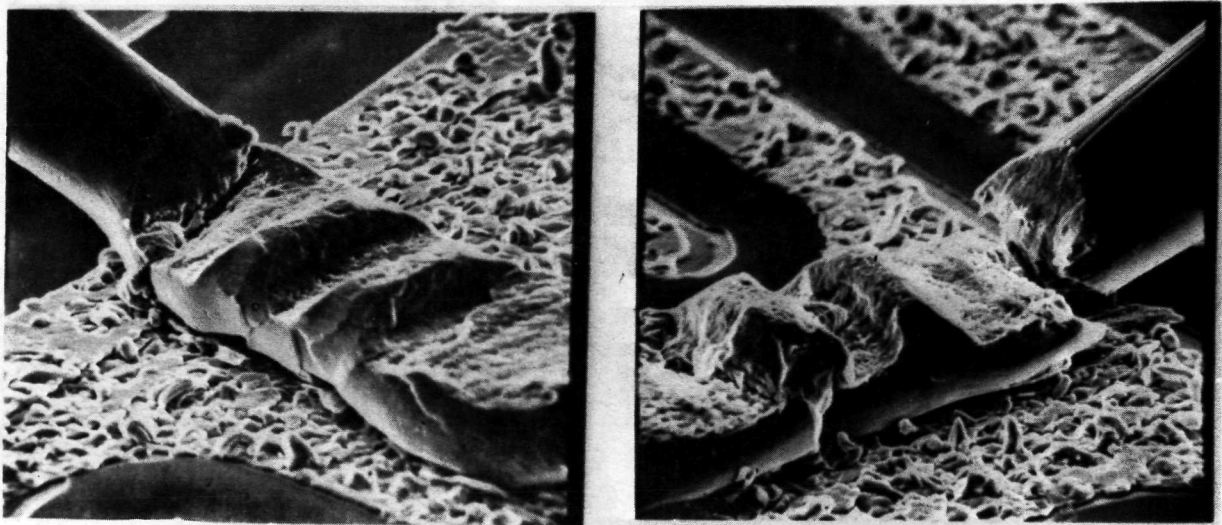


Figure 8. Manufacturer B transistor 2N2222A, serial number 75, die side bond, ultrasonic; open at heel after 14 500 power cycles.

TABLE 5. RESULTS OF BOND PULLING TESTS PERFORMED BY MSFC

Transistor	Manufacturer/ Group	Power Cycles	Devices Pulled	Average Force, g		Wire Type and Bond Type	Pull Test Remarks	
				Emitter	Base		Emitter	Base
JAN2N222A	D/8	80 430	2	5.5	5.0	Gold/TC	Wire Broke	Wire Broke
S2N910	C/9	64 730	2	5.5	5.0	Gold/TC	Wire Broke	Wire Broke
2N718A	E/10	68 880	2	8.0	8.0	Gold/TC	Bond Lifted (1) Bond Broke at Post (1)	Bond Broke at Heel (1) Bond Lifted at Heel (1)
2N718A	D/10	68 880	2	8.0	8.0	Gold/TC	Wire Broke	Wire Broke
2N2222A	B/3	44 570	5	1 to 2.5	0+ to 4	Aluminum/US	Bond Broke at Heel and Some at Post	Bond Broke at Heel and Some at Post
2N2222A	B/4	135 660	7	2.5 to 4	1 to 3.5	Aluminum/US	Bond Broke at Heel	Bond Broke at Heel and Some Lifted at Post

## CONCLUSIONS

It was concluded that the thermal deformation was related to many factors such as device power dissipation, current density, wire dress and length, thermal time constants (system), and frequency of operation. Also, it was noted that the greater the temperature differential ( $\Delta T$ ) in the systems, the greater will be the motion of the interconnecting lead wire because of thermal deformation. Therefore, if significant microcracks or tool marks are present at the heel of the bonds and if the lead does not have an adequate loop height, thermocompression wedge bonds may fail as early as 1600 cycles, and ultrasonic bonds may fail as early as 8000 cycles. When examined under the SEM, devices power-cycled under derated conditions did not exhibit bond degradation at the heel, even after 100 000 cycles.

Devices using  $2.54 \times 10^{-5}$  m (1 mil) thermo-compression bonded gold lead wire withstood the same power cycling conditions much better than either TC or ultrasonically bonded aluminum wire.

Out of a total of 179 gold wire devices tested there were two failures, one at 19 880 cycles and another at 42 060 cycles. There was virtually no degradation in the gold wire bond strength as a result of power cycling.

According to the National Bureau of Standards, a loop of adequate height significantly improves reliability by reducing the amount of flexion caused at the heel of the bond when the temperature changes.

Devices using  $2.54 \times 10^{-5}$  m (1 mil) aluminum lead wire may be used safely in power cycling applications only if very close control of the bonding process is maintained to assure that tool marks, microcracks, or insufficient cross-sectional areas are not present on the heels of the bonds. An adequate loop must also be provided in the wire. The methods or degree of control necessary to prevent said conditions have not been determined, but a study is underway with a transistor manufacturer to develop some nondestructive screening procedures and to establish the controls necessary for the variables of the bonding process.

## BIBLIOGRAPHY

Day, William; and Patridge, Jayne: Lead Failures Study, 1-Mil Wedge-Bonded 1006323 Transistor, E-2218. Massachusetts Institute of Technology Instrumentation Laboratory, Cambridge, Mass., December 1967.

Lohn, Roger L.: Reliability Limits for Power Cycling. Special Reliability Report for NASA, February 2, 1970.

Nowakowski, M. F.; and Villella, F.: Thermal Excursion Can Cause Bond Problems. 1971 IEEE Reliability Physics Symposium, Las Vegas, Nevada, March 31 — April 2, 1971.

Villella, F.; and Nowakowski, M. F.: ALERTS: MSFC-69-10, 6 October 1969; MSFC-69-10A, 10 November 1969; MSFC-69-10B, 27 February 1969. George C. Marshall Space Flight Center, Marshall Space Flight Center, Alabama.

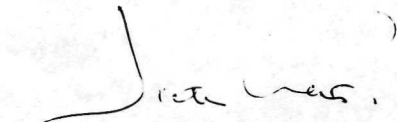
Villella, F; and Nowakowski, M. F.: Investigation of Fatigue Problem in 1-Mil Diameter Thermocompression and Ultrasonic Bonding of Aluminum Wire. NASA TM X-64566, George C. Marshall Space Flight Center, Marshall Space Flight Center, Alabama, November 30, 1970.

## APPROVAL

### RESEARCH ACHIEVEMENTS REVIEW VOLUME IV                      REPORT NO. 5

The information in these reports has been reviewed for security classification. Review of any information concerning Department of Defense or Atomic Energy Commission programs has been made by the MSFC Security Classification Officer. These reports, in their entirety, have been determined to be unclassified.

These reports have also been reviewed and approved for technical accuracy.



---

D. GRAU  
Director, Quality and Reliability Assurance Laboratory

1. Report No. NASA TM X-64666	2. Government Accession No.	3. Recipient's Catalog No.	
4. Title and Subtitle RESEARCH ACHIEVEMENTS REVIEW, VOL. IV, REPORT NO. 5 Quality and Reliability Assurance Research at MSFC		5. Report Date May 30, 1972	
		6. Performing Organization Code	
7. Author(s) J. B. Beal, M. C. McIlwain, T. F. Morris, M. J. Berkebile, and F. Vilella		8. Performing Organization Report No.	
		10. Work Unit No.	
9. Performing Organization Name and Address  George C. Marshall Space Flight Center Marshall Space Flight Center, Alabama 35812		11. Contract or Grant No.	
		13. Type of Report and Period Covered Technical Memorandum	
12. Sponsoring Agency Name and Address  National Aeronautics and Space Administration Washington, D.C. 20546		14. Sponsoring Agency Code	
		15. Supplementary Notes  Prepared by Quality and Reliability Assurance Laboratory, Science and Engineering	
16. Abstract  Recent research in quality, reliability, and checkout has been directed largely toward supplying the new and improved technologies required for long-term operation in space. The sequence and contents of the five papers included in this review of Quality and Reliability Assurance research at MSFC are as follows:  1. The operational constraints of conventional systems are compared against NASA-developed advanced X-ray and neutron imaging techniques. A solid state amplifier for X-ray imaging and a closed circuit television system for low-energy level neutron imaging are described.  2. The Space Shuttle Program has introduced a new set of materials which heretofore have had little application in space vehicle structures. These materials, namely, super-alloys, coated refractory metals and composite materials, present new and somewhat unique inspection problems which must be addressed. In-house and contractual efforts aimed at solving these problems are discussed.  3. Leak detection and flow measurement in the environment of space, as applicable to such programs as Skylab and Shuttle, are discussed. The development of a leak detector and a flowmeter, designed specifically for in-space application, and the capabilities, limitations, and present status of and future plans for the two instruments are presented.  4. Derivation of requirements and controls necessary for the production of highly reliable hybrid microcircuits of both the thick and thin film types is discussed. Microwave and power hybrid requirements are under current development, and this progress is also discussed.  5. The failure mode caused by thermal deformation is illustrated, and thermal deformation effects on bond integrity are shown. Wedge bonding in small-signal transistors and microcircuits is considered.			
17. Key Words (Suggested by Author(s)) leak detection                      composite materials flow measurement                thick film hybrid microcircuits            thin film X-ray imaging                      thermal deformation super alloys                        wedge bonding coated refractory metals        neutron imaging		18. Distribution Statement  Unclassified - Unlimited  <i>John F. Anderson</i> STE-R, MSFC	
19. Security Classif. (of this report)  Unclassified	20. Security Classif. (of this page)  Unclassified	21. No. of Pages  68	22. Price*  \$3.00

**Page intentionally left blank**

## CALENDAR OF REVIEWS

### FIRST SERIES (VOLUME I)

REVIEW	DATE	RESEARCH AREA	REVIEW	DATE	RESEARCH AREA	REVIEW	DATE	RESEARCH AREA
1	2/25/65	RADIATION PHYSICS	9	6/24/65	GROUND TESTING	16	10/28/65	ASTRODYNAMICS
2	2/25/65	THERMOPHYSICS	10	6/24/65	QUALITY ASSURANCE AND CHECKOUT	17	1/27/66	ADVANCED TRACKING SYSTEMS
3	3/25/65	CRYOGENIC TECHNOLOGY	11	9/16/65	TERRESTRIAL AND SPACE ENVIRONMENT	18	1/27/66	COMMUNICATIONS SYSTEMS
4*	3/25/65	CHEMICAL PROPULSION	12	9/16/65	AERODYNAMICS	19	1/6/66	STRUCTURES
5	4/29/65	ELECTRONICS	13	9/30/65	INSTRUMENTATION	20	1/6/66	MATHEMATICS AND COMPUTATION
6	4/29/65	CONTROL SYSTEMS	14	9/30/65	POWER SYSTEMS	21	2/24/66	ADVANCED PROPULSION
7	5/27/65	MATERIALS	15	10/28/65	GUIDANCE CONCEPTS	22	2/24/66	LUNAR AND METEOROID PHYSICS
8	5/27/65	MANUFACTURING						

### SECOND SERIES (VOLUME II)

REVIEW	DATE	RESEARCH AREA	REVIEW	DATE	RESEARCH AREA	REVIEW	DATE	RESEARCH AREA
1	3/31/66	RADIATION PHYSICS	6	1/26/67	CHEMICAL PROPULSION	10	9/28/67	TERRESTRIAL AND SPACE ENVIRONMENT
2	3/31/66	THERMOPHYSICS	7	3/30/67	CRYOGENIC TECHNOLOGY	11	11/30/67	MANUFACTURING
3	5/26/66	ELECTRONICS	8**	5/25/67	COMPUTATION	12	1/25/68	INSTRUMENTATION RESEARCH FOR GROUND TESTING
4	7/28/66	MATERIALS	9	7/27/67	POWER SYSTEMS			
5	9/29/66	QUALITY AND RELIABILITY ASSURANCE						

### THIRD SERIES (VOLUME III)

REVIEW	DATE	RESEARCH AREA	REVIEW	DATE	RESEARCH AREA	REVIEW	DATE	RESEARCH AREA
1	3/28/68	AIRBORNE INSTRUMENTATION AND DATA TRANSMISSION	5	11/21/68	COMMUNICATION AND TRACKING	10	12/18/69	MATERIALS RESEARCH FOR SHUTTLE AND SPACE STATION
2	5/22/68	ASTRODYNAMICS, GUIDANCE AND OPTIMIZATION	6	1/30/69	THERMOPHYSICS	11	1/29/70	MICROELECTRONICS RESEARCH FOR SHUTTLE AND SPACE STATION
3	7/25/68	CONTROL SYSTEMS	7	3/27/69	RADIATION PHYSICS	12	3/26/70	COMPUTATION RESEARCH (PART II)
4	9/26/68	AEROPHYSICS	8	6/26/69	METEOROID PHYSICS			
			9	9/25/69	COMPUTATION RESEARCH (PART I)			

### FOURTH SERIES (VOLUME IV)

REVIEW	DATE	RESEARCH AREA	REVIEW	DATE	RESEARCH AREA	REVIEW	DATE	RESEARCH AREA
1	5/28/70	STRUCTURES	4	3/25/71	ELECTRICAL POWER SYSTEMS	6	8/5/71	CHEMICAL PROPULSION
2	10/29/70	CRYOGENICS	5	5/27/71	QUALITY AND RELIABILITY ASSURANCE	7	9/28/71	PRODUCT ENGINEERING AND PROCESS TECHNOLOGY
3	11/19/70	INSTRUMENTATION				8	12/2/71	AEROSPACE ENVIRONMENT

\*Classified. Proceedings not published.

\*\*Proceedings summarized only.

Correspondence concerning the Research Achievements Review Series should be addressed to:  
Research Planning Office, S&E-R, Marshall Space Flight Center, Alabama 35812